

Copyright

by

Marc David Rodriguez

2003

The Dissertation Committee for Marc David Rodriguez certifies that this is the approved version of the following dissertation:

**The Development of Microbead-based Immunoassays: An
Application of the “Electronic Taste Chip”**

Committee:

John T. McDevitt, Supervisor

Eric Anslyn

Rebecca Richards-Kortum

Dean Neikirk

Jason Shear

The Development of Microbead-based Immunoassays: An
Application of the “Electronic Taste Chip”

by

Marc David Rodriguez, B.S.

Dissertation

Presented to the Faculty of the Graduate School of

the University of Texas at Austin

in Partial Fulfillment

of the Requirements

for the Degree of

Doctor of Philosophy

The University of Texas at Austin

May 2003

Dedication

This work is dedicated to my lovely wife, Debbie, for the patience and compassion she showed all throughout the long years of my education. Now that we have all the fruit trees planted, it's finally time to watch them grow.

Acknowledgements

There are many people I would like to acknowledge for making graduate school a gratifying and challenging experience. First, I owe many thanks to my supervisor, Dr. John T. McDevitt, for his guidance and leadership from the very start. I have learned many valuable lessons, both on a scientific and personal level, from our discussions. I also hope to someday emulate his democratic nature and controllability during times of crises. Furthermore, I would like to express my admiration in the creativity and scientific-aptitude shown by Dr. McDevitt, Dr. Jason Shear, Dr. Eric Anslyn and Dr. Dean Neikirk in creating the “Electronic Taste Chip” project. I know someday, if not already, this research will come to fruition and benefit the lives of many people. Indeed, I am grateful to have been a part of this intriguing, cutting-edge technology.

I would also like to acknowledge Dr. Dean Neikirk and coworkers for providing the McDevitt lab with a supply of silicon chips, Ginger Gillan for help in the early stages of immunology protocol development, and Jorge Wong who has contributed directly for the generation of the superporous beads as described in Chapters 3 and 4. Dr. Bruce Walker and Dr. William Rodriguez from the Harvard Medical School are thanked for useful discussion regarding infectious disease detection. I would also like to acknowledge the National Science Foundation IGERT Program for access to their research facilities at the University of Texas at Austin and the opportunity to meet with other excellent scientists. Although the classes and activities required more time, I feel I have gained an edge over others and feel as I am part of a very well respected program. Finally, I want to recognize my mother, father and sisters. Their support and belief in me has, and always will be, at the heart of my accomplishments.

The Development of Microbead-based Immunoassays: An Application of the “Electronic Taste Chip”

Publication No.

Marc David Rodriguez, Ph.D.

The University of Texas at Austin, 2003

Supervisor: John T. McDevitt

The development of a miniaturized microfluidic sensing device composed of individually addressable polymeric microbeads was developed for the multiplexed analysis of liquid-phase biological molecules related to human disease. This sensing device, termed here as the “Electronic Taste Chip”, makes use of an array of micromachined pits localized on a silicon wafer with trans-wafer openings forming individualized chambers that allow for both fluidic flow and optical access. The optical analysis of biological molecules was facilitated using conventional epi-fluorescent and colorimetric enzyme-linked immuno-detection techniques at each individual bead site of the sensor array enabling multiplexed analyses of antibodies and proteins. This dissertation presents the experimental efforts that led to the successful adaptation of beaded materials for use as the solid-phase matrix in the electronic taste chip. Issues such as the selection and manufacture of an optimal beaded material, protein immobilization techniques, signaling strategies and reagent penetration effects are discussed. In addition, methods to minimize variations in bead diameter and chemical reactivity were developed to improve the analytical characteristics of the bead-based immunoassays herein. Finally, to gauge the utility of the bead-based approach, the analytical characteristics of a model immunoassay performed with the optimized beaded material as the solid-phase was compared to that of a conventional 96-well microplate-based immunoassay.

TABLE OF CONTENTS

List of Figures.....	xi
List of Tables.....	xiii

OUTLINE OF CHAPTERS.....	1
---------------------------------	----------

CHAPTER 1: BACKGROUND AND INTRODUCTION.....	3
1.1 SCOPE.....	3
1.2 ANTIBODY BACKGROUND.....	3
1.3 POLYCLONAL VS. MONOCLONAL ANTIBODIES.....	5
1.4 KINETICS OF ANTIGEN-ANTIBODY INTERACTIONS.....	8
1.4.1 Antibody Affinity and Avidity.....	9
1.4.2 Rate Limitation Models.....	10
1.4.3 Experimental Methods in Determining K_{eq}	14
1.4.3.1 <i>Scatchard Plots</i>	14
1.4.3.2 <i>Surface Plasmon Resonance</i>	16
1.5 IMMUNOASSAY PRINCIPLES.....	17
1.5.1 Generalized Immunoassay Designs.....	17
1.5.2 Heterogeneous vs. Homogeneous Immunoassays.....	20
1.5.3 The Use of Avidin/Biotin in Immunoassays.....	21
1.5.4 Solid-Phase Materials and Protein Immobilization Techniques.....	21
1.6 SIGNAL GENERATION AND DETECTION SCHEMES.....	22
1.6.1 Radioactive Labels.....	22
1.6.2 Enzyme Labels	23
1.6.3 Fluorescent Labels.....	26
1.6.3.1 <i>Principles of Fluorescence</i>	26
1.6.3.2 <i>Direct and Indirect Immunofluorescence</i>	28
1.6.3.3 <i>Enzyme Labels and Fluorescent Substrates</i>	29
1.6.3.4 <i>Time-resolved Fluorescent Measurements</i>	29

1.6.4	Chemiluminescent Labels.....	30
1.6.5	Miscellaneous Labels	31
1.6.5.1	<i>Bioluminescent Fusion Conjugates</i>	31
1.6.5.2	<i>Microparticle Labels</i>	32
1.7	IMMUNOASSAY ANALYTICAL CONCEPTS.....	33
1.7.1	Analytical Terms Pertinent to Immunoassays	33
1.7.2	Assay Optimization	36
1.7.3	Data Plotting and Curve-Fitting Techniques	39
1.8	CURRENT IMMUNOLOGICAL METHODS FOR THE DIAGNOSIS OF VIRAL INFECTIOUS DISEASES	41
1.9	PROMINENT MULTI-ANALYTE DETECTION METHODS.....	46
1.9.1	Planar Microspotted Arrays for DNA/RNA Analysis.....	46
1.9.2	Planar Microspotted Arrays for Protein Analysis.....	47
1.9.3	Multiplexed Analysis Using Gel Pads.....	49
1.9.4	Multiplexed Analysis Using Polymeric Microspheres.....	50
1.10	MICRO-TOTAL ANALYSIS SYSTEMS (μ -TAS).....	51
1.11	STATEMENT OF PURPOSE	55
 CHAPTER 2: THE ELECTRONIC TASTE CHIP METHODOLOGY.....		59
 CHAPTER 3: TWO-DIMENSIONAL ARRAYS BASED ON THREE DIMENSIONAL OBJECTS FOR MULTI-ANALYTE DETECTION: MATERIALS CONSIDERATIONS.....		67
3.1	INTRODUCTION.....	67
3.2	EXPERIMENTAL SECTION.....	70
3.2.1	Reagents.....	70
3.2.2	Bead-Matrix Materials and Protein Immobilization Protocols.....	70
3.2.3	The Production of Superporous Agarose Beads.....	74
3.2.4	Bead Sorting and Activation Protocols.....	75
3.2.5	Instrumentation.....	75

3.2.6 Confocal and Scanning Electron Microscopy.....	76
3.3 RESULTS AND DISCUSSION.....	77
3.3.1 Polymer Bead Candidates.....	81
3.3.2 Optical Clarity and Background Fluorescence of Bead Candidates.....	83
3.3.3 Protein Immobilization Chemistry.....	86
3.3.4 Bead-based Immunoassay Detection Schemes.....	90
3.3.5 Gel Porosity.....	93
3.3.6 Protocol to Minimize Bead Variability.....	94
3.3.7 Integrating the Agarose Beads into the Electronic Taste Chip.....	96
3.3.8 The Characterization of Superporous and Homogenous Beads.....	99
3.3.9 Comparison of Assay Characteristics of Homogenous and Superporous Agarose Beads.....	103
3.4 CONCLUSIONS.....	106
 CHAPTER 4: A COMPARISON OF BEAD-BASED IMMUNOASSAYS USING THE ELECTRONIC TASTE CHIP APPROACH TO CONVENTIONAL MICROTITER PLATE-BASED ELISA.....	
4.1 INTRODUCTION.....	109
4.2 EXPERIMENTAL SECTION.....	113
4.2.1 Reagents.....	113
4.2.2 The Production of Superporous Agarose Beads.....	114
4.2.3 Bead Sorting, Activation and Protein Conjugation Steps.....	115
4.2.4 Instrumentation.....	115
4.2.5 Assay Procedures and Data Collection.....	116
4.2.6 Intra- and Inter assay Variation Studies.....	117
4.2.7 ELISA Studies.....	118
4.2.8 Bead Characterization.....	118
4.3 RESULTS AND DISCUSSION.....	119
4.3.1 Comparison of Signal Response Rates.....	124
4.3.2 Immunoreagent Penetration.....	129

4.3.3 Comparison of Assay Characteristics.....	134
4.3.4 Multianalyte Detection Capacity.....	140
4.4 CONCLUSIONS.....	143
REFERENCES.....	145
VITA.....	160

LIST OF FIGURES

Figure 1.1: Schematic of IgG antibody structure.....	5
Figure 1.2: Schematic of IgM antibody structure.....	5
Figure 1.3: Procedure used to produce monoclonal antibodies.....	7
Figure 1.4: Mass-transport limitation at a solid-phase surface.....	13
Figure 1.5: Scatchard Plots.....	15
Figure 1.6: Generalized immunoassay designs.....	19
Figure 1.7: Mechanism of HRP catalysis.....	25
Figure 1.8: Fluorescence energy level diagram.....	27
Figure 1.9: Direct vs. indirect immunofluorescent techniques.....	28
Figure 1.10: Schematic of dipstick-type home pregnancy tests.....	33
Figure 1.11: Various data plotting techniques.....	39
Figure 1.12: Serologic time course after Hepatitis B infections.....	42
Figure 1.13: Schematic of a demonstrative μ -Total Analysis System.....	54
Figure 2.1 SEM: image of a representative 3×4 sensor array.....	60
Figure 2.2: Diagram of the well region within the silicon wafer.....	61
Figure 2.3: Diagram depicting the sensor array flow cell housing.....	62
Figure 2.4: Schematic of fluid flow within flow cell of the sensor array.....	63
Figure 2.5: The electronic taste chip total analysis system.....	66
Figure 3.1: A 2-dimensional array assembled from 3-dimensional objects.....	79
Figure 3.2: Optical characteristics of 5 general bead types.....	85
Figure 3.3: Evaluation of protein-to-bead coupling chemistries.....	88
Figure 3.4: Bead-based immunoassay detection schemes.....	91
Figure 3.5: Effect of in-house sorting and activation of agarose beads.....	95
Figure 3.6: Integration of agarose beads into the sensor array.....	98

Figure 3.7: SEM of both homogenous and superporous bead types.....	100
Figure 3.8: Confocal images of immunoreagent penetration.....	102
Figure 3.9: Dose-response plots for bead-based CRP assay.....	105
Figure 4.1: Bead-based sensor array system.....	121
Figure 4.2: Signal response for both ELISA and electronic taste chip.....	127
Figure 4.3: Penetration of immunoreagents into agarose beads.....	131
Figure 4.4: SEM images of homogenous and superporous beads.....	134
Figure 4.5: CRP dose-response plots using ELISA and agarose beads.....	136
Figure 4.6: Multiplexing capabilities of bead-based sensor array.....	142

LIST OF TABLES

Table 1.1: Types of solid-phase materials used for immunoassays.....	22
Table 1.2: Comparison of limits of detection of various immunoassay formats.....	31
Table 1.3: Various labels and fusion conjugates used in immunoassay.....	32
Table 1.4: Advantages and limitations of common viral diagnostic methods.....	43
Table 3.1: Characteristics of various beaded materials.....	84

OUTLINE OF CHAPTERS

This dissertation will describe the contributions made towards the development of the electronic taste chip and the associated studies to validate and understand its performance. Furthermore, it presents a systematic description of the materials and methods used to develop a microbead-based sensor array capable of the measurement of proteinaceous biomarkers relevant to human disease states. Here, it is assumed that the readers are from a variety of scientific and engineering disciplines and may have only minimal knowledge of immunological analyses. Accordingly, Chapter 1 presents a rather comprehensive account of the most common immunoanalytical techniques and serum-based diagnostics. The concepts discussed here are appropriate for the understanding of the experimental procedures and mechanistic descriptions described later in the dissertation. In addition, prominent techniques relevant to multi-analyte detection such as microarrays, lab-on-a-chip, and other bead-based technologies are described. Chapter 2 presents a concise description of the instrumental design and methodological developments of the ‘electronic taste chip’ sensing strategy. This chapter summarizes the combination of instrumental and procedural parameters that have been developed collectively by the project participants at the University of Texas at Austin. Topics such as the manufacturing process of the silicon array pioneered in the Neikirk laboratory, integration of the silicon chip into a water-tight flow cell housing, incorporation and use of the microscope for optical analyses, and procedures used to extract data from the sensor array are described. Chapter 3 accounts the “process-of-elimination” approach used for the identification of the bead material for the bio-assays. Additionally, a new agarose bead matrix is introduced that contains large pores or channels that penetrate deep into the interior region of the bead. Thus, two types of agarose beads, termed here as homogenous and superporous beads, are used in the sensor array and evaluated here. Consequently, Chapter 3 adopts a materials-based approach and presents many of the physical and chemical characteristics of these materials. Furthermore, a protocol for the minimization of variation in bead size and chemical reactivity is described. Finally,

Chapter 4 integrates the use of both types of agarose beads into the sensor array as these materials are used as the solid-phase matrix for immunoassay. Chapter 4's main theme is a comparative analysis of the assay characteristics exhibited by the electronic taste chip system relative to the widely used microplate-based ELISA methodology. Issues such as the response time, detection limit, dynamic range and intra- and inter-assay variability are compared using optimized model immunoassays. Lastly, the analytical characteristics exhibited by the bead-based assays are further assessed by using analyte dissociation data derived from a bead-based experiment and compares to that of a similar surface plasmon resonance experiment. This data sheds light on the protein binding interactions occurring within the agarose matrix as well as those that occur at planar surfaces. When put into the context of the ELISA approach, these findings seek to provide a molecular-level understanding of the protein interactions occurring at the solid-phase interface of these two immuno-analytical approaches.

CHAPTER 1: BACKGROUND AND INTRODUCTION

1.1 SCOPE

This chapter provides the reader with a broad and fundamental background of the most commonly used serum-based immunoanalytical and immunodiagnostic techniques. The concepts discussed here are appropriate for the understanding of the experimental procedures and theoretical insight derived from chip-based immunology studies relayed in this dissertation. First, a background of antibodies and antibody production is presented along with consideration given to their binding constants and rates of interaction. Then, a discussion of the most widely used immunoassay techniques and detection schemes is presented to give the reader a sense of the available methods used for the solution-based analysis of biological molecules. The discussion is then directed towards the most widely accepted methods used for the medical diagnosis of viral infectious diseases. This is followed by a short summary of the most current and promising multi-analyte sensing technologies. Finally, deficiencies in current serum-based diagnostic practices are provided especially with respect to multiplexed analyses. This background information serves as a motivational basis for the completion of the research summarized in this dissertation.

1.2 ANTIBODY BACKGROUND

The vertebrate immune system consists of well-diversified molecules that recognize and respond to parasitic infection in a complex manner. A major component of this system is the macrophage. Macrophages are mononuclear phagocytes that continually roam through the bloodstream of their host. When challenged by a microbial infection, they respond by ingesting the microbes and exert a cell membrane rupturing action effectively destroying the microbe. This event, mediated by helper T cells, sets forth a complicated chain of responses that results in the stimulation of B cells. Each B cell, in turn, produces and displays a random nonspecific immunoglobulin protein on its surface. Foreign antigen (any substance that induces the antibody generating response) therefore only becomes bound to a few of these randomized B cells. However, binding to

the antigen stimulates them to divide and to mature into plasma cells that secrete large amounts of the immunoglobulin that was originally displayed on their surface. These specified immunoglobulin proteins are now termed as “antibodies”. Furthermore, during this proliferation process, cellular regulation mechanisms induce a class switching process that induces the production of a variety of antibody molecule classes (IgM, IgG, IgA, IgE or IgD). These five antibody classes differ on the basis of size, amino acid composition, carbohydrate content and abundance in serum.

The antibody classes mentioned above are variations of the basic antibody molecule structure. Figure 1.1 shows the IgG molecule consisting of two identical ‘heavy’ polypeptide chains paired with two identical ‘light’ chains, forming a flexible Y shaped molecule. These chains are linked together by disulfide bonds. The IgG molecule can be broken down into two regions, the Fc and Fab. The Fc region, so called because it is the fragment of the molecule that most readily crystallizes, is responsible for the effector functions of the antibody, i.e. interaction with Fc receptors on cell surfaces and placental transmission of IgG. The Fab region is named as such because it is the IgG fragment that contains two “antigen-binding” sites. The Fab region contains a region of highly conserved amino acids as well as a region of highly variable amino acids. It is this region that is responsible for the binding of foreign antigens via hydrogen bonding, van der Waals forces, coulombic interactions and hydrophobic bonds. Figure 1.2 provides a schematic diagram the human IgM molecule with a conjugated five-fold repeating pattern of the basic antibody molecule.¹

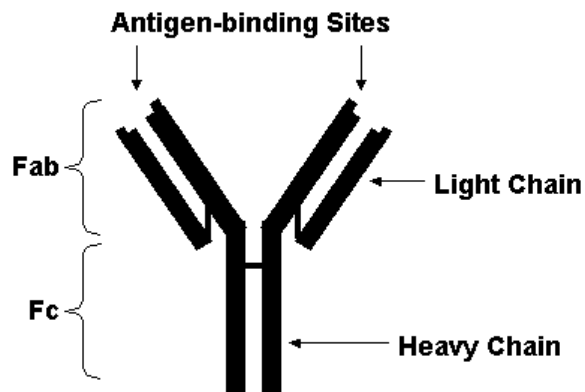


Figure 1.1: Schematic of the basic IgG antibody structure illustrating a pair of heavy chain and light chain amino acid regions that are linked via disulfide bonds. The Fc region represents the crystallizing fragment of the molecule and the Fab region contains a highly variable amino acid region responsible for binding antigen via coulombic attraction at the antigen binding sites.

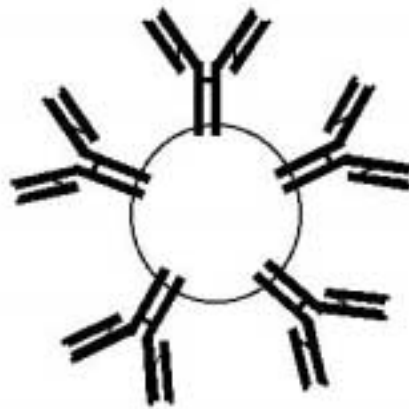


Figure 1.2: Schematic of basic human IgM structure. The IgM motif is a pentamer of the basic antibody structure joined together by disulfide bonds.

1.3 POLYCLONAL VS. MONOCLONAL ANTIBODIES

Most antibodies used for research or diagnostic purposes rely upon antibodies derived from animals. Polyclonal antibodies (Pab) are a heterogeneous mixture of antibodies of varying binding affinities and specificity. The antibodies recognize multiple epitopes (the smallest structural area on the antigen that can combine with an antibody) both on the antigen and any impurities injected with it. Polyclonal antiserum is

produced by injecting an animal (rabbit, sheep, goat, donkey, etc.) with purified antigen subcutaneously at multiple sites often near the animal's lymph nodes. Several subsequent booster shots of the same antigen are given. A standard immunization protocol would be two injections, four weeks apart, followed by a test bleed after ten days. If, after testing, the antiserum is not of sufficiently high concentration or affinity, the animal will undergo repeated boosts at monthly intervals.

The purification of the antisera could follow any of four commonly used techniques. The first method uses simple physical separation by precipitation with ammonium sulfate or sodium sulfate, also known as salting out. The IgG molecules precipitate because the solubility decreases with increasing ionic strength. Antigen-specific IgG together with non-specific IgG is precipitated followed by removal of salt by gel filtration or dialysis. The second method uses a gradient ion-exchange technique that can give a higher purity than salt fractionation, but the procedure is more time-consuming. The third method uses the specific and reversible binding properties of the antibody's Fc region with lectins (such as Protein A and Protein G). Here, the crude antibody is passed through a column containing the lectin bound to an inert support. After washing the column, IgG is eluted off the column using low pH. The fourth most specific method uses immunoaffinity techniques to isolate only specific antibody. In this case, the specified antigen of interest is covalently coupled to the support contained in a column. Crude antiserum is allowed to flow through the column and then the column is washed extensively to remove the unwanted non-specifically bound protein. Finally, the antibody of interest is collected by eluting the column with low pH or a high concentration of chaotropic agent (reagents that disrupt hydrogen bonding and promote the protein's solubility) such as guanidinium chloride.

In contrast to the molecular diversity presented by polyclonal antibody systems, monoclonal antibodies (Mabs) are identical copies of a pre-selected antibody synthesized by a single clone of B-lymphocytes. Monoclonal antibodies exhibit superb specificity and are able to distinguish very slight differences between molecules, cells or microorganisms. Likewise, Mabs are widely used in immunoassays, in the delineation of

cell surface molecules, in assays of drugs and hormones in serum and even used as therapeutic agents for disease. A schematic of the procedure used to produce these antibodies is shown in Figure 1.3. Here, a mouse or rabbit is immunized with a specified antigen. After repeated booster shots, the spleen of the animal is removed since it is responsible for the production of B-lymphocytes. Because these cells cannot proliferate in cell culture medium, they are fused with ‘immortal’ myeloma cells (neoplastic antibody-producing cells). The resulting fused cells, called hybridoma cells, are grown in a 96-well type format using cell culture techniques and will eventually begin to produce antibody. The arrayed culture supernatants are then screened according to their reactivity and specificity to the antigen of interest. Once a cell culture well has been identified as containing specific antibody-secreting cells, those cells are transferred to larger culture wells and allowed to proliferate or are cloned. Large quantities of antibody are produced by propagating the cell line in large flasks and collecting the culture supernatant that contains the antibody. Modernized methods of monoclonal antibody propagation use hollow fiber reactors.² These are essentially bundles of fine porous fibers through which culture medium is circulated. The cells are grown in the much smaller volume of the capillary or interior space of the fibers. Nutrients and waste products can pass freely in the space between the fibers but the larger molecules such as antibodies remain in the cell compartment until harvested. Large densities of cells can be maintained in this system for months producing up to several hundred mg of antibody per day.¹

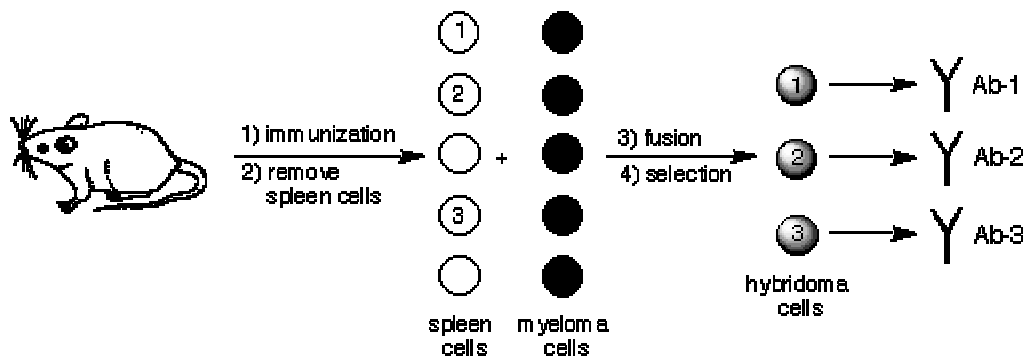
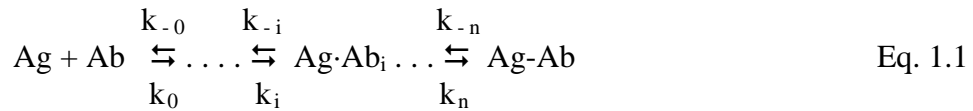


Figure 1.3: Summary of important steps used to produce monoclonal antibodies.³

1.4 KINETICS OF ANTIGEN-ANTIBODY INTERACTIONS

The antigen-antibody binding reaction occurs between a specific molecular determinant (epitope) of an antigen and the antigen-binding region (paratope) of an immunoglobulin in an aqueous environment. The forces involved in the binding between the two species are van der Waals, hydrophobic/hydrophilic interactions, electrostatic forces and hydrogen bonding events. Equation 1.1 represents the binding interaction of the antigen and antibody where Ag and Ab are the two reactants, respectively, and Ag-Ab is the final complex formed after i different intermediate states (Ag·Ab) _{i} . The notation, k_n , represents the different forward reaction rates and, k_{-n} , represents the different reverse reaction rates.



[Ag] = antigen concentration,
 [Ab] = antibody concentration,
 [Ag·Ab] = intermediate complex,
 [Ag-Ab] = bound antigen-antibody complex,
 k_{-n} = dissociation rate constant,
 k_n = association rate constant.

Many factors influence the reaction leading to the intermediate complex such as reactant size and reactivity; the diffusional or mass transport characteristics of the reactants in the reactant medium; and the conditions of the reaction medium such as pH and ionic composition. The rates of reaction for these factors are often very different in magnitude with the slowest step described as the rate-limiting factor.

Normally, as the forward and reverse reaction rates are limited by one particular factor, the overall reaction scheme is simplified to:



where k_f is the effective forward reaction rate constant and k_r is the effective reverse reaction rate constant (also known as the association and dissociation constants, respectively).⁴

1.4.1 Antibody Affinity and Avidity

The affinity constant is a key measure of an antibody's ability to function well in an immunoassay. The term "antibody affinity", therefore, refers to the strength of interaction between an antigenic determinant and the antibody-binding site. The magnitude of the antibody affinity constant is ultimately dependent upon the summation of attractive and repulsive forces involved in the relevant interactions. A high affinity antibody is thus one that forms an antigen-antibody complex with a low tendency to dissociate. A low affinity antibody, on the other hand, forms a complex with the antigen that requires less energy to dissociate.

The simplified antigen-antibody reaction described by Equation 1.2 is derived from the Law of Mass Action where the ratio of the concentration of the reactants and products is equal to the equilibrium constant, K_{eq} . Furthermore, the ratio of the forward and reverse rate constants represents the final ratio of bound to unbound antigen and antibody. This is known as the antibody affinity constant. Equation 1.3 couples these values in the context of the affinity constant, where k_f and k_r are the forward and reverse rate constants, respectively.

$$\text{Affinity constant} = K_{eq} = k_f/k_r = \frac{[Ag-Ab]}{[Ag][Ab]} \quad \text{Eq. 1.3}$$

A typical antigen-antibody reaction yields second-order reaction kinetics with units for the forward and reverse rates as $M^{-1}s^{-1}$ and s^{-1} , respectively.⁵ Overall, the units of K_{eq} take the form of M^{-1} . Likewise, an estimate for the detection threshold for a given antibody reagent is often provided by the reciprocal of the K_{eq} value which is also

expressed as Kd. The Kd value represents the concentration at which 50% of the antigen becomes bound by the antibody as expressed below⁶:

$$K_{eq} = \frac{1}{Kd} = \frac{1}{[Ag]_{50}} \quad \text{Eq. 1.4}$$

The Kd value is often used to indicate the strength of binding between the two reactants and typically range between 1 μ M to 1 nM.

Antibody avidity is a term that describes the effect of multiple binding events between an antigen with multiple epitopes and a single antibody molecule. It becomes more pronounced with antibodies with higher valencies such as IgM that possess up to 10 antigen-binding sites. The effect of these multivalent binding interactions leads to a cooperative interactivity of the antigen-antibody complex so that the probability that all AgAb interactions will dissociate simultaneously is exceedingly small. In addition, if one interaction is dissociated, the others will remain associated, thus enhancing the probability that those dissociated will reassociate. The net effect often reveals itself with an antibody with a higher effective affinity constant.

1.4.2 Rate Limitation Models

Knowledge of the rate-limiting factor of the antigen/antibody interaction is a crucial feature in the kinetic analysis of an immunoassay system. To reveal such information, the experimental data representing the binding response can be described by one of several theoretical rate-limiting reaction models in an attempt to best describe the data. The simplest of these models is the one-to-one interaction between the antigen and antibody as dictated by the Law of Mass Action where the rate of reaction is defined by reaction's equilibrium constant. The Law of Mass Action represents the reactants and products at equilibrium as would be the case where equation 1.3 is valid.

In this case, the rate of the number of moles of complex being formed is dictated only by the forward and reverse reaction rates with no other rate-limiting experimental factors being involved. This type of rate control is termed here as “reaction-limited”.

A diffusion-limited reaction is a reaction whose rate is limited (or controlled) only by the speed that the reactants diffuse to each other. The diffusion-limited model is useful to describe cases where no active fluidic is present. In these no-flow or stagnant conditions, particles in solution experience mainly random or Brownian motion where the coefficient of diffusion, D , can be estimated by the Einstein Stokes equation:

$$D = kT/6\pi\eta r \quad \text{Eq. 1.5}$$

where k is Boltzmann’s constant, T is the temperature in Kelvin, η is the viscosity of solution and r is the radius of the diffusing species. When the radius of both the antigen and antibody are known, the rate constant of a bimolecular reaction can be estimated by:

$$k = 4\pi d_{AB} (D_A + D_B)L \quad \text{Eq. 1.6}$$

where d_{AB} is the hard-sphere collision diameter of the binding complex, D_A and D_B are the diffusion coefficients of the antigen and antibody, and L is Avogadro’s number. With estimates of an average d_{AB} value at 5×10^{-8} cm and $(D_A + D_B)$ at 10^{-5} cm² s⁻¹, the above equation shows that k is estimated to be about 7×10^9 M⁻¹sec⁻¹.⁵ Consequently, in solutions, bimolecular antibody-antigen rate constants do not typically exceed 10^9 - 10^{10} M⁻¹sec⁻¹ because the rate of diffusion then becomes a limiting factor.

When binding between antibody and antigen takes place at a surface i.e. one of the binding partners is immobilized to a solid-phase and the other is distributed in solution, and flow or stirring conditions are used to deliver reagents to one another, the rate of binding and dissociation may be limited by the rate of transport of reactants to the surface where binding occurs. This occurrence becomes especially important at the

surface of some biosensors where binding interactions are monitored in real-time.⁷ Here, the rate of reactant binding and dissociation depends on the forward and reverse rate constants of the antibody and on the local concentration of reactant at the surface. A concentration gradient will form at the surface as reactants are depleted and fed back during the binding and unbinding processes. Considering the combination of multiple parameters (i.e. kinetic constants, reactant concentration, density of binding sites, flow rate and diffusion coefficients, etc.), the system can exist in a state where rates are: (i) only reaction limited, or (ii) mass transport limited.⁸ For the first case, the mass transport of reactants is able to balance concentration differences much faster than the reaction creates them. Likewise, the local analyte concentration remains essentially equal to the bulk concentration. For the second case, however, the local concentration of analyte is different at the surface than the bulk concentration and the apparent forward and reverse rate constants are different from the true rate constants of the binding reaction. This type of rate-controlled reaction is termed here as a mass-transport limited reaction. A schematic showing this situation is shown in Figure 1.4 below.

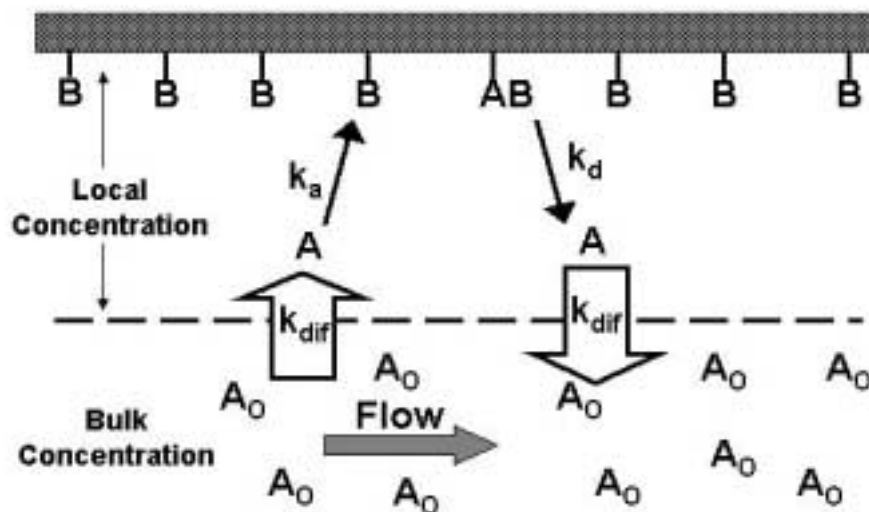


Figure 1.4: Schematic showing the mass-transport limiting rate control of binding interactions with proteins immobilized to a surface. The capture protein (B) is attached to the surface with a flexible linker. A local concentration gradient (A) is formed near the surface whereby the local analyte concentration (A) is reduced from that of the bulk analyte concentration (A₀) as it binds to the capture protein. The delivery of A₀ may or may not replenish the analyte A, diffusing to the surface at a rate k_{dif} . Here, k_a and k_d are the intrinsic forward and reverse reaction rate constants for the antigen-antibody complex binding that define the rate of formation of the complex (AB).

Determining the rate-limiting factor of solution-based and solid-phase immunoassays has been the subject of many research articles. Butler et. al. have succinctly summarized much of this work.⁴ Here, reactions with antibodies are characterized as those with small-molecule antigens (or haptens), large macromolecular antigens (proteins), and antigen-antibody reactions at surfaces. In the case of antibody reactions with haptens and after considering factors such as viscosity of the reaction medium and reactant size and reactivity, it is concluded that the diffusion rate constant for typical hapten-antibody reactions is on the order of $10^9 \text{ M}^{-1}\text{s}^{-1}$. Furthermore, it has been observed that the fastest hapten-antibody reactions in solution range from 10^5 to $10^8 \text{ M}^{-1}\text{s}^{-1}$, which is 10-10,000 slower than what is expected for the diffusion-limited rate. Likewise, the rate of typical hapten-antibody reactions in solution is often reaction-limited.

Similarly, the diffusion rate constant between antibodies and macromolecular antigens in solution is on the order of $10^7 \text{ M}^{-1}\text{s}^{-1}$. Experimental studies that were

performed to analyze the forward reaction rate between antibodies and macromolecular protein antigens reveal forward reaction rates ranging between 10^5 and $10^6 \text{ M}^{-1}\text{s}^{-1}$. These values are a factor of 10 to 100 times slower than the rate constant of a diffusion-limited reaction for these molecules and thus imply that these reactions are also reaction-limited.

In the case of antigen-antibody reactions at surfaces where an antigen is immobilized to a solid surface, the diffusional forward reaction is thought to be further reduced by the limited radius of the reactive site (as created by the immobilized antigen) and is on the order of $10^6 \text{ M}^{-1}\text{s}^{-1}$. However, the immobilization of antigens at solid surfaces introduces possible cooperative effects on the antibody reaction at the solid-liquid interface, such as the induced local concentration gradient described above. This phenomenon occurs especially at high capture protein immobilization density and often makes the antigen-antibody reaction mass-transport limited. Furthermore, these conclusions are corroborated by other the findings of other authors who also report that antigen-antibody reactions at solid-phase interfaces are typically limited by mass transport and can be considered as practically irreversible. The mechanism behind the slow dissociation described here has been suggested to be the mass transport limitation of the reverse reaction. Likewise, with a high surface concentration of immobilized receptors, there is a high probability of re-association instead of diffusion transport away from the surface after dissociation.⁹

1.4.3 Experimental Methods in Determining K_{eq}

1.4.3.1 Scatchard Plots

Assuming that a homogeneous antibody population is present, Equation 1.5 can be rearranged so that a linear relationship exists in the plot of the ratio of bound to free antigen and the concentration of bound antigen (abbreviated $[B]/[F]$ vs. $[B]$), as shown in Equation 1.7:

$$[Ab_t]K_{eq} - K_{eq}[B] = [B]/[F] \quad \text{Eq. 1.7}$$

where $[Ab_t]$ is the total antibody concentration or $[Ab] + [Ab-Ag]$; $[B]$ is the concentration of bound antigen; and $[F]$ is the concentration of free antigen. The graphic representation of this relationship is known as a Scatchard plot as shown in Figure 1.5a below.¹⁰ Two useful parameters may be derived from these plots: the equilibrium constant, K_{eq} , from the negative slope of the line and the total concentration of antibody binding sites $[Ab_t]$ from the intersection on the x-axis.

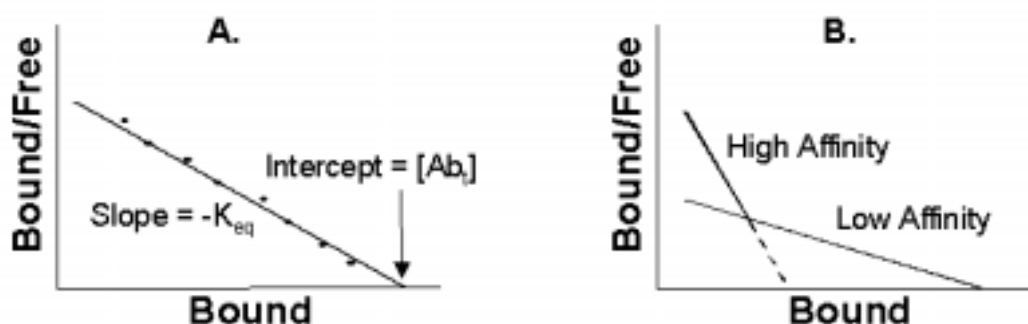


Figure 1.5: Scatchard plots. Using a homogenous antibody population, graph A demonstrates that a linear relationship exists between the ratio of $[Bound]/[Free]$ antigen and the concentration of bound antigen. Here, the slope of the line provides the equilibrium constant, K_{eq} and the x-axis intercept lends information related to the total concentration of antibody binding sites. When using a heterogeneous antibody population (i.e. a polyclonal antibody), graph B illustrates the non-linear Scatchard plots that are obtained.

To obtain experimental values for the bound and free reactants, the separation of free from bound antigen is often monitored using radioisotope-labeled antigen¹¹ with techniques such as gel filtration, sedimentation, solid-phase methods and elipsometry.^{12,13} Figure 1.5b illustrates the multiple slopes of the Scatchard plot obtained when a population of antibodies with a range of equilibrium constants is used to bind analyte (i.e. polyclonal antibodies). This gives rise to a much more complex and curved line that has, in the figure above, been simplistically resolved into two populations of high- and low-affinity antibodies. The multiple K_{eq} and $[Ab_t]$ values must now be deciphered from the

data by using a more sophisticated approach such as the nonlinear least-squares curve-fitting program reported by Munson et. al.¹⁴

1.4.3.2 Surface Plasmon Resonance

In the last decade, advances in sensor technology have enabled the binding interactions to be monitored in real-time without the use of radioactive or spectroscopic probes. For example, BIAcore® sensing technology uses surface plasmon resonance (SPR) to measure the change in refractive index at a metal/liquid interface caused by the binding of molecules. Briefly, SPR arises when light is reflected from a conducting film at the interface between two media of different refractive indices. In the BIAcore® system, the two media consist of the sample and a glass sensor chip upon which a thin film of gold is deposited. Because gold is an excellent conductor, the material has associated with it a collection of delocalized electrons that may move as a collective mass and thus form of plasma. These free electrons at the detector's gold surface are extremely sensitive to changes in the electrostatic interactions occurring in the liquid phase that result from biospecific binding interactions. Moreover, these free electrons determine the refractive index near the gold's surface. When molecules in the sample bind to the sensor surface, the concentration and therefore the refractive index at the surface changes and the SPR response is detected.¹⁵ Plotting the response against time during the course of an interaction provides a quantitative measure of the progress of the interaction. Finally, curve-fitting software is used to process the data using nonlinear least squares or numerical integration of the equations that best describes the interaction kinetics. In doing so, representative rate limiting models such as the simple bimolecular or mass-transport limited interactions are fitted to the experimental data.¹⁶ Consequently, the forward and reverse rate constants and thus the equilibrium constant of many types of biomolecular interactions can be determined rapidly and efficiently in a single manner.

1.5 IMMUNOASSAY PRINCIPLES

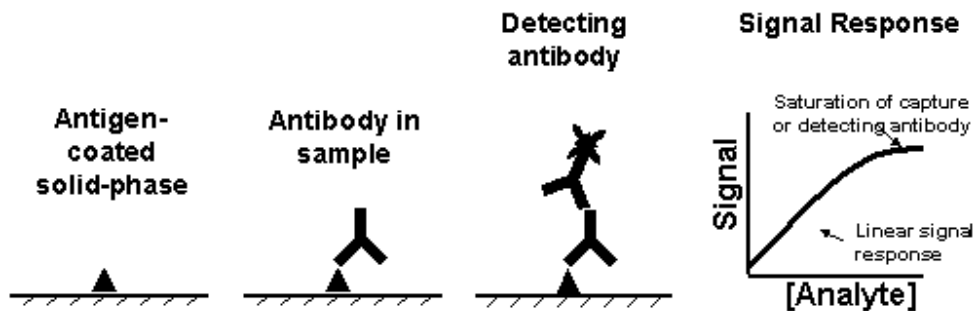
1.5.1 Generalized Immunoassay Designs

Immunoassays are analytical tests that use antibodies to bind to a target analyte and reagents to generate a signal indicating the amount of analyte present. They are widely used in fundamental life science research, clinical evaluation and medical diagnostics. For example, immune cell phenotyping and immunopathology methodologies often use fluorescent-labeled antibodies to identify disease states of cells.¹⁷ Further, infectious diseases such as those caused by viruses, bacteria, fungi, and parasites are regularly tested using antibodies.¹⁸ Immunoassay's unique characteristics are derived from three important properties of antibodies: 1) their ability to bind to an extremely wide range of natural and manmade molecules, cells and viruses. This flexibility is a direct result of the superbly evolved biomolecular selection processes of the vertebrate immune response; 2) their exceptional specificity for which each antibody binds enables minute concentrations of analyte to be assayed in the presence of many closely related substances. For example, measurements of hormones with picomolar concentrations are routinely performed in blood serum (see Table 1.2); and 3) the binding strength between antibody and analyte is exceptionally strong. These binding characteristics are required if the bound antibody/analyte complex is to survive the repeated washing and signal generation steps used in immunoassays.

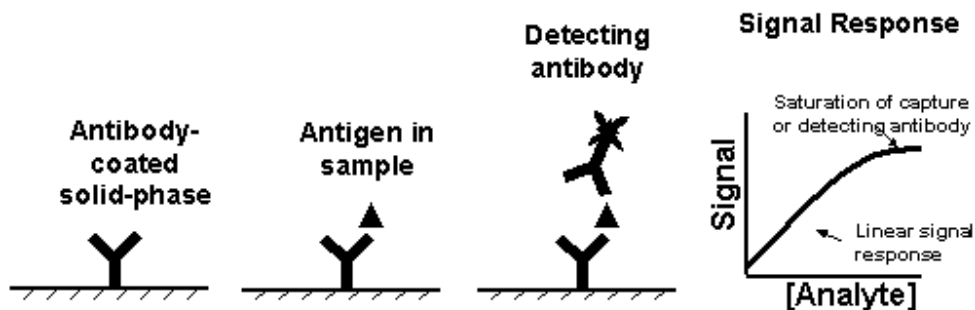
Immunoassays can be categorized as one of three generalized designs: 1) the antibody capture assay, 2) the antigen capture or sandwich assay, and 3) the competitive antigen capture assay. The antibody capture assay measures the presence or amount of specific antibody (usually in blood-based analyses) and is useful for indicating previous exposure to a selected infectious disease. Figure 1.6a illustrates a typical human serum based antibody capture assay with an antigenic protein that had been previously immobilized onto a solid-phase surface. Antibodies present in the sample that are specific to that antigen bind to the antigen. Finally, labeled polyclonal antibodies, raised against the Fc region of the human antibody are bound and used to detect the analyte. The labeled antibody is often called the detecting or tracer antibody.

Figure 1.6b illustrates a typical antigen capture or sandwich assay. Here, an antibody immobilized onto a solid-phase captures the test analyte (i.e. protein, hormone, cytokine, etc.) from the sample. A different detecting antibody, specific for another site of the analyte molecule, is used as the basis for signal generation.

a. Antibody Capture Assay



b. Antigen Capture Assay



c. Competitive Antigen Capture Assay

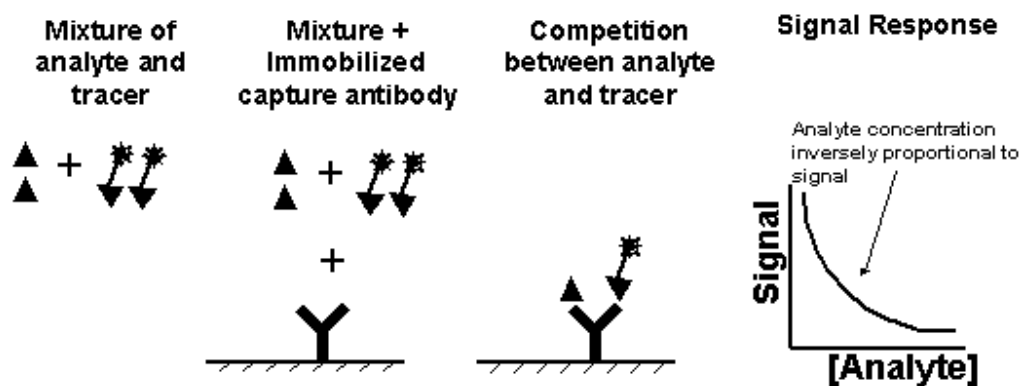


Figure 1.6: Generalized immunoassay designs: a. antibody capture assay, b. antigen capture assay also known as a “sandwich assay”, c. competitive antigen capture assay. In all cases, the capture molecule is covalently linked or bound by hydrophobic/hydrophilic interactions to a solid-phase (polystyrene of microtiter plates or beads, nitrocellulose membrane, etc.).

The immunoassay methods described above work well when the target analyte is a large molecule with the available surface area to accommodate two antibody molecules. However, many immunoassays target small molecules (i.e. drugs, toxin molecules, etc.) and a different assay design is necessary. The competitive antigen capture assay uses a capture antibody in limited quantity. The other key reagent is the tracer or target analyte labeled with a suitable signal generation material. The tracer is mixed with sample and the proportion of tracer that binds to the limited antibody sites is *indirectly* related back to the concentration of analyte in the sample. Figure 1.6c illustrates the competitive antigen capture assay and the associated signal response.

1.5.2 Heterogeneous versus Homogeneous Immunoassays

The three generalized immunoassay approaches described so far depend of the separation of bound from unbound reactants. Without such separation of reactants, the level of signal would be the same regardless of the concentration of analyte. When such separation techniques are used, the assay format is termed heterogeneous. The methods for the physical separation of reactants vary. For example, most immunoassays depend on the immobilization of the capture antibody or antigen onto a solid phase. Examples of useful solid phase materials include: nitrocellulose membranes, the walls of test tubes, polystyrene microwell plates, polystyrene or polymeric bead supports, and magnetic microparticles. Each of these materials provides a solid-phase platform for the immobilization of the immunoreagents and thus enables the separation of bound reactants by washing away the solubilized unbound reactants.

Homogeneous immunoassays require only the mixing of the sample and immunoreagents in some type of vessel without the need to separate bound from unbound reagents. Because the rate of the binding reaction is not limited by the diffusion of reactants to a surface, incubation times are faster, usually only a few minutes. An example of a homogeneous assay is the latex particle agglutination assay where colored microspheres with immobilized antibody are mixed with the sample. A positive result is indicated when the microspheres cross-link to form a colored agglutination pattern.¹⁹

1.5.3 The Use of Avidin/Biotin in Immunoassays

Biotin is a small water-soluble vitamin with an extremely high binding affinity for the egg-white protein, avidin. The affinity constant for the two molecules is $\sim 10^{15} \text{ M}^{-1}$, considered to be one of the strongest biological interactions. This molecular interaction has been widely exploited for use in immunoassay techniques. In this case, avidin is coated to the solid-phase surface just as the capture antigen/antibody would have been. The biotin-labeled protein is then allowed to bind to avidin producing the irreversible binding interaction.

1.5.4 Solid-Phase Materials and Protein Immobilization Techniques

There are a wide variety of materials that are used as the solid phase in heterogeneous immunoassays. For example, many immunoassay systems use injection-molded supports, such as microtiter plates, as the solid phase for capture protein immobilization. The individual wells of the microtiter plate serve as the reaction vessel to perform the antigen/antibody binding interactions and for separation steps necessary for the immunoassay. Other examples include membranes that are used in immunoblotting techniques and beads or microparticles that are used in many automated clinical assays. The factors that define the selection of the solid phase have to do with convenience, laboratory tradition, and specialized conditions. In addition, existing technological advances can also influence the selection of the solid phase. For example, the immunoassay industry has recently focused its efforts on microtiter plate robotic automation for high-throughput analyses.²⁰

Table 1.1 below summarizes the solid phases in common use with a listing of relative protein loading capacity and predominant protein binding forces.

Table 1.1: Types of solid-phase material used for immunoassays.²¹

Type	Capacity	Binding Force
Membranous Forms		
Nitrocellulose	High	Hydrophobic
Polyvinylidene difluoride	High	Hydrophobic
Nylon	High	Hydrophobic
Modified membranes	High	Covalent, hydrophilic, hydrophobic
Plastic Plates and Tubes		
Polystyrene (PS)	Low	Hydrophobic
Polyvinyl	Low	Hydrophobic
Derivatized microtiter plates	Low	Covalent, hydrophilic, hydrophobic
Beads and microparticles		
PS beads	Moderate	Hydrophobic
Derivatized PS beads	High	Covalent, hydrophilic, hydrophobic
Microparticles (latex, agarose, etc.)	High	Covalent and hydrophobic

Typically, immunoreactants are immobilized to the solid-phase in one of three ways: (1) direct adsorption of the protein to the solid-phase surface, (2) covalent attachment to an activated surface or 3) the immobilization of high affinity binding proteins such as avidin using methods (1) or (2) above then the subsequent binding of the biotin-labeled ligand. The method of immobilization is dictated by the solid-phase material, ligand chemistry and immunoassay conditions.²¹

1.6 SIGNAL GENERATION AND DETECTION SCHEMES

1.6.1 Radioactive Labels

A number of radioisotopes are used in immunoassays to generate the signal required to quantify the analyte. The most common is ¹²⁵I with a half-life of 60 days. Tritium or ³H, ⁵⁷Co and ¹⁴C are also occasionally used. Methods for labeling antigen or antibody have been developed that substitutes the radiolabel onto the aromatic rings of

the amino acids tyrosine or histidine of the analyte or antibody.²² The labeled analyte is then detected by means of a scintillant that emits flashes of light when struck by gamma emissions. Finally, these emissions are counted by using a photomultiplier tube that converts the light flashes from the scintillant into electrical pulses, which trigger electronic counting circuits. Since the decay of ^{125}I is a two-photon event, the background of a radioimmunoassay can be reduced by setting the detection system to register only two-photon events as signal. By doing so, background counts fall to 0.5 counts per week and ^{125}I can be detected down to 0.1 attomole. However, even radioactive labels have limited sensitivity since each radioactive atom only gives off its energy on one occasion. In the case of ^{125}I , only one atom disintegrates per second in every 7.5×10^6 radioisotopic atoms.²³

Radiolabels were among the first to be used in immunoassays. However, concerns of radiation exposure and the problems associated with regulation and disposal of radioactive waste have stimulated the development and widespread use of other signaling agents as described below.

1.6.2 Enzyme Labels

Enzyme labels have been developed in response to the shortcomings of radioactive signal generators. Enzymes can be covalently linked to proteins creating an extremely efficient method for signal amplification. Likewise, enzymes are now used more than any other type of label creating the well-known enzyme-linked immunosorbent assay or ELISA (or EIA enzyme immunoassay). Here an enzyme is measurable at very low concentrations by catalyzing the generation of a soluble colored product from a colorless precursor substrate. Enzymatic substrates that catalyze the generation of precipitated end products are also available. A single molecule of enzyme can catalyze the conversion of up to 10^7 molecules of substrate per minute, greatly increasing the sensitivity of the assay compared to a label that produces just one signal event.²³ Since the enzyme acts only as a catalyst, it brings about the molecular change in the substrate

without itself being chemically altered. Enzymes can continue to convert the substrate until the reactants become limited or the reaction itself is terminated.

Three of the most popular enzymes used in ELISA are β -galactosidase, alkaline phosphatase and horseradish peroxidase (HRP). The HRP system is the most commonly used because it is smallest in size of the three and therefore minimizes steric hindrance effects upon conjugation to antibody or analyte. It also has been shown to be superior to alkaline phosphatase and β -galactosidase in terms of assay sensitivity and time.²⁴ For these reasons, HRP will be used as an illustrative example for further discussion. In addition, HRP is extensively used in ELISA and bead array applications in chapters that follow.

The HRP macromolecule is a 44kDa glycosylated hemoprotein. It is an oxidoreductase that catalyzes the reduction of hydrogen peroxide with the concurrent oxidation of the substrate. Consequently, the reaction involves the two electron oxidation of the enzyme by hydrogen peroxide to yield an intermediate compound I. As shown in Figure 1.7 below, compound I (the enzyme) is in turn reduced by the hydrogen donating substrate (the chromophore) via a one-electron transfer to form an intermediate compound II and a donor radical. In the presence of excess substrate, compound II is further reduced by the hydrogen donor via a one-electron transfer to regenerate a free enzyme and another donor radical. The two donor radicals may combine to produce a stable end product.²⁵

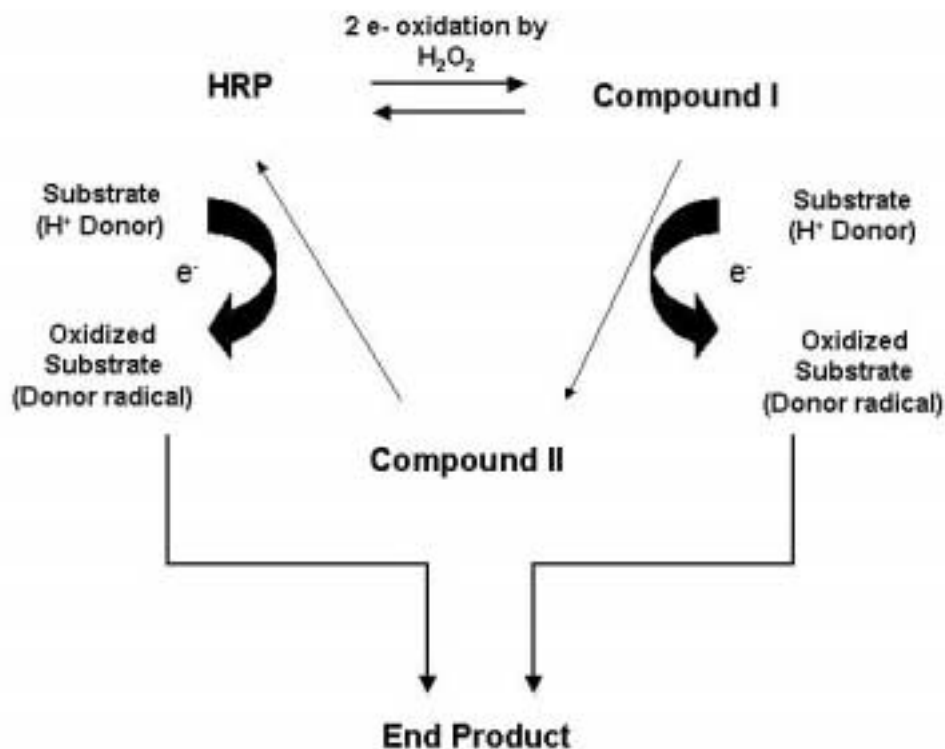


Figure 1.7: Mechanism of HRP catalysis. HRP, a hemoprotein, undergoes a two electron oxidation by H_2O_2 to form Compound I. The iron in the heme group is oxidized from the Fe(III) state to Fe(IV) plus a porphyrin π -radical cation heme. Subsequent reduction of Compound I by a proton donating substrate reduces iron to its Fe(IV) state and yields a donor radical. This reduction occurs again to regenerate the active HRP in the Fe(III) state and another donor radical. Two donor radicals may react to form the colored, fluorescent or chemiluminescent end product.²⁵

A number of soluble and precipitable colorimetric substrates are available for use with horseradish peroxidase. The most common soluble colorimetric substrates used with HRP are *O*-phenylenediamine (OPD), 2,2'-azino-di (2-ethyl-benzthiazoline) sulfonic acid (ABTS) and 3,3',5,5'-tetramethylbenzidine (TMB). A useful precipitating colorimetric substrate most often used in gel blotting experiments is 3'-aminomethyl carbazole (AEC).

To determine the magnitude of the signal generated by the colorimetric enzymatic reaction, the signal is measured using a spectrophotometer where the absorption of light in solution is quantified using Beer's Law:

$$A = \epsilon Cl \quad \text{Eq. 1.8}$$

where A is the absorbance of the solution, ϵ is the molar absorptivity, C is the molar concentration, and l is the path length in centimeters. Currently, microtiter plate readers are available that are capable of the making parallel absorbance measurements in the microtiter plate format.²⁶

1.6.3 Fluorescent Labels

1.6.3.1 Principles of Fluorescence

In addition to colorimetric methods for generating signals for immunoassay, fluorescent techniques are also employed. Fluorescence may be derived from a single class of luminescent dyes that, following their electronic excitation by light absorption, return to the ground state by re-emission of the photonic energy. As the molecule returns to the ground state, it emits a photon of light at a lower energy (i.e. longer wavelength). The difference between the excitation and emission wavelengths is known as the Stoke's shift and the proportion of energy re-emitted is referred to as the quantum efficiency. Many inorganic substances fluoresce such as fluor, spar, rare-earth metals, and semi-conducting nanoparticles. However, fluorescence is much more common among organic compounds such as the naturally occurring phycobiliproteins, the amino acids tyrosine and tryptophan, and manmade molecules such as fluorescein and rhodamine.²³

Figure 1.8 illustrates the energy level diagram of absorption and fluorescence transitions. The absorption of light by an electron in the lowest vibrational state of the electronic ground state (S_0) excites it into one of the vibrational levels of the first excited electronic state (S_1) or into a higher excited state (S_2 , S_3 , etc. not shown). Non-radiative transitions, also known as internal conversion (IC), occur among the vibrational levels of a given electronic excited state. The excited electron rapidly falls to the lowest vibrational state of S_1 . Light emission by fluorescence occurs when the electron returns from this state to one the vibrational levels of the electronic ground state.

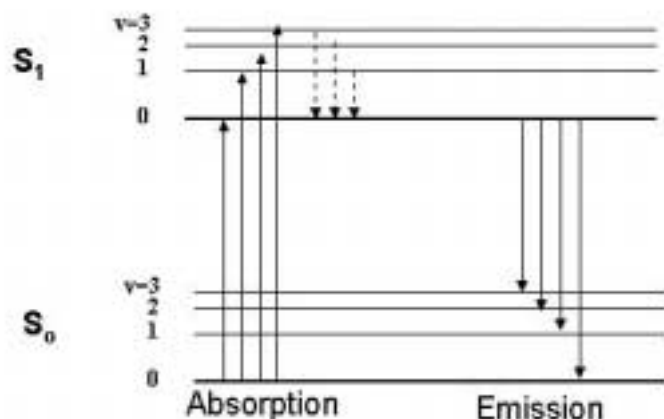


Figure 1.8: Energy level diagram showing absorption and fluorescence emission transitions.

Fluorescent emission usually occurs on the order of 1-100 nanoseconds after excitation. The emitted photons can be measured either by steady-state techniques using a simple fluorimeter or time-resolved techniques using a fluorimeter with pulsed light capabilities. Steady-state methods use a continuous light source to excite the fluorescent compound. A simple fluorimeter includes a light source, an excitation monochromator, a sample holder, an emission monochromator and a photomultiplier detector. This setup can be used in two modes. To obtain an emission spectrum, the excitation monochromator is held at a single wavelength while the emission monochromator is scanned. To obtain the excitation spectrum, the emission monochromator is held at a single wavelength while the excitation monochromator is scanned. Such steady-state fluorescence techniques are ideal if excitation and emission spectra are required or if fluorescent intensities are to be investigated.

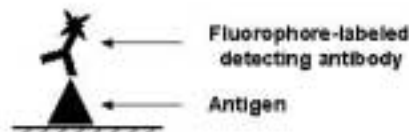
Time-resolved data can provide information not available from steady-state data. For example, these measurements reveal distinct decay times when multiple fluorophores have overlapping excitation or emission spectra. In time-domain methods, the sample is excited with a pulse of light. The width of the pulse is made as short as possible and is preferably much shorter than the decay time τ of the sample. The time-dependent intensity is measured following the excitation pulse, and the decay time τ is calculated

from the slope of a plot of $I(t)$ versus t , or from the time at which the intensity decreases to $1/e$. The measured fluorescent lifetime value is a statistical average of the time all fluorophores emit.²⁷

1.6.3.2 Direct and Indirect Immunofluorescence

There are a variety of immunoassay techniques that use fluorophores as signal generators. The first are those that employ a fluorophore that is directly labeled to the antigen or antibody to signal the presence of analyte. When a fluorophore-linked antibody is used to visualize an antigen, the method is termed direct immunofluorescence. This method has long been used to visualize antigens in microscopic sections of tissue.²⁸ In indirect immunofluorescence techniques, an intermediate antigen or antibody is used with a fluorophore-labeled secondary antibody to indicate the presence of analyte. Figure 1.9 illustrates in schematic form the differences between direct and indirect immunofluorescence techniques.

a. Direct immunofluorescence technique



b. Indirect immunofluorescence technique

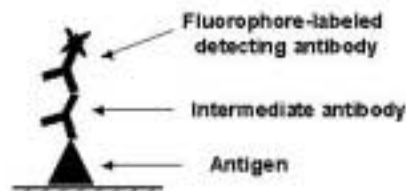


Figure 1.9: Direct vs. indirect immunofluorescent techniques.

1.6.3.3 Enzyme Labels using Fluorescent Substrates

Another technique that generates a fluorescent signal is the ELISA methodology previously adapted for use with fluorescent substrates. Some examples of fluorescent substrates include homovanillic acid, tyramine, and 3',6'-diacetyl-2',7'-dichlorofluorescein. The enzyme catalyzed redox reactions using fluorescent substrates are variations of the redox reaction previously described for HRP. To determine the strength of the fluorescent signal generated by the enzymatic reaction, the signal intensity is measured typically using steady-state techniques with a fluorimeter or fluorimeter-like microtiter plate reader.

1.6.3.4 Time-Resolved Fluorescent Measurements

The performance of the fluorescent immunoassays described above can be diminished by the background fluorescence created from matrix components such as serum proteins, NADH (the reduced form of nicotinamide adenine dinucleotide) and bilirubin. Lower detection thresholds can be obtained when the fluorescence of a long fluorescent lifetime label is discriminated from the short fluorescent lifetime usually found in background fluorescence (1 – 20 ns decay time). The development of long-lifetime labels, such as lanthanide chelates, with decay times ranging from 10 to 1000 μ s, enable the possibility to increase the sensitivity of a fluorescent-based immunoassay.

An example of this technique is commercialized under the name DELFIA™ or "Dissociation Enhanced Lanthanide Fluoroimmunoassay". Here, an europium ion is bound to an immunoreactive antibody through a chelating agent such as ethylenediamine tetra-acetic acid (EDTA). After the immunoreactions are completed and the free and bound reactants are separated, the europium ions are released from the chelate by dissociation at low pH. An enhancement solution is added containing a diketone such as naphthoyl trifluoroaceto-acetonate (NFTA), a detergent and trioctylphosphine oxide to exclude the quenching effect of water from europium's coordination sphere. The

solution is then excited using a pulsed xenon flash lamp and the emitted light intensity is measured after a 100 μ s delay.²⁹

1.6.4 Chemiluminescent Labels

Chemiluminescence is the chemical generation of electronically excited states and subsequent light emission. The use of the enzymatic-catalyzed oxidation of chemiluminescent substrates has also become widespread in clinical laboratory analysis. In the case of the enhanced chemiluminescence reaction (ECL), certain phenol derivatives enhance the light emission from the horseradish peroxidase-catalyzed oxidation of luminol, a cyclic diacyl hydrazide. The light emission decays slowly (several minutes) and its intensity may be 1000-fold greater than that of the unenhanced reaction. This system allows for the detection of HRP labeled antigen or antibody and has been incorporated into immunoassays using beads, microtiter plates and gel blotting techniques.³⁰ A luminometer (a light-measuring device) is used to quantify the light intensity of the reaction in microtiter plate format while instant photographic film or digital imaging is used to provide quantifiable results for gel blots. Other chemiluminescent substrates include the enzyme-catalyzed oxidation of dioxetane and acridinium ester compounds triggered by alkaline peroxides.²³

Chemiluminescent (CL) signaling schemes offer the potential to reach extremely low detection thresholds.³¹ Table 1.2 illustrates that the CL assays for the detection of thyroid stimulating hormone (TSH) are able to detect the lowest concentrations, 10⁻¹⁴ M, compared to the enzymatic colorimetric, enzymatic fluorescent and time-resolved fluorescent signaling strategies. The reasons for this are: 1) No excitation light source is used, so the problems associated with excitation are alleviated such as fluctuation of light intensity and stray light contamination; 2) There is no need for filters or wavelength selection, so the full photon flux from the sample is detected; 3) The blue CL emissions are maximal from 420-450 nm. This range is optimal for many photomultiplier tubes in terms of high quantum efficiency and low dark current.³²

Table 1.2 lists various signaling strategies with their associated lowest detectable concentrations in a collection of studies detecting thyroid-stimulating hormone (TSH).³³

Table 1.2: Comparison of the lowest detectable concentration of different heterogeneous immunoassay formats.³³

Method of Assay	Analyte	Lowest detected Concentration, Molarity
1. CL (dioxetane) ¹	TSH	3.5×10^{-14}
2. CL (acridinium) ²	TSH	5.0×10^{-14}
3. TRF (DELPHIA TM)	TSH	1.0×10^{-13}
4. CL (acridinium) ³	TSH	1.4×10^{-13}
5. CL (enhanced luminol)	TSH	3.0×10^{-13}
6. ELISA (fluorescence) ⁴	TSH	2.5×10^{-13}
7. ELISA (absorbance) ⁵	TSH	2.5×10^{-13}

¹ Using alkaline phosphatase-catalyzed dioxetalle from commercial kit.

² Using coated tubes.

³ Using magnetizable microparticle separation.

⁴ Abbott Laboratories label claim.

⁵ Using HRP label and OPD substrate.

1.6.5 Miscellaneous Labels

1.6.5.1 Bioluminescent Fusion Conjugates

Components of bioluminescent reactions, such as firefly luciferases and bacterial phosphatases, are attractive as immunoassay labels because of the efficiency of bioluminescent reactions. However, the preparation of conjugates of firefly luciferase and other enzymes has been problematic because these enzymes are easily deactivated by the chemical reactions used to prepare conjugates with antigens and antibodies. To remedy this problem, many of the genes for bioluminescent proteins have been cloned and as a result the splicing of these genes with the genes for other proteins (i.e. protein A, IgG heavy chain) has provided a route to a reproducible supply of active fusion conjugates that retain the biological activity of the bioluminescent protein and the

specific binding properties of the protein.³⁴ Table 1.3 lists a few examples of fusion conjugates and other novel labels that have been used in immunoassays.

Table 1.3: Examples of labels and fusion conjugates used for immunoassays.²³

<u>Type</u>	<u>Examples</u>
Fusion Conjugates	firefly luciferase-protein A, aequorin-IgG heavy chain, bacterial alkaline phosphatase-IgG Fc binding protein
Metal and Metalloid	gold, silver, selenium
Microparticle	latex, erythrocytes, liposomes
Phosphor	europium-activated yttrium oxysulfide
Photoprotein	aequorin
Quantum dots	zinc sulfide-coated CdSe microparticle
Redox complex	ferrocene
Virus	Bacteriophage T4

1.6.5.2 Microparticle Labels

Another label commonly used in immunoassay involves the use of latex microparticles. Latex particles are widely used as the solid-phase in latex agglutination assays³⁵⁻³⁸ and they are also commonly used as the indicator in immunochromatographic assays (ICA) as is present in over-the-counter home pregnancy tests.^{39,40} This method uses an absorbent material (i.e. nitrocellulose membrane) to mobilize or wick the sample across zones of pre-adsorbed reagents. These tests commonly test for high levels of human chorionic gonadotropin (HCG). Figure 1.10a shows how the reagents are pre-absorbed onto such a dipstick-like device. The device has a number of active and inactive zones through which the lateral flow assay is completed. The first zone has colored latex particles sensitized with antibodies to HCG. These particles are free to move along the membrane via capillary action created by the user's urine sample. The second zone has immobilized antibody to HCG. As shown in Figure 1.10b, once the sample is introduced, HCG in the urine sample attaches to the latex-bound HCG antibodies and moves by capillary action to the second test zone where it forms a

‘sandwich’ of antibody thereby producing a colored line. The sandwich complex does not form if HCG is not present making this a simple and effective procedure for following hormone levels in the course of home pregnancy tests.

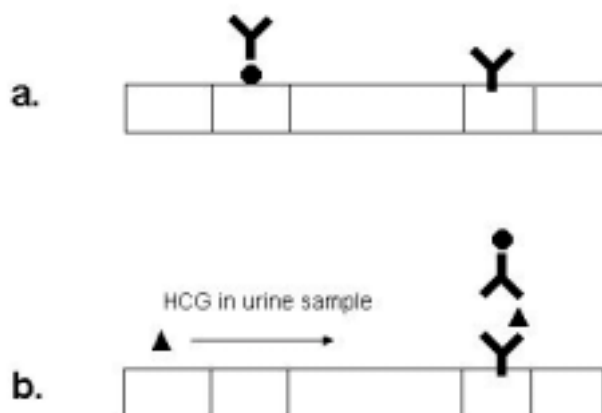


Figure 1.10: a) Schematic of dipstick-type home pregnancy test showing the HCG antibodies bound to colored latex particles are at the base of the strip and a band of HCG antibodies is at a point further along the strip. b) HCG in the urine sample attaches to the latex-bound HCG antibodies and moves by capillary action to the HCG antibodies bound to the strip (second zone) producing a colored line.

1.7 IMMUNOASSAY ANALYTICAL CONCEPTS

1.7.1 Analytical Terms Pertinent to Immunoassays

This section will address many of the essential concepts related to the analysis of biomolecules and will focus mainly on those issues pertaining to solid-phase immunoassays. First, non-specific binding (NSB) is defined as the binding of immunoreactants or labeled conjugate by nonimmune-specific means such as unanticipated electrostatic effects or antibody cross-reactions. These effects become more pronounced when excessively high concentrations of reactants are used. Blocking is a process that uses high concentrations of an irrelevant protein or detergent to minimize

these nonspecific interactions. Blocking steps are essential for high quality solid-phase immunoassays.

Many definitions concerning an analytical technique's ability to distinguish low concentrations of analyte are used and have become intermingled throughout some branches of science. In this writing, the sensitivity of an analytical detection technique is defined by the slope of the dose-response curve. Thus, a highly sensitive method, by this definition, has a higher signal-to-noise ratio (S/N) and is capable of detecting small changes in analyte concentration. The detection threshold is the *minimal detectable difference* in concentration. Finally, the limit of detection (LOD) is the smallest response that can be deciphered with reasonable probability that a particular analyte is present. The LOD is a quantity that reflects the precision of the zero concentration and, as shown in Equation 1.9, is expressed as the mean of the blank readings plus some factor, k , multiplied by the standard deviation of the blank readings. The k factor is chosen according to the confidence level desired.⁴¹

$$\text{LOD} = \text{mean}_{\text{blank}} + k(\text{st.dev.})_{\text{blank}} \quad \text{Eq. 1.9}$$

As a side note, the limit of detection can be estimated for sandwich-type immunoassays by the following relationship:

$$\text{Minimum [Analyte]} = K_3 CV_{\text{nsb}} / K_2 \quad \text{Eq. 1.10}$$

where K_3 is the fractional non-specific binding (expressed as a percent), CV_{nsb} is the error in signal response at zero analyte concentration and K_2 is the detecting antibody equilibrium constant. For example, given an antibody affinity of $1 \times 10^9 \text{ M}^{-1}$, non-specific binding of 0.1% and an error in the signal response of 1%, an estimate of the lowest analyte concentration detectable is of the order of $1 \times 10^{-14} \text{ M}$.⁶

Diagnostic sensitivity and specificity, on the other hand, are terms used to assess the accuracy of a medical diagnostic test. The diagnostic sensitivity is the proportion of individuals with the disease who test positively with the test. It is expressed as a percentage as follows:

$$\text{Sensitivity (\%)} = \frac{100 \times \text{the \# of diseased individuals with a positive test}}{\text{total \# of diseased individuals tested}} \quad \text{Eq. 1.11}$$

The diagnostic specificity of a test is the proportion of individuals without the disease who test negatively for the disease. It is expressed as follows:

$$\text{Specificity (\%)} = \frac{100 \times \text{the \# of individuals without the disease with a negative test}}{\text{total \# of individuals tested without the disease}} \quad \text{Eq. 1.12}$$

Ideally, the diagnostic sensitivity and specificity should each be 100%. The sensitivity and specificity of a diagnostic test depend on the distribution of test results for the diseased and not-diseased individuals and also on the value of the test that defines the abnormal levels, the cutoff value.

The precision of an immunoassay is important because it enables an assessment to be made of the probability that a given concentration differs from a specified value. It also describes the repeatability of the test. An immunoassay's repeatability is usually measured as its imprecision and often expressed as the percent coefficient of variation (%CV) at a particular analyte level as shown below:

$$\%CV = \frac{100 \times \text{standard deviation of replicate test values}}{\text{mean of replicate test values}} \quad \text{Eq. 1.13}$$

The within-run precision is defined as the precision of the same sample run on several occasions within the same assay. This is also known as intra-assay variation. The

between-run precision is a measure of the assay to reproduce the same result on the same sample from run to run and from day to day. It is also known as the inter-assay variation. The between-lot precision is an estimate of the variability of results using a variety of different lots (batches) of reagents.

1.7.2 Assay Optimization

The development of an immunoassay culminates with the assay's ability to accurately quantify or identify the presence of a specified analyte. In doing so, samples of known analyte concentration are tested according to an optimized procedure and a calibration curve (or dose-response curve) is usually plotted of the signal response as a function of the analyte concentration. The concentration of analyte in the unknown sample may then be interpolated from the calibration curve. An assay's performance can be gauged on its ability to accurately detect: 1) low concentrations of analyte, 2) a wide range of analyte concentrations based on the linearity of the calibration curve or 3) high concentrations of analyte without the calibration curve becoming saturated. However, the wide variety of assay designs dictates that optimal assay conditions and reagent concentrations must be experimentally determined to provide the desired analytical information. This aspect of immunoassay development is termed here as assay optimization and should accommodate several variables. For example, the following factors should be considered when optimizing a typical solid-phase sandwich immunoassay:

- the solid-phase capture antibody concentration
- the blocking concentration and incubation times
- the sample volume and incubation time
- the detecting antibody concentration
- the agitation speed (or flow rate) of reagent delivery
- the signal generation scheme

If a sandwich assay were optimized for its lowest detection threshold, the Law of Mass Action dictates that if high concentrations of both capture and labeled antibody are used, the antigen-antibody binding reaction will be pushed to the right and a high proportion of antigen will be bound leading to lower detection thresholds. Increasing the amount of detecting antibody, however, also increases the amount of its non-specific binding (and its associated error). Eventually a point is reached where the level of non-specific binding increases faster than the rate of specific binding and the S/N begins to drop. Thus, a balance must be found in the optimization procedure so that the highest signal is attained with the lowest level of non-specific binding. Furthermore, the major determining factors of detection threshold are the level and imprecision of the non-specific binding and error in measurement of the signal and not necessarily the antibody's equilibrium constant. Thus, an assay with a low detection threshold will 1) be optimized with high concentrations of antibody in relation to the antigen, 2) have low non-specific binding of the detecting antibody, and 3) have a signal generator with high activity.

Strobel has summarized the pertinent methods used to optimize a scientific technique.⁴² For example, an immunoassay could be optimized for the highest S/N using a sequential technique. This method is designed to permit one to start with a few initial experiments and vary the conditions for later experiments as suggested by the response obtained. In this case, the results are monitored as one factor is tested (i.e. vary the detecting antibody concentration as high, med, and low) until an optimal S/N is reached. This set of conditions is then used to test the next experimental factor, and so on. These sequentially optimized factors would ideally be even further optimized by continually testing each factor as in a bootstrap method.

Another optimization technique is that of a simultaneous random design method such as that provided by "Experimental Design" methods. This approach provides experimental designs that economically reveal the manner in which experimental factors influence a measurement. In this case, pertinent experimental factors (i.e. a 3 factor experiment testing antigen incubation time, antigen delivery rate, detecting antibody concentration) are input into the routine. The algorithm generates a model of random

experiments the investigator will perform that encompass the full range of applicable experimental conditions for each of the experimental factors (i.e. high, med, low values of the 3 factors). After the experiments are performed, the investigator inputs the results of the experiments back into the routine and the algorithm generates a report revealing the effect of the factors on the measurement. The algorithm also proposes the optimized experimental conditions that lead to the desired effect (i.e. highest S/N). A benefit of this approach is that a complex optimization procedure can be simplified to a fewer number of experiments. However, arguments could be made concerning the reliability of any “black-box” approach. Convenient commercial software programs are available for the completion of such multi-variable optimization tasks.⁴³

1.7.3 Data Plotting and Curve-Fitting Techniques

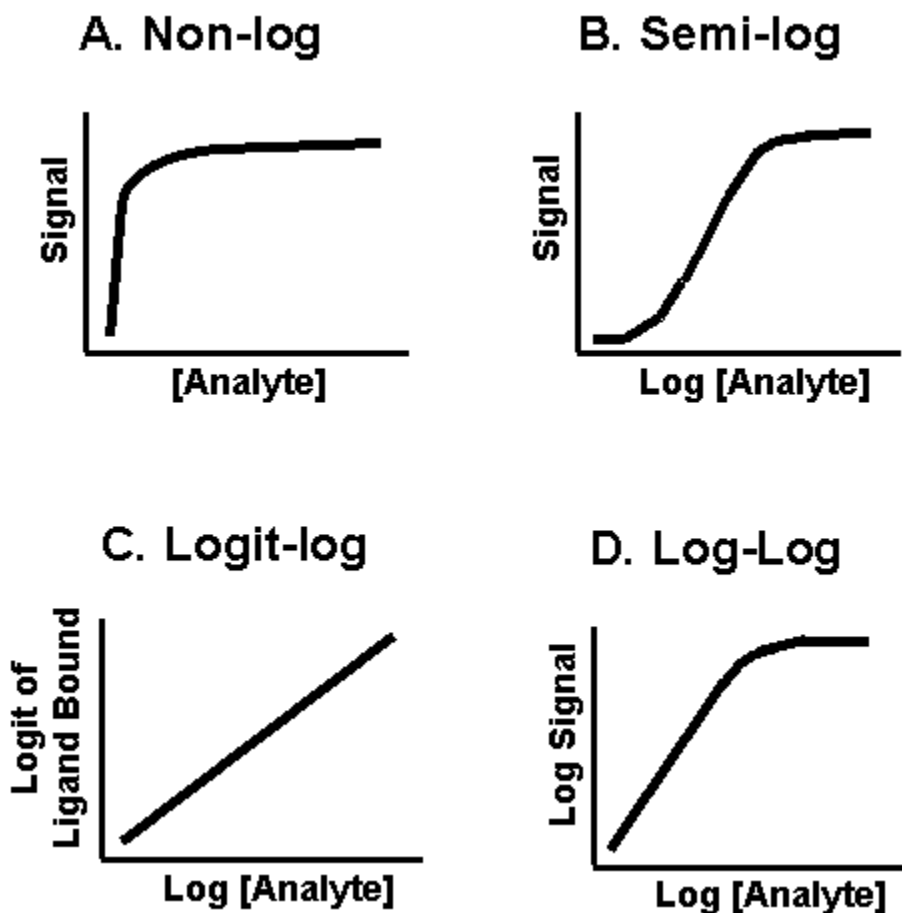


Figure 1.11: Plots of simulated dose-response data presented in the following formats: A) non-log, B) semi-log, C) logit-log and D) log-log.

Once the assay procedures have been optimized, it becomes important to measure experimentally the dose dependence of the assay signals. Figure 1.11 illustrates various techniques of plotting solid-phase immunoassay dose response data. Figure 1.11A shows a non-log or linear plot of a simulated immunoassay dose-response where both axes are linear. Here the data appears to be compressed at the low analyte region where the signal is found to plateau at low concentrations. As a result, these plots are rarely used for calibration curves.

The semi-log plot shown Figure 1.11B only partially overcomes the problems of the linear plot. Here, the y-axis is plotted linearly as the amount of ligand bound (i.e. the final absorbance value) and the x-axis is the log of the analyte concentration. Solid-phase immunoassays are usually performed using serial dilutions of the analyte; thus the dilutions are logarithmic. The data plotted in this format yields the S-shaped sigmoidal curve. A linear regression analysis (such the least-squares) fits only the pseudolinear region around the inflection point. This plotting method greatly restricts the usable range of the standard curve. On the other hand, a polynomial equation (i.e., the third degree polynomial $S = ax^3 + bx^2 + cx + d$, where a, b, c, and d are constants) may be fitted to the sigmoid.

On the other hand, more useful is the logit-log plot illustrated in Figure 1.11C. The logit transformation is a mathematical conversion that transforms the S-shaped curve of the typical semi-log plot into a straight line. In non-competitive assays, the logarithm of the concentration is plotted against the logit of the amount of bound ligand (L_b), where the amount of bound ligand can be expressed as the signal (i.e. final absorbance). Here, the logit function is the $\log L_b / (L_m - L_b)$ where the L_m is the amount of ligand bound at saturation. The magnitude of the transformation is thus proportional to the value of L_b . Logit-log plots require an accurate estimate of L_m ; overestimates will not completely straighten the curve while underestimates will result in an upward-curving line.

Finally, the log-log plot in Figure 1.11D has the advantage of having a linear region at concentrations where the capture antibody is not saturated with analyte. The complexity of curve fitting is greatly reduced if this plot is used and if the analysis is restricted to non-saturated regions. Such data is more reliable and can be readily fitted by a least-squares analysis.⁴⁴

1.8 CURRENT IMMUNOLOGICAL METHODS FOR THE DIAGNOSIS OF VIRAL INFECTIOUS DISEASES

Immunology and immunological-based methods have in the past and will continue to play key roles in the understanding and diagnosis of infectious diseases.⁴⁵ Progress in the study of the immunological mechanisms involved in infection resistance and the immune responses elicited by viral infections and vaccines has been instrumental for the prevention, treatment and monitoring of infections and for the design and implementation of vaccines. For example, immunological methods using monoclonal antibodies are convenient for deciphering the antigenic mosaic of pathogens and for mapping epitopes on molecules from them and thus guiding vaccine design and preparation.¹⁸ In order to emphasize the widespread use and impact of immunological methods, the sections below present current practices for the clinical diagnosis of infectious diseases. However, since a comprehensive description of the broad variation of viral, bacterial, fungal, and parasitic pathogens and the multitude of available techniques used to identify them would be beyond the scope of this writing, only the most common techniques will be emphasized for the clinical diagnosis of viral pathogens.

The human immunological and biological events associated with a viral infection are illustrated in Figure 1.12 where the serologic time course is illustrated of an individual infected with Hepatitis B virus (HBV).

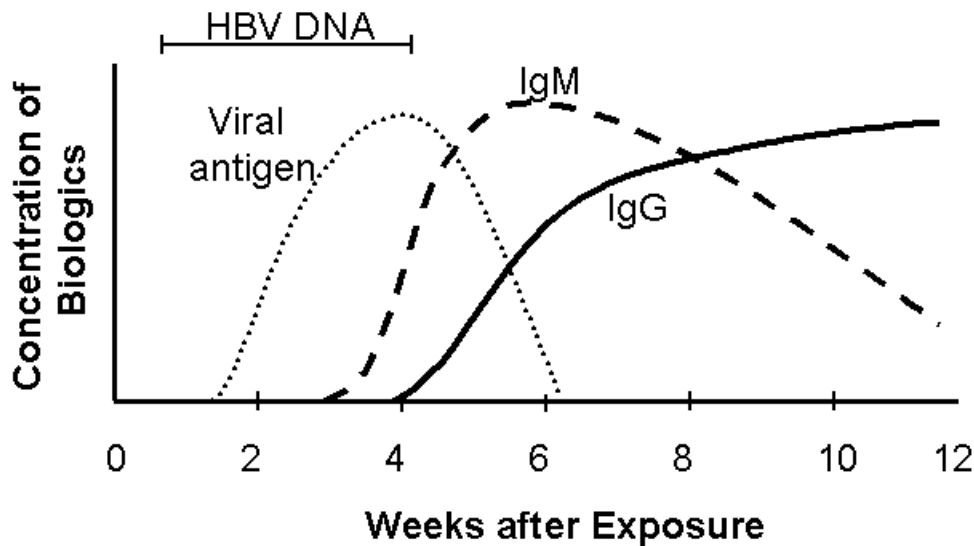


Figure 1.12: Typical human serologic time-course of Hepatitis B virus (HBV) infection. Virus is detectable in blood ~2 weeks after infection. IgM antibody concentration becomes detectable ~3 weeks and peaks at ~6 weeks then drops. IgG antibody concentration becomes detectable ~4 weeks into the time course and increases throughout. DNA detection methods decrease the time necessary for diagnosis of virus.

The incubation period for an HBV infection ranges from the time of infection to 10-50 days afterwards. Using current detection strategies, the viral particle or viral antigen is not detectable until ~2 weeks after infection. However, current developments in DNA isolation and amplification techniques enable the identification of the virus about one week sooner than direct detection of the viral antigen.⁴⁶ The IgM antibody response is the first to become detectable about 3 weeks after exposure while the IgG antibody response can be detected anytime after ~4 weeks.

The methods used for viral diagnoses can be generally grouped according to the following strategies: (i) direct detection of viral antigens, nucleic acid, or particles in clinical specimens, (ii) biologic amplification of infectious virus in cell culture, followed by detection of viral antigens in cultured cells, and (iii) detection of the antibody response to viral infection, usually immunoglobulin M (IgM) or immunoglobulin G (IgG). The advantages and limitations of the most commonly used techniques are listed in Table 1.4.

Table 1.4: Advantages and limitations of common viral diagnostic methods.

Method	Applications	Time	Advantages	Limitations
Immunostaining	RSV, VZV, HSV, etc.	0.5-5h	Can detect single cell or multiple pathogens	Endpoints subjective
EIA (membrane)	RSV, rotavirus, Influenza A & B, etc.	0.5h	No major equipment; can test single or multiple samples	Expensive per-test reagent costs; NSB difficult to detect
EIA (microtiter plates)	Hepatitis, HIV, Adenovirus, RSV, etc.	2-4h (after overnight plate incubation)	Objective endpoints, automated format possible	Sensitivities varies with virus and kit used, controls needed
Latex Agglutination	Rotavirus, etc.	0.5h	Simple, quick, suitable for subjective & single sample testing	Difficult to read; not as sensitive as EIA
Nucleic acid hybridization	EBV, CMV, Adenovirus, etc.	4h-2days	DNA more stable than antigens; methods with chemiluminescence highly sensitive	Expertise in molecular and electrophoretic methods required; time consuming
PCR amplification	HIV-1 RNA, etc.	6h-2days	Very sensitive; potentially quantitative; high-quality standardized kits available	Cross contamination potentially a problem; QC essential
Cell Culture	HSV, VZV, CMV, etc.	16-48h	Sensitive due to amplification	Time and reagent consuming; tissue facilities required
Immune Response	EBV, Hepatitis, rubella, measles, parvo- and arboviruses, etc.	2-4h (after overnight plate incubation)	Valuable when culture or antigen methods not available	Delay in antibody response;

Table 1.4 List of acronyms: HSV=herpes simplex virus; VZV=varicella zoster virus; CMV=cytomegalovirus; EBV=Epstein Barr virus; RSV=respiratory syncytial virus; HBV=hepatitis B virus; EIA=enzyme immunoassay; NSB=nonspecific binding. Note: the applicable diseases tested is not limited to those stated above.

Inspection of Table 1.12 suggests there are a wide variety of techniques for the clinical diagnosis of viral diseases. However, as a case in point, the CDC suggests that the solid-phase based enzyme immunoassay (EIA) is the most widely used screening test for detecting antibody to HIV-1.⁴⁷ To narrow the “window of detection”, the Food and Drug Administration approved the first HIV-1 antigen screening test based on EIA in 1996 for use at blood donor facilities. These assays represent the generation of simple/ rapid test devices (S/RTDs)⁴⁸ that have been developed to meet the demand for rapid small-scale or point-of-care testing devices. Here, the development of simple and inexpensive immunological tests that deliver quick and accurate results without the use of complicated instrumentation or time-consuming techniques (cell culture, PCR, etc.) has become important for point-of-care treatment. Furthermore, the less complex immunological methods of the EIAs are essential for use in resource poor settings that lack sophisticated clinical diagnostic and laboratory networks.

In many hospital laboratories and blood donor facilities, the normal practice to screen for infectious diseases is to test specimens by automated EIA.⁴⁹ If a positive reaction is detected, the sample is then retested with a supplemental and more specific test that serves as a gold standard method. To date, the most common confirmatory test is the Western Blot. For example, an antibody screening test would be confirmed by the Western Blot as follows: individual proteins of the viral lysate are separated according to size on a gel membrane (usually agarose) using polyacrylamide gel electrophoresis (PAGE).⁵⁰ The viral proteins are then transferred onto nitrocellulose paper by capillary action and reacted with the patient’s serum. Any virus-specific antibody present in the patient’s serum is detected by a labeled anti-human IgG antibody (an antibody raised against human IgG) and will produce a colored band. Positive and negative serum specimens are run simultaneously to allow identification of viral proteins.

Automated immunoassay systems continue to be an innovative and dynamic area of research for the clinical diagnostics industry. Pressures to decrease sample analysis times, increase sample throughput, and expand the number of analytes tested are the challenges faced

by the clinical laboratory. A review by Sokoll et.al. describes many of the current automated immunoassay systems.⁵¹ Here, a typical system has the capability to analyze up to 120 samples per hour (sometimes more) using either homogenous or heterogeneous assay formats. Numerous approaches have been taken as the separation mechanism in heterogeneous assays with a common approach being magnetic particles, or antigen- or antibody-coated beads, tubes or wells. Detection schemes most often use chemiluminescence, enzyme-mediated colorimetric or fluorescence signaling agents, or particle-enhanced turbidometric⁵² or nephelometric^{53,54} techniques (measures forward light attenuation or light scattering based on the aggregation of sensitized particles, respectively). A typical system consists of a sample handler where barcoded samples are loaded onto a carousel. Controls and reagents are often stored in an on-board refrigerated compartment. Specimens, reagents, calibrators and controls are then transported individually to the appropriate modules using robotics. Many systems can analyze up to 80 different biomarkers including thyroid, fertility, cardiac and tumor markers, therapeutic drugs, drugs of abuse, toxicology, allergy, infectious diseases, bone metabolism, cytokines and other special proteins.

Clearly, assay automation has made significant progress for the advancement of clinical analyses and disease diagnostics and has become irreplaceable for routine analyses. However, these modern automated systems are typically limited to the traditional “single-analyte per test”. Likewise, large sample volumes and high amounts of reagents are required to test for multiple biomarkers. To fill this void, other technologies capable of “multiple-analyses per sample” must be developed to provide even more efficient, systematic and timely testing.

1.9 PROMINENT MULTI-ANALYTE DETECTION METHODS

Another approach, which has the capability to revolutionize bio-analytical techniques and medical diagnostics, is the parallel analysis of multiple targets per sample run (termed here as multiplexing). By using an array of differential sensors, with each sensor being highly selective for a targeted analyte, it is possible to maximize the analytical output of an assay to encompass the measurement of a variety of different analytes. Compared to a sequential “single analysis per test” approach, the key advantages of multiplexing is that (1) sample and reagent volumes are reduced, (2) analysis times are reduced with a concurrent reduction of manpower and cost, and (3) assay protocols are simplified, (4) the complete investigation of the biological (and/or chemical) content of a complex multi-component fluid can potentially be performed in a single run. Furthermore, by sufficiently expanding the sensor diversity in the array, the detection of analytes that were previously unexpected is possible.

Generally, multianalyte methods employ either multiple labels or spatial resolution to discriminate between different analyte specificities. The former approach uses various labels such as fluorophores, enzymes, metal ions, or isotopes. Another approach is the development of spatially resolved sensor arrays in which the location of each sensor identifies its specificity. Such sensor arrays are typically manufactured using high precision ink-jet printers, robotic deposition, or photodeposition techniques.⁵⁵

1.9.1 Planar Microspotted Arrays for DNA/RNA Analysis

Much of the initial development of multiplexed bioassays has been in the genomics arena where miniaturized arrays of nucleic acid probes are microspotted with extremely high spatial density onto filter membranes or glass microscope slides (for a review see Young, 2000).⁵⁶ These DNA microarrays allow complex mixtures of RNA and cellular DNA (cDNA) to be interrogated in a parallel and quantitative fashion and are currently used in profiling levels of gene expression (messenger RNA abundance)⁵⁷, sequencing human mitochondrial DNA,⁵⁸ identifying appropriate target molecules in drug discovery and therapeutic intervention⁵⁹; and diagnosing infectious diseases⁶⁰ and cancer.⁶¹ Here, the arrays are generally produced in one of two ways: by robotic or ink-jet deposition of nucleic acids (PCR products, plasmids,

oligonucleotides) directly onto a chemically activated glass slide⁵⁵ or the *in situ* synthesis of oligonucleotides on the glass surface using photolithographic techniques (such as the Genechip® technology by Affymetrix; Santa Clara, CA). Currently, arrays with > 250,000 different nucleotide probes or >10,000 different cDNAs per square centimeter can now be produced in significant numbers. The most common detection scheme uses fluorescent labeled probes with laser scanning, but ellipsometric and interferometric techniques have also been reported.⁶²

To provide an example of the detecting capabilities of the microspot array approach, Cheung et. al. fabricated a microspotting apparatus and sample scanning device for use in an academic setting and reports their combination of lasers (10mW; green and red channels) and photomultiplier tubes can detect as few as 10^5 target molecule in a 100 μm spot with a dynamic range of 3 orders of magnitude. In addition, the apparatus required ~40 minutes to raster scan an average sized array (26 \times 19 mm) for each color channel.

As a case study, Affymetrix Inc. (Santa Clara, CA) offers genome arrays that contain >24,000 gene sequences per array (18 μm spot diameter). The introduction of sample and reagent solutions occurs in an automated fluidics unit where the glass slide is enclosed in a plastic cartridge and sample is introduced using a peristaltic pump. The cartridge is removed from the fluidics unit and hybridization occurs as the slide cartridge is rotated in a heated carousel for a minimum of 16 hours. The slides are then visualized using laser-induced fluorescence.⁶³ This system allows access to genetic information as polymorphisms in DNA or RNA are compared to standards. These methods can be used to address a variety of questions in molecular genetics including gene expression, genetic linkage, and genetic variability.⁵⁸ Similar methods are now being developed for protein microarrays.⁶⁴⁻⁶⁸

1.9.2 Planar Microspotted Arrays for Protein Analysis

While the vast majority (up to 95%) of microarray-based research utilizes nucleic acids for analyte recognition, descriptions of protein-, peptide-, or small molecule-based arrays are increasing (for a review see MacBeath, 2002).⁶⁹ These latter arrays have been used for such diverse applications as antibody screening,^{64,70} protein-ligand or protein-protein interactions,^{65,68}

and diagnostics/proteomics.⁶⁶ These techniques use the selectivity of antibody (or ligand/receptor) binding in typical sandwich or antibody capture assay formats using filter membranes or glass surfaces as the solid support. For example, a glass microtiter plate-based multiplexed ELISA was reported that uses a precipitating enzyme-linked fluorescent detection scheme (Genometrix; The Woodlands, TX). Here, the deposition of arrayed capture antibodies was demonstrated using a robotic capillary print head that deposits four identical 36-element arrays in each well of a customized 96-well glass microscope plate. Each well of the plate can then be tested in four-fold replicate against a different antigen. Accordingly, up to 3,456 immunoassays could be performed simultaneously using standard microplate ELISA incubation and washing procedures and CCD camera fluorescent imaging techniques.⁶⁷

Another microspotting technique reported by Francis Ligler et. al. exploits the internal reflective properties of glass slides for use in multiplexed analyses. This sensor technology utilizes evanescent wave excitation to interrogate patterns of fluorescent immunoassays immobilized to the surface of glass slides. In brief, columns of capture antibodies are directed and immobilized onto a chemically derivatized glass by the use of a removable siloxane flow cell. After immobilization, another flow cell (oriented perpendicular to the columns) delivers the sample and appropriate immunoreagents across the columns of immobilized capture antibodies. Laser light (635 nm) is then directed into the end of a glass slide resulting in the evanescent excitation of the surface-bound fluorophores of the completed fluorescent immunoassay. Finally, optical lenses direct the spatial image of the fluorescent sensing region onto a cooled charge-coupled device (CCD) where the signals from the digitized image are analyzed based on fluorescent intensity. This technique has successively demonstrated the simultaneous identification of biologically dangerous agents such as Staphylococcal enterotoxin B (SEB), ricin and cholera toxin^{71,72} while a variety of immunoassay formats (direct, competitive, displacement, and sandwich) was shown to be effective using this approach.⁷³ Moreover, this technology has been incorporated into a portable and rugged apparatus the size of a tackle-box for use in biological warfare detection operations.⁷⁴ Clinical fluids such as whole blood, plasma, urine, saliva and nasal secretions can be tested in 10 min assays with detection limits in 1-10 ng/mL range.⁷⁵

1.9.3 Multiplexed Analyses Using Polymeric Gel Pads

As opposed to the planar arrays on glass slides, different antibodies and antigens, enzymes or nucleic acids can be immobilized within the three-dimensional regions of polyacrylamide gel pads^{76,77}. Using this technique, arrays of up to 4200 of 5% polyacrylamide gel pads ($100 \times 100 \times 20 \mu\text{m}$ spaced by $200 \mu\text{m}$) are prepared on a glass slide by photopolymerization and proteins or oligonucleotides are subsequently transferred onto the pads via manual handling or robotic processes. The immobilization of the receptor occurs by reductive coupling of their amino groups with aldehyde groups of the gel. Immuno-, enzymatic and nucleic acid hybridization assays are then performed with the aid of electrophoresis and detected using common fluorescence detection techniques.

The gel pads in the array are separated from each other by the hydrophobic surface of the glass. Therefore, the gel pad arrays can be used as a large number of individual mini-tubes to carry out specific biological and chemical interactions. In addition, three-dimensional immobilization in the gel pads provides a higher receptor binding capacity and a more homogenous environment than the heterophase immobilization on glass or filters. Arenkov et. al. claim “This prevents the aggregation of immobilized proteins or their interphase-induced denaturation on a solid surface.” Finally, the three-dimensionality of the pads serves to provide a thicker layer for specific interactions to occur that can potentially lead to higher signal intensities.⁷⁸

Perkin ElmerTM has taken advantage of the benefits derived from three-dimensional matrices and developed a HydrogelTM coated slide for microarray analyses.⁷⁹ Here, slides are coated with a $12 \times 40 \times 0.02 \text{ mm}$ “lawn” of acrylamide film to be used with any microspotting equipment. The manufacturer claims the film has been optimized to maintain protein activity for a variety of assays including protein-protein interaction studies, protein profiling, antibody screening, and sandwich assays. The film has a high protein binding capacity, low intrinsic fluorescence and low non-specific binding yielding signal to noise ratios ranging from ~8 to 16. Receptor proteins in the range of 60-160 kDa were found to occupy binding sites from the surface of the substrate to a depth of 20 –50% or $4\text{--}10 \mu\text{m}$ and target molecules were shown to

penetrate to a depth as great as the receptor depth. Finally, in a model study using microspotted IgG and an anti-IgG probe, the intra-assay variation was ~10% and the inter-assay variation was ~15%.

1.9.4 Multiplexed Analyses Using Polymeric Microspheres

Polymer microspheres (or beads) have historically been utilized¹⁹ as the solid-phase in turbidimetric/nephelometric immunoassays⁵²⁻⁵⁴ and in latex agglutination tests (LATs) for the rapid clinical analysis of serum-based proteins and infectious disease diagnostics (for a review see Bangs, 1996).¹⁹ For example, many commercial LATs are available for diseases such as infectious mononucleosis³⁵, Methicillin-resistant *Staphylococcus aureus* (MRSA)³⁶, *Escherichia coli* verocytotoxins or (Shiga toxins)³⁷, and rotavirus.³⁸ These optimized assays offer excellent assay characteristics with diagnostic sensitivities and specificities approaching 100% and are often easy and fast to perform. However, the detection thresholds are generally not as low as other more quantitative techniques⁸⁰ and the LATs cannot be utilized for multiple analyte detection schemes as the nature of the response intrinsically depends on a cooperative effect of the entire collection of microspheres.

Multiplexed concepts using microspheres as the solid-phase in immunoassays⁸¹⁻⁸⁴ have been successfully demonstrated using a variety of techniques. For example, David Walt and coworkers have developed a fiber optic bead-based sensor array. This technique uses a high-density fiber optic bundle (500 μm) that contains ~6000 individually addressable 3-6 μm etched wells capable of housing functionalized microspheres. Sensor arrays are then created by randomly distributing a mixture of functionalized microspheres in the wells on the fiber tip using a drying deposition process. The different microsensors in the array are identified by an optical encoding method in which unique combinations of fluorescent dyes are attached to each type of microsphere. Applications of these methods have been reported for the multiplexed analyses of soluble odor compounds⁸⁵, cellular response of live cells⁸⁶, haptens and proteins⁸⁷, and DNA oligomers.⁸⁸

Perhaps the most commercially successful microsphere-based multiplexing methods available to date are those that use flow cytometry for analyte interrogation such as the methods developed for the FlowMetrix™ system (Luminex; Austin, TX). The flow cytometer simultaneously analyzes individual polystyrene microspheres (~5 µm diameter) by size and fluorescence intensity distinguishing three fluorescent colors -green (530 nm), orange (585 nm), and red (>650 nm). Microsphere size is determined by 90° light scatter, and is used to eliminate microsphere aggregates from the analysis. A fluorescent barcoding system is utilized by varying the concentration of orange and red fluorophores conjugated to the spheres and thus orange and red fluorescent signals are used to classify sets of analyte specific microsphere populations. At the same time, the green fluorescent channel is monitored for the quantitative measurement of the analyte. Luminex has developed at least 64 distinct sets of microspheres for the analysis of human cytokines, allergen-specific antibodies and DNA sequence analysis.⁸⁹⁻⁹¹ Further, customized immunofluorescent assays have been developed for infectious disease diagnostics.⁹²

1.10 MICRO-TOTAL ANALYSIS SYSTEMS (µ-TAS)

Another strategy important to chemical and biological analysis is the micro-total analysis system (µ-TAS), also called “lab-on-a-chip”. Research and development in this area has grown very rapidly since the last decade (for reviews, see Reyes,2002 and Auroux, 2002).^{93,94} In general, the µ-TAS concept integrates all the steps required of a chemical analysis, such as sample injection and mixing, reaction of sample (separation, binding events, etc.) and detection, within the same miniaturized device. Applications of such total analysis devices includes electrically driven separation techniques such as capillary electrophoresis^{95,96}, capillary gel electrophoresis^{97,98}, DNA analysis devices^{99,100}; and bead-in-channel analyte detection strategies.^{81,101-103} In parallel, systems that perform chemical reactions within the device were developed and include arrays for solid-phase chemistry¹⁰⁴, methods to perform polymerase chain reactions within the device (PCRs)¹⁰⁵, and manifolds for homogeneous enzyme assays.¹⁰⁶

The methods predominantly used in μ -TAS device manufacturing were borrowed from the silicon microprocessor industry, and as a result, silicon wafers and glass⁹⁵ are the materials most often used for device construction. However, polymeric materials such as plastics¹⁰⁷ and elastomers such as poly-dimethyl siloxane (PDMS) have also been successful when used for device construction.^{93,101} The silicon chip-based devices can be fabricated by conventional photolithographic techniques in single-crystalline silicon bulk material.¹⁰⁸⁻¹¹¹ These methods are used to create channels, capillaries reservoirs and other specialized structures within the device to permit the continuous flow of reagents for sample reaction and analysis. Otherwise, many new approaches in the fabrication of microfluidic systems have been developed.⁹³ For example, a fabrication method called buried channel technology, in which channels, cavities, and connection holes in the bulk of a silicon wafer were constructed by several steps of trench etching and sidewall coating.¹¹² Further, by depositing a thin layer of silicon nitride on a silicon wafer, then anodically bonding it to a glass substrate, and subsequently removing the silicon, a transparent 390-nm free-standing silicon nitride microchannel was fabricated by Schasfoort et. al.¹¹³

Miniaturized analysis systems depend on the precise control of fluids through the network of channels. One approach is to use pressure-driven flows delivered by off-chip pressure sources or micropumps.^{75,81,101,111} Another approach becoming rather common in electrophoretic separations and other microfluidic applications is electrokinetic flow, also known as electro-osmotic flow (EOF).^{95,113} As demonstrated by Manz et. al., micromachining technology was used to prepare capillaries on glass chips for the separation of amino acids that utilize electroosmotic pumping to drive fluid flow. With the manipulation of applied voltages, the directions of fluid flow within the glass manifold could be controlled.⁹⁵ This effect was investigated in depth by Schasfoort et. al. who reported, “The flow could also be controlled by manipulating the chemical composition of the buffer solution, thereby influencing the zeta potential, the potential difference across the mobile part of the electrical double layer of the channel wall.”

Here, the surface of the channel (such as silica), when filled with a solution of $\text{pH} > 3$, becomes negatively charged as a result of the dissociation of its surface silanol groups. When a voltage is applied across the fluid at the two ends of the channel, the positive ions of the double layer move under the influence of the longitudinal electric field, E , dragging the fluid with them through viscous coupling.⁹⁵

Figure 1.13 is a schematic of the enzyme analysis chip as reported by Hadd et. al. Electrokinetic flow is used to pump fluids and is controlled by regulating the applied potentials at the terminus of each channel of the microchip. Within the channel network, cross intersections and mixing tees are used for valving and dispensing fluids with high volumetric reproducibility (0.3% RSD). The mixing tee can also be used to mix two fluid streams in any ratio from 10-100% from either stream simply by varying the relative field strengths in the two channels. Electro-osmotic pumps offer a number of advantages over miniaturized pressure-driven pumps, such as ease of fabrication and absence of moving parts. Moreover, sample plugs suffer little from dispersion because the fluid velocity is nearly constant across the channel diameter.

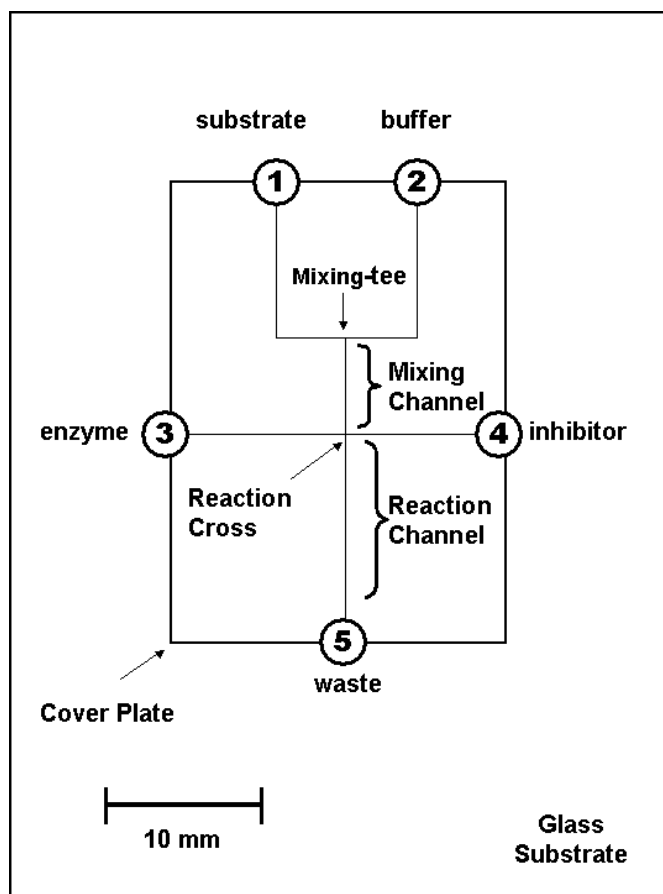


Figure 1.13: Schematic of the enzyme analysis chip demonstrated by Hadd et. al. This is an example of a micro-total analysis system (μ -TAS) that uses electrokinetic flow to mobilize fluid streams. Platinum electrodes are placed in the wells of each reservoir with a grounded electrode submersed in the buffer solution of the waste reservoir. As derived from Kirchoff's rules and Ohm's law, current through a channel approximates the electrokinetic transport of material and microfluidic control is realized by adjusting the applied potentials at each channel reservoir (up to 1000 V). Proportions of substrate and buffer are mobilized from their respective reservoirs and mixed in the mixing channel. The fluidic streams then meet with enzyme or inhibitor at the reaction cross and reaction products are measured by, in this case, monitoring the fluorescence of the hydrolysis product, resorufin, using laser-induced fluorescence.¹⁰⁶

Initially, the micro concept was primarily implemented to enhance the analytical performance rather than to reduce the size of the device. However, it was recognized that chemical analyses on micro-fluidic devices can be highly automated with reduced analysis times and can reduce the consumption of reagents by several orders of magnitude.^{99,105,113} Other advantages arise as a result of the smaller size of the device.

For example, improved thermal diffusion gives rise to faster heating and cooling within the system. This effect becomes important in electrophoretic separations where higher voltage gradients may be used without extensive Joule heating of the system as the power is more efficiently dissipated within the microstructures. This characteristic provides the possibility of improved speed and separation efficiency when compared to conventional electrophoretic methods. Another feature derived from the smaller channel dimensions is that the microfluidic systems generally render laminar flow. As a result, band broadening and increased pressure from turbulent flow is avoided. Furthermore, laminar flow adds the possibility of faster separation speeds with less diffusional band broadening. Furthermore, the efficiency of electrophoretic and chromatographic separations, measured as the number of theoretical plates, is proportional to the length of the separation channel over the diameter of the channel. This means that reduction in size can be successfully facilitated without any loss in the number of theoretical plates. Finally, the chip-based systems allow for a number of valveless systems to be used for material transportation, such as the electrokinetic flow described above. Consequently, these systems are also readily parallelized, allowing multiple analyses on a single chip. This is a well-recognized attribute that provides the possibility to achieve the high sample throughput required for both genomics and proteomics.¹¹⁴

1.11 STATEMENT OF PURPOSE

The multitude of immunoassay techniques that are currently implemented for the clinical analysis of human biomarkers are constantly being driven to achieve better analytical results with combined efforts to reduce analysis times and sample/reagent volumes. For example, the microtiter plate-based ELISA is often used in clinical diagnostic settings as well as in scientific studies for a number of disciplines. These assays are used extensively due to their high diagnostic selectivity and sensitivity and have largely replaced earlier radioimmunoassay technologies. However, testing for antibody responses or presence of disease-specific antigens requires a separate assay for each analyte. Moreover, the dynamic range of the current ELISAs is limited so that repeated testing after additional dilutions is often required. These aspects are

not desirable for routine and repetitive testing since many manual liquid-handling procedures and wash steps are necessary evolving into a complicated and time-consuming process that uses a proportionate amount of reagents and manpower.

As a result, the development of multiplexed approaches such as microspotted arrays and microsphere-based techniques seeks to overcome these barriers by making bio-analyses more efficient while at the same time greatly increasing information content. Indeed, the scientific community is now faced with exciting opportunities that may enable lab-on-a-chip developments suitable for high quality multiplexed bio-assays.

On the other hand, these techniques are quite complex requiring sophisticated instrumentation and software to gather and decipher usable information. Unfortunately, large monetary investment in equipment, facilities and qualified personnel is required before analyses can begin. Furthermore, several aspects inherent to the predominant multiplexing strategies have limited their analytical capabilities. For example, RNA/DNA and protein microarrays on glass surfaces have a history of being problematic for assay optimization and the practice often requires the biomolecules to be dried as part of the preparation and storage, which may potentially affect the assay performance. In addition, the use of “planar” platforms results in small signal generating path-lengths that necessitates either the use of high-powered light sources for their readout or the use of amplification procedures that serves to slow analysis times.

Another aspect that current multiplexed technologies cannot fulfill is the need to perform medical diagnoses at the point-of-care. In most hospitals and physician’s clinics, the normal practice in performing disease diagnoses requires a thorough physical examination of the patient along with a review of his/her medical history and lifestyle. The physician often requires blood and urine tests (or other specialized procedures) to make informed diagnoses. The time to obtain the test results may take a few hours (in a hospital setting with integrated testing facilities) to days or even weeks (in neighborhood physician clinics for example). This postponement in obtaining laboratory test results serves to delay therapeutic strategies and may even increase the probability of the patient transmitting the disease to others. Performing blood or urine tests at the patient’s bedside or in a doctor’s office and being able to rapidly obtain the results at the point-of-care enable better patient management decisions, improved patient and societal outcomes, and

a reduction in the overall cost of care. The predominant multiplexing approaches, however, are currently limited for use in the research or specialized laboratory setting. Clearly, the widespread implementation of these methods in common doctor's offices seems improbable due to their complexity.

Finally, it is highly desirable to be able to diagnose or differentiate between multiple diseases having the same preliminary symptoms. For example, infection with human immunodeficiency virus type 1 (HIV-1) is often confused with infectious mononucleosis and influenza because the initial symptoms of HIV-1 are similar (fever, fatigue, etc.) Although many patients seek medical attention during the onset of HIV-1 infection, the diagnosis is often dismissed as being the flu or infectious mononucleosis. In a case study, ~2% of the patients suspected of infectious mononucleosis were in fact HIV-1 positive.¹¹⁵ Thus, the capability to tailor a differential disease diagnostic test according to relevant medical research findings would greatly improve the efficiency and accuracy of current diagnostic practices.

A niche, therefore, has formed requiring the development of an inexpensive and portable flow device facilitating a simple, flexible and cost effective approach to multiplexed disease diagnoses. This device should be usable in a point-of-care approach that simultaneously screens for a variety of disease-specific biomarkers while being capable of rapidly delivering the results to the physician. In addition, common immunoassay formats and strategies should be capable of being incorporated with this approach facilitating the usage of commercially available immunoreagents and detection schemes. Finally, the analytical performance characteristics (analysis times, sample and reagent volumes, assay dynamic range and detection thresholds, etc.) of the new diagnostic device should be comparable or improve upon those of the current state-of-the-art techniques.

With the collaborative efforts of the Neikirk, Shear, Anslyn and McDevitt research groups and other technical experts at the University of Texas at Austin, a silicon chip-based sensor array, termed here as the "electronic taste chip", was integrated with pressure driven fluidics and conventional microscopy to create a miniaturized and optical-based flow-through analytical device. Previous reports have demonstrated the utility of this approach for the detection of cation, anions, solubilized metals, sugars, enzymes, DNA/RNA fragments and

nucleotide phosphates.^{111,116-120} Furthermore, this strategy makes possible the simultaneous analysis of multiple targets with minimal reagent and sample requirements. In this dissertation, experimental research was completed to facilitate the analysis of biological molecules using this new approach. In addition, specialized experiments were completed in an effort to understand on a molecular-level the factors that influence immunoassay analytical characteristics as performed using this electronic taste chip methodology.

CHAPTER 2: THE ELECTRONIC TASTE CHIP METHODOLOGY

Before discussing the specific details of bead-based immunoassays as will be completed in the following two chapters, this chapter will provide a short summary of the relevant instrumentation and measurement protocols specific to the taste chip approach.

The Electronic Taste Chip can be described as an analyte detecting strategy that has evolved from the combination of the microfluidics and sensor array technologies. The heart of the system is the arrangement of individualized beaded sensing elements in a specially designed holding chip. The approach makes use of an array of micromachined pits localized on a silicon wafer with trans-wafer openings forming individualized chambers that allow for both fluidic flow and optical access. The investigation of complex fluids has been demonstrated for a variety of important classes of analytes including acids, bases, metal cations, enzymes, and DNA/RNA oligonucleotides.^{111,116,117,121,122} Identification and quantitation of analytes occur via colorimetric and fluorescence changes to receptor and indicator molecules that are covalently attached to termination sites on the polymeric beads. Crude spectral data is extracted from the array using a charge-coupled device (CCD) allowing for the near-real time extraction of digitized data. Furthermore, the analysis of proteins has been demonstrated using conventional direct and indirect fluorescent and colorimetric enzyme-linked immuno-detection techniques.¹¹⁹ This arrangement of the silicon chip-based array and multiple sensing elements affords the concurrent analysis of multiple target analytes. Finally, by using computer software, the patterns created by the differential optical output of the sensor array can be compared to internal data sets thus enabling the identification and quantitation of a complex mixture of analytes through pattern recognition schemes.¹²³

Figure 2.1 illustrates the cavities or wells of the micromachined bead array as prepared by the Neikirk laboratory at UT. The wells are chemically etched in a square arrayed pattern on silicon wafers (230-380 μm thick). The chemical etching process uses KOH anisotropic etching of the silicon substrate.^{110,111,124} To mask the substrate during to etching process, a silicon nitride layer is prepared using a low-pressure chemical vapor

deposition (LPCVD) process. Removal of the mask layer from one side of the silicon is carried out by protecting the other side with photoresist and then by plasma etching (CF_4 and O_2) the silicon nitride layer. The silicon substrate is then etched anisotropically using a 40% KOH solution. After the etching process, the nitride masking layer is completely removed from both

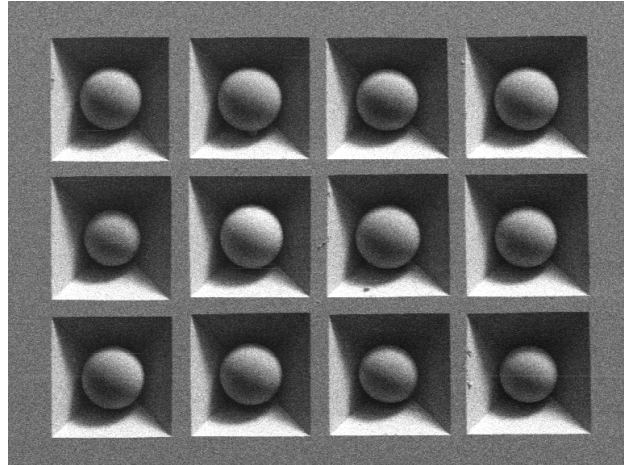


Figure 2.1: A scanning electron micrograph showing a 3×4 array of chemically etched wells of a silicon wafer. The wells extend through the entire thickness of the silicon creating square openings on the bottom side of the chip. These openings provide both optical access to the bead sensing element and serve as a drain for the reaction/analysis chamber. Glass beads have been placed in the beads to illustrate the dimensionality of the beads as they are located within the wells (Photograph provided courtesy of Dwight Ramanovics).

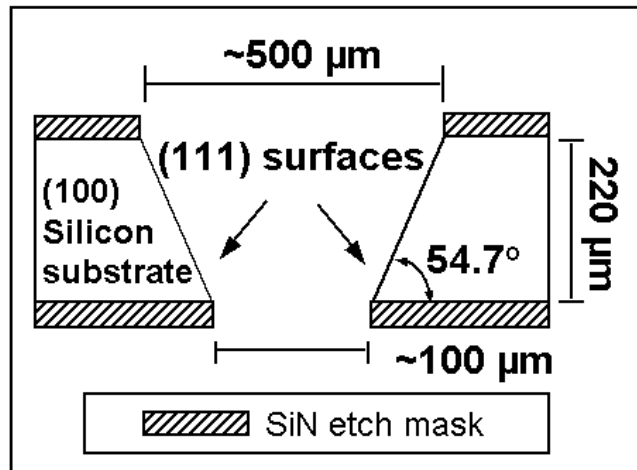


Figure 2.2: A cross-section diagram displaying the well region within the silicon wafer. The area created by this structure serves to confine the beaded sensing element within. Here a square opening ($\sim 500 \times 500 \mu\text{m}$) within the SiN etch mask layer is used in conjunction with an anisotropic etch to expose the silicon (111) surfaces. The resulting inverted pyramidal well extends through the entire thickness of the wafer, creating square openings ($\sim 100 \times 100 \mu\text{m}$) on the bottom side of the chip. These openings provide both optical access to the bead element and serve as a drain for the reaction/analysis chamber.

surfaces of the wafer using plasma etching. Figure 2.3 illustrates a cross-sectional diagram of the silicon wafer displaying a well that is used to confine the beaded sensing element. Here, a square opening ($\sim 500 \times 500 \mu\text{m}$) within the silicon etch mask layer is used with the anisotropic etch to expose the (111) surfaces, each at 54.7° from the horizontal surface of the wafer. The etching process creates wells that have an inverted pyramid shape with the apex of the pyramid being truncated by the bottom surface of the silicon wafer. This design serves as a chamber to contain the beaded sensing element while allowing both bottom-illuminated light to be transmitted through the bead and fluid to flow perpendicular through the wafer. Furthermore, patterns of these wells have been etched to create 3×3 , 3×4 , 4×5 , 5×7 , or 10×10 arrays.

After the all silicon micromaching steps are completed, a silicon dioxide layer is deposited over the entire silicon structure to enhance surface wetting characteristics for subsequent sample and reagent introduction. The chip is then loaded (i.e. maneuvered with a needle point) with selected biologically reactive beads with known location in the array. The bead-loaded chip is then encased into a fluid flow cell that is held together by

a stainless steel housing. The flow cell is constructed with see-through plastic support layers that creates microfluidic channels and reservoirs above and below the silicon chip while still allowing optical access, as shown in Figure 2.4.

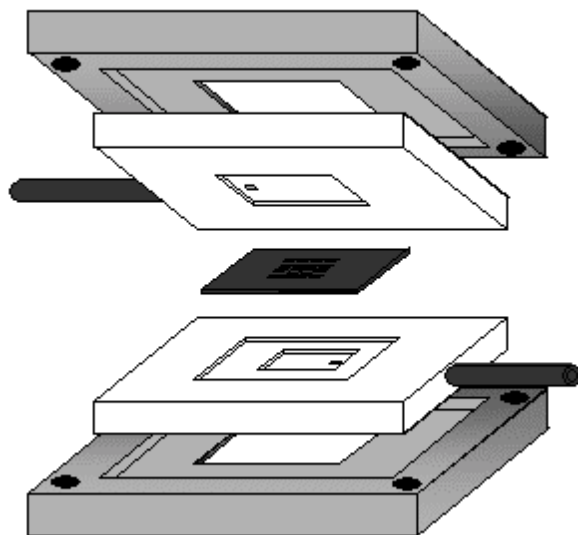


Figure 2.3: A schematic diagram depicting the flow cell housing. Here two layers of see-through plastic were designed to hold the bead-loaded silicon chip. Fluids are introduced into the flow cell using flexible, chemically inert plastic tubing.

The flow cell assembly is positioned onto the stage of either an Olympus SZX12 stereo microscope or an Olympus BX60 compound microscope (Olympus America Inc.; Melville, NY). The microscope allows for the detailed observation of the beads from both transmitted (bottom illumination) and epi-fluorescent (top-illumination) perspectives.

Solutions are then introduced into the flow cell in an automated fashion using an Amersham Pharmacia Biotech ÄKTA high-pressure liquid chromatography system controlled by Unicorn 3.0 software (Amersham Pharmacia Biotech; Piscataway, NJ). The beads within the silicon array are exposed to sample and signaling reagents using the pressure-driven flow created by the pumps of the liquid handling system. As shown in

Figure 2.5, the fluid flow pattern is directed into an upper reservoir of the flow cell and forced through the wells containing the beads. Finally, the fluid is directed into a bottom reservoir leading to an exit drain. The flow cell is designed to ensure that all introduced fluids passed only through the wells of the sensor array. Consequently, the wells are observed through the microscope optics, and images are captured using a 12-bit charge-coupled device (CCD) as supplied by DVC Company (Austin, TX) in conjunction with Image Pro Plus 4.0 software (Media Cybernetics; Silver Spring, MD).

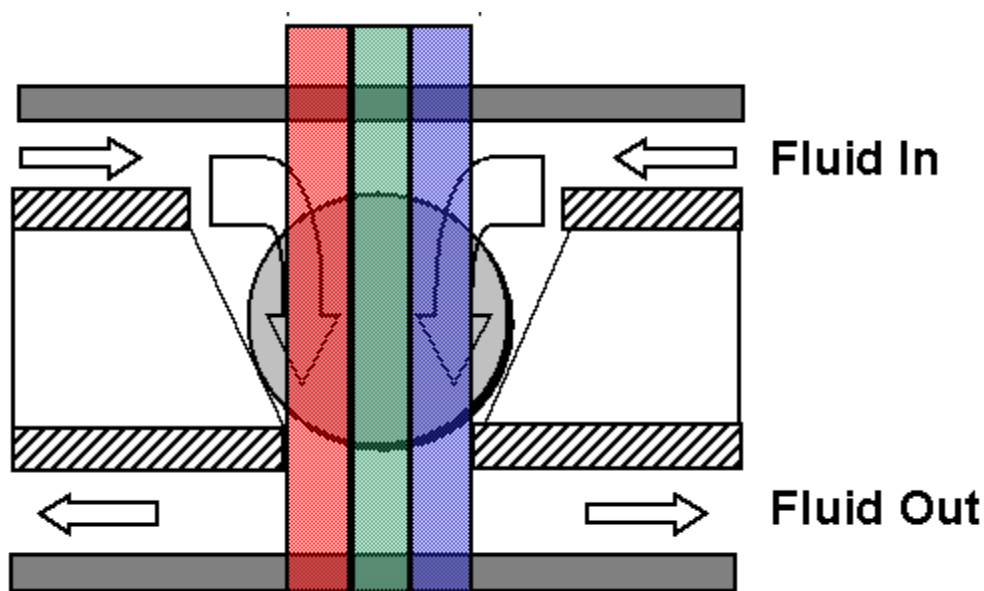


Figure 2.4: Schematic depicting route of fluid flow in the flow cell housing. Fluid samples containing the various reagents and analytes are introduced from the top side of the chip, pass through the analysis/reaction chamber holding the beaded sensing element, and exit out of the bottom region of the assembly. In addition, optical analysis of the bead is made possible with this construction either by using transmitted light (bottom illumination) or epi-fluorescent signaling schemes. Here, specific chemical and biological reactions within the bead are monitored by conventional colorimetric or fluorescent signaling strategies and quantified by measuring the red, green and blue pixel intensities that were derived from the CCD camera and imaging software.

To obtain quantitative data from enzyme-based colorimetric assays, the colorimetric signal is developed using conventional enzyme-amplified colorimetric substrates. For example, the enzyme horseradish peroxidase (HRP) is commonly used as an enzymic label for detecting antibodies. This label is often used with a precipitable

chromophore such as 3-amino-9-ethylcarbazole (AEC) for color development. Upon the addition of peroxide, the HRP readily converts the uncolored substrate into a reddish-brown colloidal precipitate. A mechanism is provided in Chapter 1 that describes the process. Furthermore, when the detecting antibody is bound to the bead, the precipitated AEC reagent becomes effectively trapped within the bead matrix. As a result, the bead turns reddish-brown indicating the presence of detecting antibody.

To obtain numerical data concerning the degree of coloration, and hence the amount of detecting antibody present, images of a bead are captured before and after the delivery of reagents. First, an image of the bead is captured before the delivery of reagents. The degree of coloration is quantified by measuring the pixel intensity, I_{Before} , yielded by the CCD. Here, the pixel intensity values are derived from circular areas of interest (AOIs) drawn in the inner region of each bead as yielded by the imaging software. Next, after all reagents have been delivered, another image is captured of the same bead (at the same magnification and at the original illumination conditions). The pixel intensity after the reagents, I_{After} , is quantified by the imaging software as above and the “effective absorbance” value, A_B , is calculated using Beer’s law:¹¹¹

$$[A_B = -\log(I_{\text{After}}/I_{\text{Before}})] \quad \text{Eq. 2.1}$$

To obtain fluorescent intensity data, the sensor array is held secure on the microscope stage at a suitable magnification and illuminated with the appropriate excitation light as afforded by the microscope’s epi-fluorescent capabilities. Here, fluorescent filter sets are chosen to match the excitation and emission wavelengths of the fluorescent label being monitored. Images of the bead, before and after the delivery of reagents, are captured and the intensity of the fluorescent emission is obtained directly from the imaging software.

Lastly, Figure 2.5 illustrates the total integration of the electronic taste chip system showing the fluidic pump unit, the sensor array encased in the flow cell, a compound microscope with an attached CCD camera and the computer used to derive

digital data. With this arrangement in instrumentation, the following important accomplishments have been demonstrated to date:¹¹¹ 1) near real-time collection of absorbance or fluorescence signals at multiple sites, 2) production of a polymer bead-based sensor array with site-to-site optical variance of 2-4%, 3) uniform flow characteristics with little noticeable motion of the sensitized beads, 4) the ability to pass a large number of fluid dead volumes through the sensor array leading to efficient washing and sample delivery, 5) incorporation of receptors/signaling agents suitable for the analysis of acids, bases, numerous metal cations, enzymatic substrates, DNA/RNA oligonucleotides, proteins and antibodies.^{111,117,119,122}

Furthermore, the beads localized in the wells of the silicon chip serve both as microreactors and as miniaturized analysis chambers. When interfaced with the CCD camera and fluid delivery system, these beads serve as the heart of the electronic taste chip sensing system. The next chapter presents in detail the steps that were taken to identify the most appropriate polymer bead material that would serve as a “3-dimensional cuvette” for the efficient detection of biological analytes.

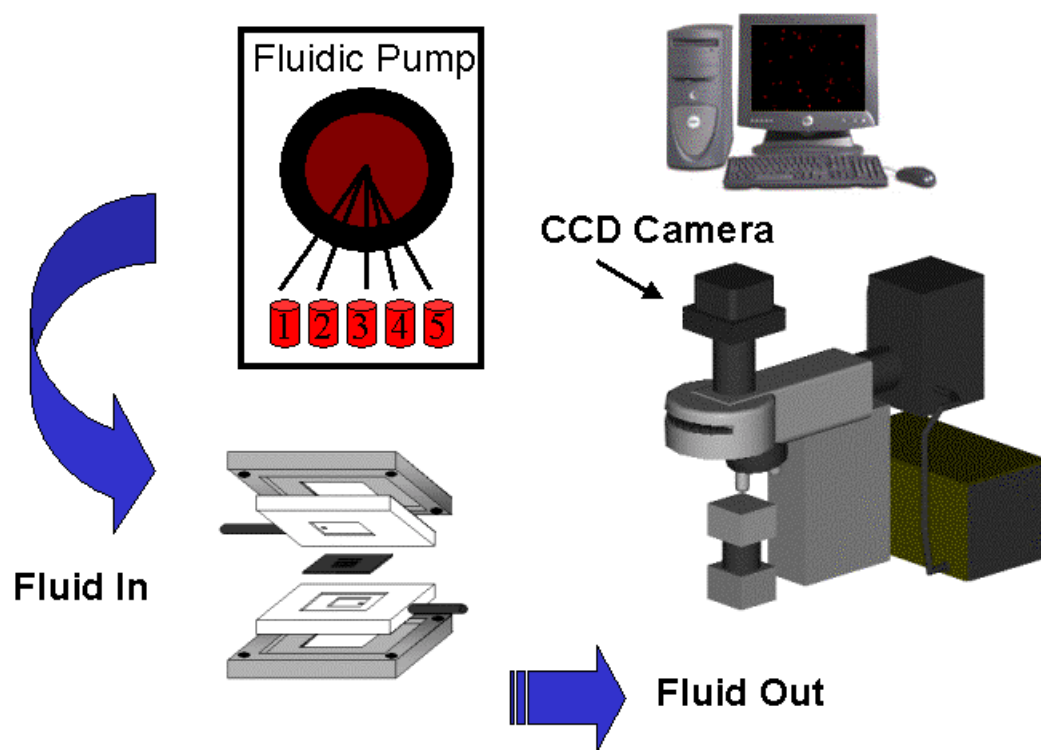


Figure 2.5: The electronic taste chip total analysis system.

CHAPTER 3: TWO-DIMENSIONAL ARRAYS BASED ON THREE-DIMENSIONAL OBJECTS FOR MULTI-ANALYTE DETECTION: MATERIALS CONSIDERATIONS

3.1 INTRODUCTION

The last decade has witnessed remarkable advancements of new microarray-based analytical techniques allowing for the parallel analysis of multiple biological analytes.^{57,69} Recent developments in the area of lab-on-a chip devices, also known as micro-total analysis systems^{93,114} (μ -TAS), have also incorporated the technological developments in the areas of photolithography, microfluidics and microelectromechanical systems (MEMS) for the construction of miniaturized monolithic testing devices.^{95,101,105,125} The advantages conferred by these microfabricated systems include a reduction in size and reagent consumption leading to lower assay costs, shortened analysis times, increased mass transport and improved thermal diffusion.¹¹⁴ Furthermore, these miniaturized systems when fully developed will lend themselves to multiplexed detection themes.^{105,125,126} However, a limitation of current lab-on-a-chip strategies is the ability to detect multiple analyte classes (i.e. proteins, DNA fragments, small organic molecules, metal cations, acids and bases, etc.).¹¹¹

The solid-phase material used for the immobilization of specific receptor molecules is a major consideration when designing such sensors. For example, much of the initial focus of microarray technology has been placed in the field of genomics where miniaturized arrays of cellular DNA (cDNA) are immobilized onto treated glass microscope slides with a high spatial density enabling investigators to perform highly parallel measurements of DNA/RNA content in genotyping and gene expression experiments.^{55-58,70,127} These concepts have also been implemented for protein analyses with antibody-based protein array systems.⁶⁵ For example, antigen specific capture antibodies have been immobilized in a patterned array on the surface of glass microscope slides⁷¹ and on the interior surface of glass capillary tubes⁷⁵ where the multiplexed

analysis of various bacterial, viral and protein analytes is performed using fluorescent tracer antibodies. Multiplexed immunoassays have also been demonstrated on the surface of polystyrene¹²⁸ and silanized glass¹²⁹ microtiter plates and on the surface of polyvinylidene difluoride⁶⁴ and nitrocellulose^{70,130} filter membranes.

The use of planar substrates for the immobilization of receptor molecules has been the predominant approach for microarray-based nucleic acid and immunoassay methodologies. However, proteins are more sensitive to their environment than nucleic acids and as a result, the hydrophobicity of many plastic and glass surfaces cause proteins to lose their native structure resulting in the loss of specific binding activity.^{131,132} In addition, the use of planar microarrays results in small signal generating path-lengths that necessitates either the use of high-powered light sources for their readout or the use of amplification methodologies that serves to lengthen the analysis time.

To overcome these limitations, the use of 3-dimensional substrates in nucleic acid and protein biosensor methodologies has been studied recently.^{76,77,133} The approaches appear to provide essential advantages over the use of standard planar surfaces. Immobilization of receptor molecules in 3-dimensional elements provides: 1) a higher binding capacity allowing more receptor/analyte interactions; 2) a consequential increase in the signal generating pathlength of the biosensor; 3) potentially a more homogenous environment than the heterophase immobilization on planar surfaces; and 4) an opportunity to select or design a suitable “scaffold” to enhance the stability of the receptor/ligand interaction. Accordingly, arrays of polyacrylamide gel pads ($100 \times 100 \times 20 \mu\text{m}$) have been used for the multiplexed analysis of proteins and enzymes,⁷⁶ as well as nucleic acids.⁷⁷ Further, a thin layer of hydrophilic polyacrylamide gel¹³³ ($12 \text{ mm} \times 40 \text{ mm} \times 20 \mu\text{m}$) and agarose¹³⁴ has been coated to glass slides facilitating their use with conventional microarray spotting and analysis equipment.⁵⁵

Beaded supports have become established also as the solid-phase platform in several promising multi-analyte sensing strategies.^{81-83,103,135} For example, the use of fluorescent encoded sets of polystyrene microspheres ($\sim 5 \mu\text{m}$ diameter) allows for the

multiplexed interrogation of immunochemical and DNA hybridization reactions on the surface of the spheres using flow cytometric techniques.^{89,91} In addition, Walt and coworkers have developed a high-density fiber optic bundle (500 μm) that contains ~6000 individually addressable 3-6 μm etched wells capable of housing functionalized poly(methylstyrene)divinylbenzene microspheres.^{87,88} Sensor arrays are then created by randomly distributing a mixture of microspheres on the fiber tip whereby specific receptor/ligand interactions are monitored and identified by optical encoding methodologies. While these technologies are suited for high-throughput biological sensing, the above-specified advantages derived from using a 3-dimensional reaction vessel for the micro-localization of receptor/ligand binding interactions have not been exploited given that these prior bead approaches have relied most upon surface interactions for signal generation.

To this end, we have developed recently a flow-based sensor array^{111,116-118} that exploits the 3-dimensionality of beaded polymer microreactors and combines the chemically etched pits of a silicon chip and video chip optical analyses thereby allowing for the simultaneous completion of multiple immunoassays. This work expands upon our prior efforts using the same “electronic taste chip” methodology whereby acids, metal cations, proteins, antibodies, sugars and biological cofactors in solution samples were identified rapidly and with high quality assay characteristics.^{111,118,119} The central component of this system is an extremely versatile silicon chip-based platform into which individual microbead sensors are positioned so that the combination of these sensors can be tailored to fit any number of customized applications. For example, applications of the taste chip approach have been demonstrated for the multiplexed analysis of the human cardiac risk factors, C-reactive protein (CRP) and interleukin-6,¹¹⁹ viral infectious diseases (see Chapter 4), and DNA hybridizations.¹²²

This chapter describes the selection, design and preparation of the polymer-beaded materials for use as immunological sensing elements in the taste chip integrated system. In addition, the penetration of immunoreagents into the 3-dimensional network

of the bead matrix is demonstrated here and the advantages of utilizing the 3-dimensionality of the porous bead as immunological reaction vessels are revealed and compared to planar immunoassay strategies.

3.2 EXPERIMENTAL SECTION

3.2.1 Reagents

For the bead characterization experiments, normal mouse IgG was used as a general protein that was obtained from Caltag Laboratories (Burlingame, CA). A rat monoclonal anti-mouse IgG₁ (Biosource International; Camarillo, CA) was used as a detecting antibody. This antibody was conjugated either with the fluorophore, Alexa Fluor® 546 or Alexa Fluor® 488 obtained from Molecular Probes (Eugene, OR) or was purchased with a conjugated horseradish peroxidase (HRP) enzyme label from Biosource International (Camarillo, CA). Sandwich immunoassays were performed using human C-reactive protein (CRP) as the analyte. Details describing the generation of CRP dose-response have been described previously.¹¹⁹ The bead-based precipitable colorimetric signal was developed using the substrate 3-amino-9-ethylcarbazole (AEC) from Pierce Biotechnology Inc. (Rockford, IL) while the bead-based soluble colorimetric signal was developed using 3,3',5,5'-tetramethyl benzidine (TMB). Both these reagents were purchased from Pierce Biotechnology (Rockford, IL). Agarose powder (type I-B), sorbitan triolate (Span 85), and polyoxyethylenesorbitan monooleate (Tween 80) were purchased from Sigma Corporation (St. Louis, MO). Hexane (mixture of isomers) was obtained from Fisher Scientific (Fair Lawn, NJ).

3.2.2 Bead Matrix Materials and Protein Immobilization Protocols.

The bead selecting process explored the physical and chemical characteristics of 5 generalized beaded matrices as follows: unmodified polystyrene (PS), divinylbenzene cross-linked polystyrene (DVB-PS), polystyrene-polyethylene glycol graft co-polymer (PS/PEG), polyethylene glycol dimethyl acrylamide co-polymer (PEGA), and cross-

linked beaded agarose. All DVB-PS, PS/PEG and PEGA beaded supports (~130 μm diameter) were purchased from Novabiochem Corporation (San Diego, CA). The unmodified PS beads (175-260 μm diameter) were purchased from Polysciences, Inc. (Warrington, PA). And the cross-linked agarose beads (75-450 μm) were purchased in both the amine- and aldehyde-functionalized formats from Agarose Bead Technologies (Tampa, FL).

Evaluations of the optical clarity and background fluorescent readings of the beaded materials were performed using conventional light microscopy and epi-fluorescent techniques. Samples of unmodified polystyrene, chloromethylated DVB-PS, amine- and carboxylate- functionalized PS-PEG, amine-functionalized PEGA, and amine- and aldehyde-functionalized agarose beads were each solvated in aqueous solution. To evaluate the optical clarity of each bead type, samples were placed on glass microscope slides and viewed under an Olympus SZX12 stereo microscope (Olympus America Inc.; Melville, NY) at ~30x magnification using transmitted light (bottom illumination). Images of the beads were captured using an 8-bit charge-coupled device (CCD) as supplied by DVC Company (Austin, TX) in conjunction with Image Pro Plus 4.0 software (Media Cybernetics; Silver Spring, MD). Absorbance values were calculated using Beer's law, $[A_B = -\log(I_{\text{Bead}}/I_{\text{Background}})]$, where the blue pixel intensity attenuated by the bead, I_{Bead} , was compared to the reference blue pixel intensity of the background illumination, $I_{\text{Background}}$. These values were derived from circular areas of interest (AOIs) drawn in the inner region of each bead using the imaging software. The values derived for the background illumination was an arbitrarily selected AOI in the image where a bead was not present. Similarly, the amount of light transmitted by the bead matrix was also reported transmittance ($\%T = I_{\text{Bead}}/I_{\text{Background}} \times 100$) and was calculated as the ratio of the blue pixel intensity transmitted from the bead sample divided by the blue pixel intensity from the background illumination and expressed as a percentage.

To evaluate the fluorescent background reading of each bead type, the bead samples were placed on microscope slides and illuminated with blue light ($\lambda_{\text{max}} = 488$ nm) from above as afforded by the microscope's epi-fluorescent capabilities. The green fluorescent emission ($\lambda_{\text{max}} = 520$ nm) was measured by capturing images of the various bead samples with the CCD. Here, the green pixel intensity of selected AOIs containing the beads were compared to the green pixel intensity of the image background (i.e. location where no bead was present) and reported as an average signal-to-noise ratio ($S/N = \text{bead fluorescent intensity} / \text{background fluorescent intensity}$). The CCD exposure time for the fluorescent images was 5 seconds and the gain of the CCD was increased to ~75% maximum to accentuate the fluorescent readings.

Experiments were performed to evaluate effectiveness of established protein-to-bead immobilization procedures.¹³⁶ The protein immobilization procedures used here include: the physical adsorption of analyte capturing protein directly to the surface of the unmodified polystyrene bead; the covalent coupling of protein to aldehyde-functionalized agarose beads using reductive amination procedures;¹³⁷ the covalent coupling of proteins to amine-functionalized beads (i.e. PS-PEG, PEGA and agarose materials) using glutaraldehyde as a cross-linking reagent;¹³⁸ and the covalent coupling of proteins to carboxylate-functionalized bead matrices (i.e. PS-PEG) using carbodiimide activation procedures.¹³⁶

In the experiments evaluating the efficiency of the physical adsorption of capturing protein directly onto the bead matrix, ~50 μL aliquots (settled volume) of chloromethyl terminated DVB-PS and unmodified polystyrene beads were individually isolated in separate capped micro-centrifuge tubes (0.7 mL maximum capacity). The beads were gently agitated in a 1 mg/mL solution of mouse IgG overnight at room temperature. The aliquots were then rinsed with at least 3 volume washes of PBS. Coomassie protein stain (Pierce Biotechnology Inc.; Rockford, IL) was used to evaluate the efficiency of protein adsorption by gently agitating the bead sample for 20 minutes in a 100% by volume solution of the liquefied protein stain. The beads were then rinsed

with at least 3 volume washes of PBS. The presence of protein was then measured by evaluating the degree of blue color of the beads as caused by the protein stain. Here, the stained beads were placed on a glass microscope slide and viewed under the Olympus SZX12 stereo microscope at ~30x magnification using transmitted light (bottom illumination). Images of the beads were captured using the CCD in conjunction with the imaging software. Absorbance values were calculated as described above, where the red pixel intensity of the bead, I_{Bead} , was compared to the red pixel intensity of the background illumination, $I_{\text{Background}}$, as derived from the imaging software.

The coupling of protein to the aldehyde-functionalized agarose beads was performed using established reductive amination procedures.¹³⁷ More specifically, a ~50 μL aliquot of aldehyde-functionalized agarose beads (settled volume) was isolated in an individual capped micro-centrifuge tube. The beads were agitated with 500 μL of a 1 mg/mL mouse IgG and 4.8×10^{-4} moles NaCNBH_3 overnight at room temperature with end-over-end tumbling. The next day the beads were rinsed with at least 3 volume washes of phosphate buffered saline (PBS). The remaining active sites were deactivated with the amine-containing TRIS buffered saline and a similar amount of NaCNBH_3 by tumbling for 1 hour. The beads were then rinsed with 3 volume washes and evaluated using the Coomassie protein stain as described above.

Protein coupling procedures were performed using glutaraldehyde as a cross-linking reagent between amine-functionalized beads and protein. Approximately 50 μL aliquots (settled volume) of amine-functionalized PS-PEG, PEGA, and agarose beads were individually isolated in separate capped tubes. A volume of 0.5 mL of a 6% (vol/vol) glutaraldehyde solution pH 7.4 was mixed with the bead samples for 6 hours at room temperature with end-to-end mixing. The aliquots were then rinsed with 3 volume washes of PBS followed by an end-over-end incubation with 500 μL of a 1 mg/mL mouse IgG solution overnight at room temperature. Afterwards, the aliquots were rinsed again with 3 volume washes of PBS. The remaining active sites were deactivated with

0.5 mL of 0.2M ethanolamine for 30 minutes followed by rinsing with 3 volume washes of PBS. The beads were then evaluated with Coomassie protein stain as described above.

Carboxylated PS/PEG beads were also coupled with mouse immunoglobulin protein and evaluated by the protein stain. In this case, ~ 200 μ L aliquots (settled volume) of beads were isolated in a separate tube and mixed 4 hours end-over-end with 0.5mL of a 2% (wt/vol) carbodiimide solution pH 4.5. The aliquots were then rinsed with 3 volume washes of PBS. The beads were incubated with end-over-end mixing with 500 μ L of a 1 mg/mL mouse IgG solution pH 4.5 overnight at room temperature. Afterwards, the aliquots were rinsed again with 3 volume washes of PBS and then resuspended in borate buffer. A volume of 50 μ L of 0.1M ethanolamine was added and mixed for 30 minutes to deactivate the remaining active sites followed by rinsing with 3 volume washes of PBS at pH 7.4.

3.2.3 The Production of Superporous Agarose Beads.

Superporous agarose beads were prepared by adapting a procedure previously described.¹³⁹ An agarose solution was prepared by heating ~2 g of agarose in 50 mL of water to 92°C. The solution was stirred slowly and cooled to 62°C. The stir rate was increased to 1000 rpm and a 62°C suspension consisting of 1.4 mL Tween 80 and 20 mL hexanes was added with agitation for 4.5 min. A second 62°C solution consisting of 14 mL Span 85 and 150 mL hexanes was added and mixed for 1.5 min. The stir rate was then reduced to 500 rpm and the reaction was cooled to 30°C. The resulting mixture was transferred to a wire screen sieve (W.S Tyler; Mentor, OH) and washed with water. The beads were then washed with a water:ethanol (50%:50%) solution. Particles with diameters ranging from between 250 and 300 μ m were isolated with the sieves and sonicated in the water:ethanol (50%:50% vol) solution for 30 minutes followed by another rinse with pure water.

3.2.4 Bead Sorting and Activation Protocol.

Populations of beads that were of a useful size range and uniform diameter were isolated and chemically functionalized to contain reactive aldehyde groups. First, samples of non-functionalized commercial agarose beads or the freshly prepared superporous beads were size selected using a series of graded sieves. The bead fractions between 250-300 μm diameter were then sorted to a more defined diameter range using an automated high-throughput particle analysis/sorting instrument (Union Biometrica; Sommerville, MA). The instrumental parameters were set to analyze the bead population based on object length and subsequently separate beads that fit predefined criteria. As a result, a population of beads was obtained with a variation in diameter of ~5%.

To incorporate reactive aldehyde groups into the agarose matrix for protein immobilization, a procedure by Shainoff was adapted and optimized here. A volume of ~2 mL settled size selected beads were placed in a 10 mL beaker (2.5 mL total volume deionized (DI) water). Then an aliquot of 0.7 mL of a solution comprised of 7mL 1M NaOH, 2 mg/mL 0.1M NaBH_3 and 3 mL glycidol was added in the reaction vessel that was then gently rocked with circular motion overnight at room temperature. The vessel was covered with wax film to prevent evaporation of reactants. To prevent the aggregation of beads into clumps, the mixture was periodically checked and if clumping was noticed, the vessel was mixed with vigorous agitation. The beads were then filtered in a sintered glass funnel with ~1 L DI water. Next, 0.7 mL of a 0.16 M NaIO_4 solution was added to the beads (2.5 mL total volume of DI water) and gently rocked with circular motion for 1 hour. The beads were then rinsed again in the sintered glass funnel with ~1 L DI water. Finally, The beads were rinsed with ~ 10 mL PBS pH 7.4 and immobilized with protein using reductive amination as described above.

3.2.5 Instrumentation.

The components of the taste chip analysis system have been described^{111,117,119} in Chapter 2. Briefly, individual beads were placed into photolithographically etched

cavities patterned in a square array on a silicon wafer chip. The cavities were created by an anisotropic etch which yielded inverted pyramidal wells with trans-wafer openings. Patterns of these wells were arranged to create 3×3 , 3×4 , 4×5 , 5×7 , or 10×10 arrays. The chip was loaded (i.e. maneuvered with a needle point) with beads selected biologically reactive beads with known location in the array. The bead-loaded chip was then encased into a fluid flow cell that was held together by a stainless steel housing. The flow cell was constructed by vinyl adhesive sheeting and see-through plastic support layers that created microfluidic channels and reservoirs above and below the silicon chip while allowing optical access. Solutions were introduced into the flow cell in an automated fashion using an Amersham Pharmacia Biotech ÄKTA high-pressure liquid chromatography system controlled by Unicorn 3.0 software (Amersham Pharmacia Biotech; Piscataway, NJ). The flow cell assembly was positioned onto the stage of the Olympus SZX12 stereo microscope that allowed for the microscopic observation of the beads from both transmitted (bottom illumination) and epi-fluorescent (top-illumination) perspectives. The beads within the silicon array were exposed to sample and signaling reagents using fluid flow that was directed into an upper reservoir of the flow cell and forced through the wells containing the beads. The fluid then was directed into a bottom reservoir leading to an exit drain. The flow cell was designed to ensure that all introduced fluid passed only through the wells of the sensor array. Finally, the wells were observed through the microscope optics, and images were captured using a 12-bit charge-coupled device (CCD) in conjunction with Image Pro Plus 4.0 software (Media Cybernetics; Silver Spring, MD).

3.2.6 Confocal and Scanning Electron Microscopy.

To evaluate the penetration of immunoreagents, medial cross-sectional images of beads were obtained on a LEICA (Exton, PA) TCS 4D laser scanning confocal microscope. Fluorophore-labeled CRP capture antibody was immobilized to both types of beads using reductive amination. These beads were then imaged with the confocal

microscope to obtain the medial cross-sectional image. Next, beads with unlabeled capture antibody were reacted with fluorophore-labeled CRP antigen and imaged as such. Likewise, beads with unlabeled capture antibody and bound unlabeled CRP antigen were reacted with fluorophore-labeled detecting antibody then imaged. All reagents were allowed to react overnight to ensure diffusion processes had equilibrated.

Scanning electron micrographs of the plain agarose and porous bead types were obtained on the LEO Model-1530 scanning electron microscope (Carl Zeiss Inc., North America). The physical structure of the agarose was preserved for SEM imaging by drying the beads in a carbon dioxide critical point drying apparatus (Tousimis Research Corp.; Rockville, MD).

3.3 RESULTS AND DISCUSSION

The electronic taste chip sensing methodology makes use of multiple micromachined wells localized on a silicon wafer with trans-wafer openings forming a 2-dimensional array of individualized analysis/reaction chambers. Figure 3.1A is a schematic illustration of a single micromachined well that is used to confine the beaded sensing element. Figure 3.1B illustrates an actual 3×4 array with localized beads. The wells of the array are chemically etched in a square arrayed pattern on a silicon wafer (230-380 μm thick) using a KOH anisotropic etching process of the bulk silicon substrate and a silicon nitride masking layer.^{110,111,124} Here, a pattern of square openings ($\sim 500 \times 500 \mu\text{m}$) formed by the silicon nitride mask layer is used with the anisotropic etch to expose the (111) surfaces of the silicon. The etching process creates wells that have an inverted pyramid shape with the apex of the pyramid being truncated by the bottom surface of the wafer. This configuration generates multiple analysis/reaction chambers with square openings ($100 \times 100 \mu\text{m}$) on the bottom surface of the wafer that allows liquid to drain and bottom illuminated light to be transmitted through the well. Patterns of these wells have been etched to create 3×3 , 3×4 , 4×5 , 5×7 , and 10×10 arrays. After all silicon micromachining steps are completed, a silicon dioxide layer is deposited

over the entire silicon structure to enhance the surface wetting characteristics for subsequent sample and reagent introduction.

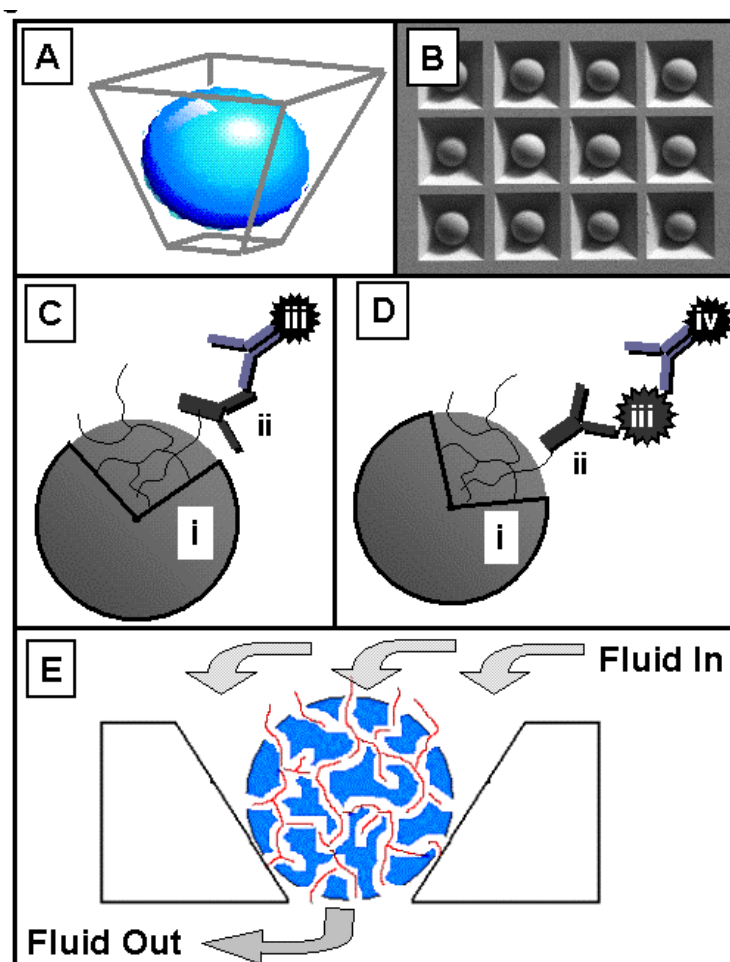


Figure 3.1: A 2-dimensional sensor array is assembled from a series of 3-dimensional objects. As illustrated in (A), the fundamental sensing element is a spherical bead placed inside the confines of a micromachined well. Here, a microwell has been chemically etched in a silicon wafer (230-380 μm thick) to form an inverted pyramid shaped chamber with a square opening ($500 \times 500 \mu\text{m}$) on the top surface of the silicon chip and square opening ($100 \times 100 \mu\text{m}$) on the bottom surface of the wafer. These openings both provide optical access to the bead element and serve as a drain for the reaction/analysis chamber. The structure of the sensor array is demonstrated in (B) where the scanning electron micrograph shows a 3×4 array of beads as localized in the etched wells of the silicon wafer. Case (C) shows the immunocomplex schematic for the detection of mouse IgG protein. Here, a bead (i) is conjugated with mouse IgG protein (ii) and detected by a fluorescent- or enzyme-labeled and mouse IgG specific detecting antibody (iii). Case (D) shows the immunocomplex schematic for detection of C-reactive protein (CRP). Here, a bead (i) is conjugated with CRP specific capture antibody (ii). The CRP protein analyte (iii) binds to the capture antibody and is visualized with the enzyme-labeled and CRP specific detecting antibody (iv). Color development is achieved with an enzyme-catalyzed precipitating chromophore that effectively stains the bead a reddish-brown color. Case (E) illustrates a cross-sectional schematic of a superporous bead as placed within an etched well of the silicon chip. The fluid flow pattern created by the external pumps forces sample and reagents to around and through the sensitized bead and finally out to waste. The meandering pores and channels within the superporous bead is also illustrated.

With the development of these 2-dimensional arrays composed of 3-dimensional objects having integrated fluidic systems, the selection of materials for the various components, especially the beads, becomes particularly important. The ideal systems that would be expected to deliver optimal analytical performance characteristics should have rapid, efficient and selective analyte permeation to occur throughout the entire volume of the bead microreactor. Accordingly, our pre-defined criteria for the selection and design of such a substrate includes the following considerations. The beaded material should: 1) facilitate common receptor immobilization chemistries with high receptor binding capacities for a wide range of bio-molecules including proteins, enzymes, DNA/RNA oligonucleotides, 2) it should withstand the harsh chemical reagents used in such immobilization methods, 3) it should possess optical properties amenable to the predominant signaling strategies used in the approach (i.e. mainly absorbance and fluorescent measurements for the taste chip approach here studied). Hence, the material should be optically transparent and have a negligible background fluorescent signature, and 4) it should have sufficient mechanical stability to withstand the fluidic flow rates and pressures sustained within the micro-fluidic chamber of the chip-based sensor system. Furthermore, it is desired that the selected matrix material be: 5) hydrophilic and biocompatible, 6) show little nonspecific binding of biomolecules, and 7) allow access of biomolecules (i.e. antibodies and proteins) to the interior of the matrix. In addition, methods must be developed to achieve a high degree of uniformity in both the size of the bead and its chemical reactivity to ensure consistent and dependable results. Thus, the initial goal here is to evaluate the physical and chemical parameters of a variety of polymer bead matrices and identify an optimized material that follows the criteria as defined above.

To evaluate the protein detecting capabilities of the sensitized bead materials, a series of model bead-based immunoassays are used. These assays use either a fluorescent or colorimetric signaling scheme that is deemed appropriate when evaluating the optical characteristics of the assay as defined by the integrated sensor array approach. Figure 3.1C illustrates the relevant immunocomplex of the simple 2-component bead-based

model immunoassay that is used extensively in this report. Here, a generic mouse antibody protein (mouse IgG) is immobilized to the bead and acts as the specific target for the fluorophore or enzyme-labeled detecting antibody. Identification and quantification of the analyte follows by discriminating the fluorescent or colorimetric optical signals acquired by the charge-coupled device (CCD).

3.3.1 Polymer Bead Candidates. Polymer bead materials that have established good track records as the solid-phase supports in macroscopic particle-based medical diagnostic assays,^{19,21} solid-phase peptide synthesis^{140,141} or immunoaffinity chromatography techniques¹³⁶ are selected for the initial evaluation. Accordingly, the first material chosen for the evaluation is unmodified polystyrene microbeads due to the extensive use of polystyrene in conventional microtiter plate- and bead-based immunoassays.²¹ In addition, polystyrene beads are widely used in medical diagnostic applications and automated clinical assays.^{19,51} Typically, the immobilization of the solid-phase reactant to the polystyrene surface occurs via hydrophobic adsorption effects (i.e. physical adsorption).

Cross-linked polystyrene and polystyrene copolymer beads are also chosen for the evaluation since these materials are commonly used in solid-phase peptide synthesis methodologies.¹⁴² Advances in polystyrene co-polymer formulations have created materials with increased swelling capacities in solvents of related polarity enabling the supports to accommodate growing peptide chains into the interior regions of the beads.¹⁴³ The first material selected from this category for the evaluation is polystyrene cross-linked with 1-2% divinylbenzene (PS/DVB). This beaded matrix appears as a hard glassy transparent material that is hydrophobic and exhibits minimal swelling in aqueous solvent. Another candidate chosen for the evaluation is the co-polymer polystyrene-poly(ethylene glycol) composite material (PS/PEG).¹⁴⁴ This supports has cross-linked polystyrene (1-2% divinylbenzene) as its backbone, but also grafted onto this are long poly(ethylene glycol) side chains (PEG) enabling relatively high ligand loading levels of >0.3 mmol/g (active sites per dry gram resin). These composites are comprised of ~70

wt% poly(ethylene glycol) and ~30 wt% PS/DVB and typically swell 2-4 times their dry diameter when placed in water. Poly(ethylene glycol)-acrylamide or PEGA resin is another co-polymer chosen for the evaluation.¹⁴⁵ This material is largely hydrophilic and freely permeable to macromolecules up to 35 kDa¹⁴⁰ making it potentially suitable for the above described application. Finally, beaded agarose is selected for the evaluation due to its widespread use as the solid-phase support in affinity chromatographic techniques^{136,146,147} and size exclusion chromatography (SEC).^{148,149} Polymerized agarose is a hydrophilic linear polysaccharide derived from algae consisting of alternating residues of D-glucose and 3-anhydrogalactose units. Agarose beads are typically generated¹⁵⁰ in a liquid emulsification procedure where heated aqueous agarose and the appropriate cross-linking reagents (i.e. epichlorohydrin or divinyl sulfone) are added to an organic solvent under stirring conditions. After a gradual temperature decrease, the liquid agarose gels to form cross-linked agarose beads in a wide range of diameters. The secondary and tertiary structures of agarose can be described as single fibers spun into a yarn of multiple fibers that is in turn “loosely wound into a ball” of extraordinarily complex tertiary structure. This feature builds a large network of accessible pores enabling the penetration of macromolecules into the interior regions of the beaded superstructure. Agarose bead-based SEC makes use of this in its ability to filter or separate a mixture of macromolecules based on their rate of migration through the porous agarose matrix.^{151,152} Additionally, several established protocols have been developed for the immobilization of proteins to beaded agarose.^{136,153} These attributes further incite the possibility to exploit the 3-dimensionality of beaded agarose and use advantageously in the bead-based immunoassays described here.

As described above, 5 general categories of beaded materials are evaluated for use as the primary solid-phase matrix in bio-analytical applications of the electronic taste chip approach. These materials are all commercially available and functionalized with a wide variety of chemically active pendant groups suitable for the protein immobilization chemistries investigated here. Accordingly, these bead types are chosen to possess chemical functionalities that function well with established protein coupling chemistries

(see below). In doing so, a total of 7 bead materials are evaluated for use in the sensor array as follows: 1) unmodified polystyrene (PS), 2) chloromethylated- PS/DVB (CM-PS/DVB), 3) amine-functionalized PEGA (NH₂-PEGA) , 4) amine-functionalized PS/PEG (NH₂-PS/PEG), 5) carboxylate-functionalized PS/PEG (COOH-PS/PEG), 6) amine-functionalized cross-linked agarose (NH₂-Agarose), and 7) aldehyde-functionalized cross-linked agarose (COH-Agarose).

3.3.2 Optical Clarity and Background Fluorescence.

To evaluate the optical properties of these 7 beaded materials, conventional light microscopy and epi-fluorescent techniques are employed. For the conventional light microscopy measurements, transmitted white light images are acquired for the beads placed in the water pool supported on a glass slide. Measurement of the intensity transmitted through the bead as well as through the adjacent regions lacking beads is used to obtain a quantitative measure of the bead matrix transparency. Similarly, the bead matrix background fluorescent properties are evaluated using similar water soaked beads that are examined using epi-fluorescent images with blue light excitation (480 +/- 20 nm bandpass filter) and green emission (505 nm longpass filter). Here the bead signal versus the adjacent background levels are measured. The resulting optical clarity and background fluorescence measurements are summarized in Table 3.1 Additionally, Figure 3.2 presents digitized images depicting the optical clarity and background fluorescent readings of the 5 representative bead types.

Table 3.1. Characteristics of various beaded materials.

	Optical Clarity		Background Fluorescence	Protein Coupling Chemistry	Wetted Bead Diameter	
	ABS	T%	S/N	Corrected ABS	Range (μm)	Variation (CV)
Unmodified PS	0.032	93%	1	PA 0.052	175-260	22%
CM-DVB/PS	0.21	62%	4.40	PA Negligible	65-110	20%
NH₂-PS/PEG	0.011	97%	1.83	Glut 0.24	190-250	10%
COOH-PS/PEG	0.010	98%	3.0	Carb 0.074	170-210	10%
NH₂-PEGA	0.002	99%	1.86	Glut 0.033	100-250	28%
NH₂-Agarose	0.009	98%	1	Glut 0.56	75-250	38%
COH-Agarose	0.012	97%	1	RA 0.40	250-450	18%

PA=passive/physical adsorption; Glut=glutaraldehyde cross-linker; Carb=carbodiimide activation; RA=reductive amination.

Inspection of the images and optical constants for the CM-PS/DVB beads show that the material exhibits poor optical clarity and a high fluorescent background reading. The beads are tinted a yellowish-gray color and exhibited a significant amount of surface roughness along with bubble-like features within the bead matrix. These features hinder both absorbance and fluorescent readings as measured in the sensor array. Likewise, the candidate-beaded material is here eliminated as a viable choice for the matrix material. A close inspection of the polystyrene beads reveals an acceptable standard of optical clarity and background fluorescent readings. These beads are also reasonably uniform in size and shape. Further, the average diameter of this bead type is deemed appropriate for use in the wells of the electronic taste chip. However, due to polystyrene's hydrophobic nature, the matrix is difficult to solvate and tends to float in aqueous solution. Only after

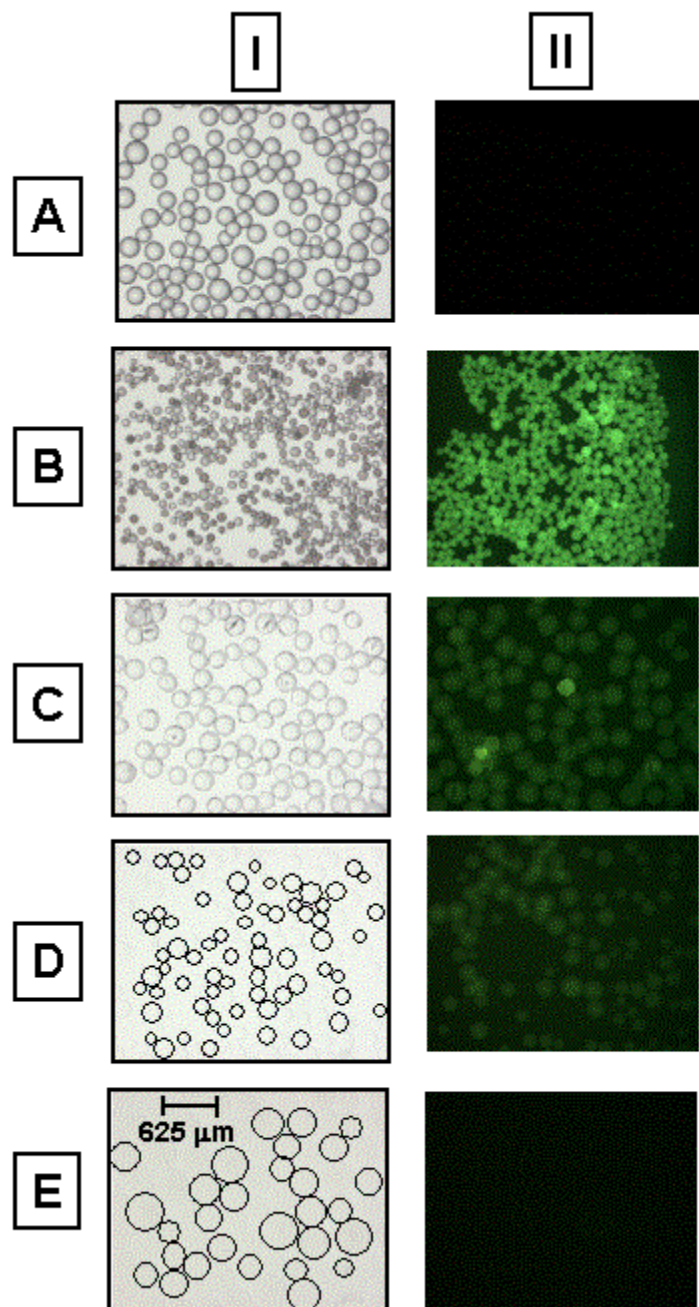


Figure 3.2: Images showing optical features and background fluorescent characteristics of the 5 generalized bead types. Here, images of beads were captured by CCD camera as solvated in a pool of water on glass microscope slides. The optical features (I) of the beads were evaluated using transmitted white light while background fluorescent readings (II) were evaluated using blue excitation and green emission filters. The bead materials used here are as follows: A) unmodified polystyrene, B) polystyrene cross-linked with 1-2% divinylbenzene (PS/DVB), C) cross-linked polystyrene/poly(ethylene glycol) grafted co-polymer (PS/PEG), D) poly(ethylene glycol)-acrylamide (PEGA), E) cross-linked agarose.

vigorous shaking in an Eppendorf tube would the beads become solvated by water. The NH₂-PS/PEG beads are easily solvated and had a slight yellowish tint in the transmitted light. This material exhibits a high level of optical clarity (97% transmittance) and had an acceptable fluorescent background reading (S/N=1.83). Previously, this material has been used extensively as a sensing element in the electronic taste chip for the detection of small molecules, anions, and cations^{111,116,117} and is of an appropriate size range for placement in the wells of the silicon chip. The PEGA matrix exhibits a high level of optical clarity (99% transmittance) and also had an acceptable fluorescent background reading (S/N=1.86). However, the size range of this bead type is deemed inappropriate for use in the current generation of taste chip arrays. Finally, the COH-agarose beads are very easily solvated in aqueous solution and are reasonably consistent in size and shape. They exhibit high optical clarity (~97% transmittance) with a negligible background fluorescent reading (S/N=1). Further, the NH₂-Agarose beads are similar in these respects.

Evaluating the relative attributes of the 7 candidate bead matrices, the unmodified PS, the PS/PEG co-polymer and the agarose beads are found to exhibit high optical clarity, low fluorescent background and are available in a size range suitable for the taste chip sensor array. Accordingly, these beads are selected as candidates for further evaluations.

3.3.3 Protein Immobilization Chemistry.

Having identified beads with suitable size ranges and optical properties, the next materials selection stage involves consideration of the protein immobilization characteristics. To compare the effectiveness of several methods used to immobilize capture antibodies onto the polystyrene, PS/PEG and agarose beads, purified mouse antibody (mouse IgG) is immobilized to the beads using established procedures.^{136,137} The degree of protein loading is subsequently evaluated by using a general protein indicator (Coomassie protein stain) to visualize the amount of protein. The protein immobilization strategies here examined include: 1) the physical adsorption (PA) of

protein directly to the surface of the unmodified polystyrene beads; 2) covalent linkage of the amine-containing protein to amine-functionalized PS/PEG or agarose beads via the glutaraldehyde cross-linking reagent (Glut); and 3) the covalent linkage of the amine-containing protein to aldehyde-functionalized cross-linked agarose beads using reductive amination procedures (RA). Color photomicrographs are provided in Figure 3.3 showing the Coomassie stained beads after the immobilization of mouse IgG. Separate control tests are performed prior to the protein staining procedure to confirm that only the mouse IgG and not the bead material itself is stained by the protein indicator (data not shown). Additionally, Table 3.1 provides information relating the degree of protein immobilization as indicated by the effective absorbance of the protein indicator.

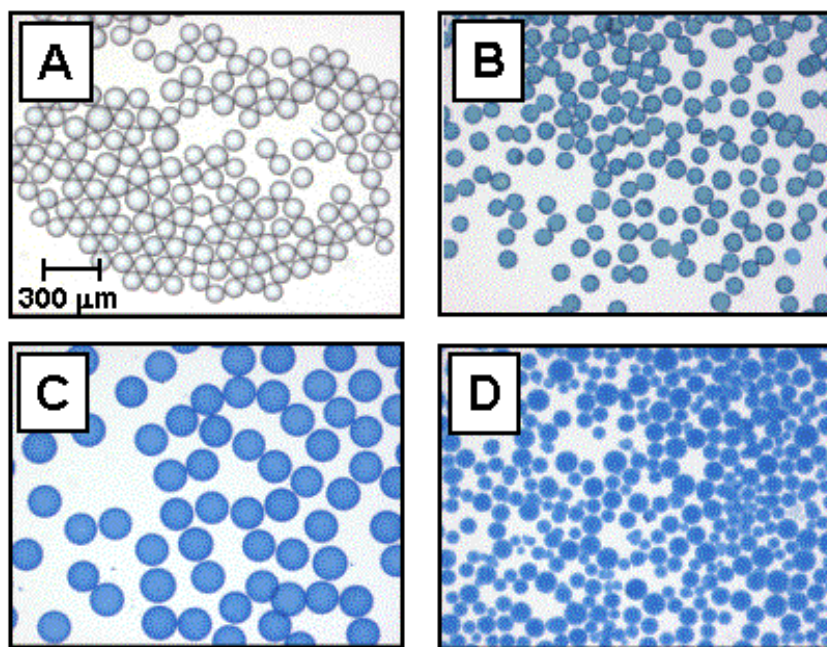


Figure 3.3: Evaluation of protein-to-bead coupling chemistries. The degree of protein loading of various protein immobilization procedures was evaluated on 4 different bead types by using a general protein indicator. Here, Coomassie protein stain was used to reveal the amount of mouse IgG bound to the bead matrix after the coupling procedure. The protein immobilization procedure used for each bead type is as follows: A) physical adsorption of mouse IgG onto the surface of polystyrene beads, B) covalent linkage of amine-containing protein to amine-functionalized PS/PEG via the glutaraldehyde cross-linking reagent, C) the covalent linkage of amine-containing protein to aldehyde-functionalized agarose beads using reductive amination, D) covalent linkage of amine-containing protein to amine-functionalized agarose via the glutaraldehyde cross-linking reagent.

As revealed by the protein indicator, the physical adsorption of the mouse IgG onto the surface of the unmodified polystyrene beads is uniform throughout the surface of individual beads and consistent within the population of beads shown in Figure 3.3A. However, the low effective absorbance value (0.052) indicates that only a low density of protein adsorption occurs here. This observation is most likely due to the limitation of protein binding to the outer surface of the polystyrene bead. Water permeation, and thus protein penetration from aqueous samples, into the interior region of the polystyrene matrix is generally limited to the outer surface of the beads.^{19,142} Consequently, use of such beads would be expected to result in surface localized analysis as is common in

ELISA and other microarray methodologies^{6,75,154} thus preventing the acquisition of the full advantages of a bead-based assay described above. These issues point to the importance of selection of a bead matrix that readily allows the penetration of immunoreagents into the 3-dimensional regions of the bead.

On the other hand, previous studies have established the utility of PS/PEG beads for use in applications which require small molecule and dye penetration in the central region of these beads.¹¹¹ Likewise, the use of the PS/PEG matrix is included in these evaluations where both the amine- and carboxylate-functionalized form of the material is used with the glutaraldehyde and carbodiimide protein immobilization chemistries, respectively. Coomassie staining of PS/PEG beads reveal that the protein immobilization procedure using the glutaraldehyde cross-linker provided a moderate protein loading (Abs=0.24). However, the immobilization of protein to the COOH-PS/PEG matrix using the carbodiimide coupling chemistry is found to be rather ineffective as indicated by low absorbance of the protein stain (Abs=0.074). Possible reasons for the lower protein immobilization efficiencies include the lack of penetration of protein throughout the PS/PEG matrix and use of non-optimized protein-coupling procedures. Previously, similar carbodiimide coupling procedures have been used to anchor a number of low molecular weight receptor and signaling agents to PS/PEG. Likewise, the high molecular weight restriction appears to be the more plausible explanation currently for the lack of protein immobilization to the matrix. Further studies are needed, however, to define this issue more conclusively.

Interestingly, the protein immobilization procedure using reductive amination on aldehyde-functionalized agarose beads reveal a deep blue staining (Abs=0.40) compared to the polystyrene beads. This behavior suggests a uniform protein loading is formed consistent with immobilization into the bead interior region as shown in Figure 3.3C. Similarly, the protein immobilization procedure using the glutaraldehyde cross-linker with the amine-functionalized agarose beads is very effective at protein loading (Abs=0.56). However, these beads are exceedingly polydisperse in size and exhibit

inconsistent protein loading levels as illustrated by the variation of blue color intensity shown in Figure 3.3D.

Collectively, the protein immobilization efficiencies as visualized by the presence of protein indicator suggests the reductive amination of protein to the aldehyde-functionalized agarose matrix to be the most effective combination of bead matrix, chemical functionality, and protein coupling chemistry. Furthermore, initial work with this material reveals that it has negligible non-specific protein binding effects and a high protein binding capacity, observations consistent with the findings of others.^{148,150}

3.3.4 Bead-based Immunoassay Detection Schemes.

Having down selected to appropriate matrices and protein conjugation methods, it becomes important to define signal generation methodologies as well as quantify non-specific biological background issues. To evaluate the detection schemes that are most appropriate for colorimetric and fluorescence bead-based immunoassays, soluble and precipitable colorimetric signaling strategies as well as fluorescent methods are evaluated for both the aldehyde-functionalized agarose and unmodified polystyrene beads. The polystyrene beads are included here to serve as a useful reference for the analogous planar approaches. Because the polystyrene beads possess spherical shape, their exterior protein immobilization provides a useful reference for the surface approaches. As depicted in Figure 3.1C, mouse IgG is physically adsorbed or covalently linked to the polystyrene or agarose beads, respectively. A rat anti-mouse IgG detecting antibody specific for the immobilized mouse IgG protein is used in conjunction with its direct conjugation to either a fluorophore or the enzyme horseradish peroxidase (HRP). For the latter, upon the addition of peroxide, the HRP readily converts an uncolored chemical substrate into its colored analog. The enzyme is used here with the precipitable substrate, 3-amino-9-ethylcarbazole (AEC), or the soluble substrate, 3,3',5,5'-tetramethyl benzidine (TMB).

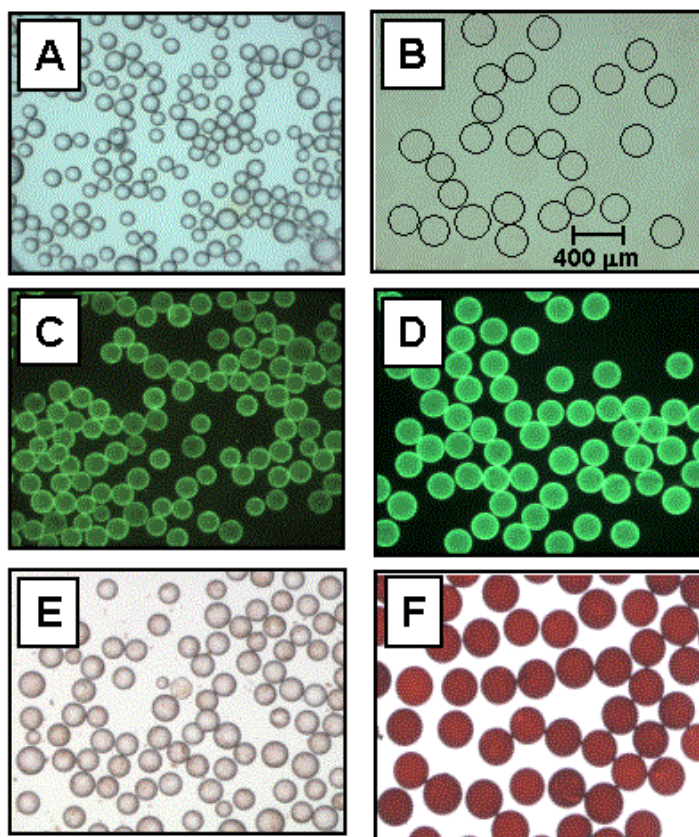


Figure 3.4: Bead-based immunoassay detection schemes. To compare the protein loading capacity of polystyrene vs. agarose beads, mouse IgG is adsorbed onto the polystyrene beads and covalently linked to the aldehyde-functionalized agarose beads using reductive amination. Similar volumes of each bead type was placed in adjacent wells of a microtiter plate where the amount of mouse IgG protein immobilized to the beads was measured by using an enzyme-labeled detecting antibody and an enzyme-catalyzed soluble chromophore. The degree of color development was monitored for the polystyrene (A) and agarose beads (B) and was observed to be much darker for the agarose beads. To evaluate the signaling strategies most appropriate for optical bead-based immunoassays, precipitable colorimetric and fluorescence detection schemes were evaluated for both the polystyrene and cross-linked agarose beads. The mouse IgG protein was detected with a fluorophore-labeled detecting antibody and is shown for the polystyrene (C) and agarose beads (D). Similarly, the protein was detected using an enzyme-catalyzed precipitable chromophore for the polystyrene (E) and agarose beads (F).

To demonstrate the effect of using soluble chromogenic substrates in bead-based assays, the signal generating capabilities of the bead-based IgG immunoassays is examined inside the confines of a microtiter plate well (300 μ L total well volume). Similar volumes of the agarose and polystyrene beads are each distributed into separate wells and the presence of detecting antibody is probed with a fixed volume of TMB.

Figure 3.4A and B shows the results of these experiments where the catalysis of clear to colored substrate is more pronounced for the agarose beads compared to the polystyrene beads (measured absorbance of the solution with polystyrene and agarose beads is 0.05 and 0.16, respectively). The larger signal response is consistent with a greater concentration of HRP-labeled detecting antibody associated with the agarose beads. While these experiments lend some information related to signal generating capacities of the various approaches, the use of a soluble substrate is not practical in the electronic taste chip approach as the colorant is rinsed away from the analysis chambers during the normal course of the assay.

The use of fluorescent or precipitable colorimetric signaling schemes is, however, more appropriate for the taste chip approach. As further illustrated in Figure 3.4 C and D, when probed with the fluorophore-labeled detecting antibody, the polystyrene beads are moderately fluorescent and reasonably consistent in signal intensity. On the other hand, the fluorescent-probed agarose beads are very consistent in signal intensity and are nearly 2× brighter compared to the fluorescent-probed polystyrene beads (S/N=5.9 vs. 2.8 for the agarose and polystyrene beads, respectively) suggesting that more signal generating detecting antibody is present.

In the evaluation of the precipitable colorimetric signaling scheme, the polystyrene beads are lightly (corrected Abs=0.052) and sporadically covered with the reddish-brown precipitated AEC substrate as shown in Figure 3.4 E. Furthermore, small “flakes” of particulate matter can be recognized at higher magnification on the bottom surface of the microscope slide indicating that the precipitate has detached from the hard surface of the polystyrene. The agarose beads, on the other hand, have a much darker (corrected Abs=0.70) and consistent staining. The liquid-phase colorimetric reagent appears to penetrate deeper into interior region of the bead and the ensuing insoluble chromophore becomes effectively trapped within the porous agarose matrix as it precipitates. Accordingly, the “molecular scaffold” constructed by the penetrable 3-dimensional structure of the agarose bead matrix significantly enhanced the light

attenuating capabilities of the model colorimetric immunoassay. This feature serves to increase the sensitivity of analytical measurements in the bead-based immunoassays as performed here (see below). The agarose bead matrix also produces a much more pronounced fluorescent signal than, for example, the single layer of molecular interactions presumably limited by the impenetrable surface of the polystyrene beads. Collectively, these results corroborate the enhanced signaling effects resulting from the increased pathlength that is generated by the penetration of the immuno-reagents into the 3-dimensional scaffold created by the macroporous agarose matrix.

3.3.5 Gel Porosity.

To further isolate the optimized cross-linked agarose matrix, the gel porosity of the agarose matrix is also investigated. Agarose gel porosity is a continuous function of the agarose concentration used during bead formulation affecting both the molecular sieving properties and the gel strength of the material. As the agarose concentration of the gel formulation increases, the gel's mechanical strength also increases.¹⁵¹ However, the molecular fractionation range exhibited by the bead formulation decreases with increased agarose concentration. To explore the effect of various agarose concentrations on the physical and analytical characteristics of the bead-based immunoassays used here, experiments are performed to probe these features on separate bead samples of various agarose gel formulations. Here, aldehyde-functionalized beads of cross-linked agarose in 1, 2, 4, 6, 8, 10, and 12 wt/vol % agarose concentrations are tested using the fluorescent-based model immunoassay depicted in Figure 3.1A and visualized on microscope slides using epi-fluorescence microscopy. The results reveal (data not shown) that the 1 and 2%, and to some degree the 4%, agarose formulations exhibit very little gel mechanical strength as illustrated by the fact that many of the beads are amorphous and non-spherical in shape. The 8, 10 and 12% formulations are spherical in shape, but produced only a nominal fluorescent signal in the model immunoassay suggesting a restriction in the penetration of the immunoreagents. The beads of the 6% agarose formulation, however, are sufficiently spherical in shape and displayed the brightest fluorescent signal in the

immunoassay. As a result, the 6% cross-linked beaded agarose are identified as an optimized formulation. Further, the 6% wt/vol agarose concentration exhibits a protein fractionation range suitable for the majority of the protein analytes investigated here (see discussion of protein penetration below).

3.3.6 Protocol to Minimize Bead Variability.

In the early developmental stages of the electronic taste chip methodology, 6% cross-linked agarose beads were purchased pre-activated with reactive aldehyde functional groups ready for capture protein immobilization. However, a close examination of a population of these beads reveals significant variations in size and chemical reactivity. Since the development of the taste chip methodology seeks to provide miniaturized and multiplexed bioassays for bio-analytical and medical diagnostic applications, it is essential to minimize all sources of potential assay variability. Undeniably, a considerable source of variation is revealed in the batches of pre-activated beads as purchased from the commercial source. Figure 3.5 column I presents data showing the variation in bead size, shape and immunological reactivity of the pre-activated commercial source of agarose beads as investigated by the fluorescent-based mouse IgG immunoassay. Size measurements of a population of the pre-prepared beads, indicated a coefficient of variation (CV) of 28% in diameter. Furthermore, the fluorescent intensity measurements of the completed fluorescent immunoassay reveals a CV of 61%. While this variation in size and immunological reactivity may be tolerable for the packed columns used in size exclusion and affinity chromatographic separations, the nature of taste chip bioassays emphasizes the individuality of each agarose bead. Thus, the intra-assay (bead-to bead) and inter-assay (run-to-run) variation would be intolerable. To remedy this problem, a protocol is developed to generate a highly selected population of beads with a minimal deviation in size. Here, beads are obtained in their native form (i.e. no added functionality) so that the appropriate optimized chemical reactions could be performed to deliver a series of highly reactive beads with minimal variability in chemical and thus immunological reactivity.

In brief, the non-functionalized agarose beads are coarsely separated within a functional size range by use of graded particle sieves. These beads are then further sorted in a computer-aided bead-sorting unit that delivers highly selected bead populations

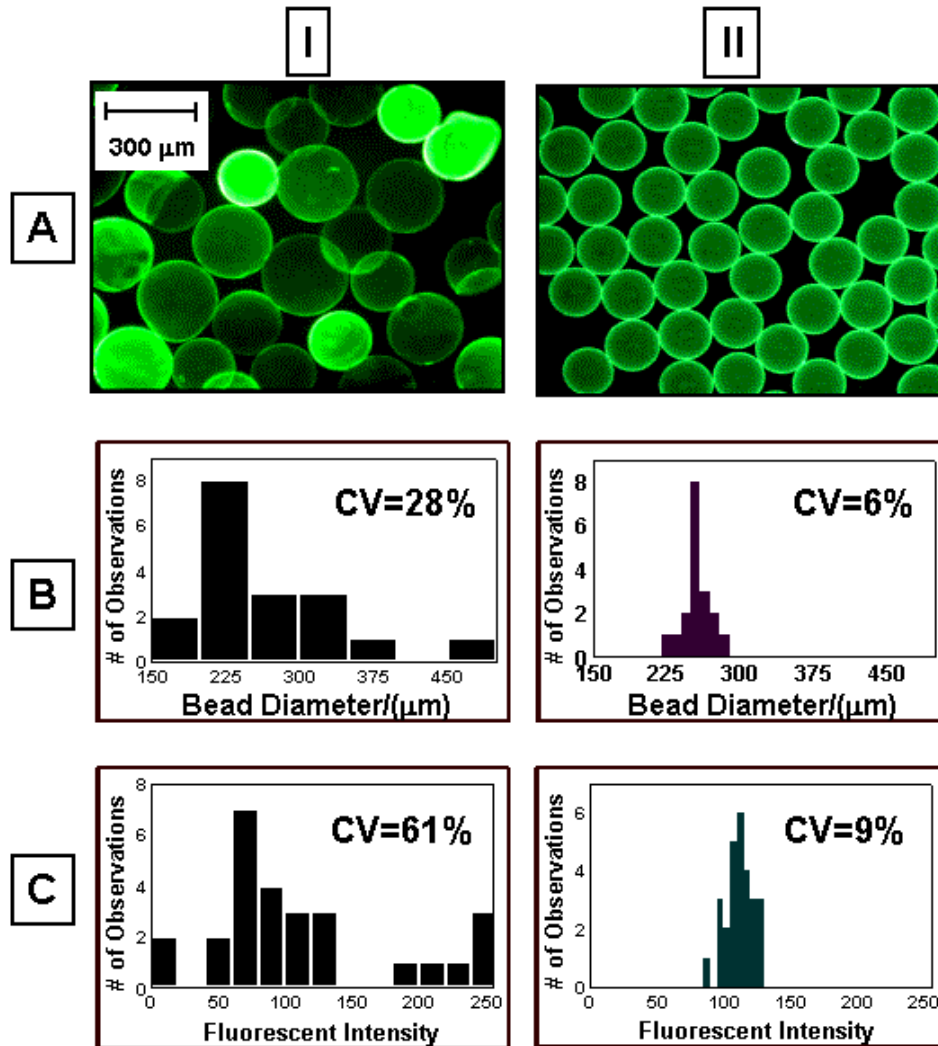


Figure 3.5: The size distribution and immunological reactivity variability of a commercial source of cross-linked agarose beads (Column I) is compared to beads that have been size sorted and chemically functionalized in-house (Column II). Row A presents images acquired by the CCD camera depicting both the variation in size and immunological reactivity of a fluorescent-based mouse IgG immunoassay. Row B presents data demonstrating the variation in bead diameter while row C illustrates the variation in fluorescent intensity of the bead-based immunoassay.

based on user-defined criteria. These beads are then chemically modified by procedure adapted by Shainoff where glycidol is used to introduce adjacent hydroxyl groups within the saccharides of the polymerized agarose.¹⁵³ This added functionality is then oxidized by sodium meta-periodate to form aldehyde groups suitable for the reductive amination coupling of the amine-containing protein. Moreover, the proportions of chemical reagents and procedural details are optimized to provide the highest immunological reactivity and lowest variation in the model fluorescent immunoassay. For example, beads sorted and activated in-house are shown in Figure 3.5 column II where the fluorescent mouse-IgG immunoassay is used as a signaling scheme. The variation of the diameter of this population of beads was ~6% as defined by the bead-sorting procedure. Importantly, the intra-bead fluorescent intensity variation has been reduced from 61% to 9%. Thus, the in-house bead sorting and activating protocol decreased the variation in bead size and reactivity by almost 7-fold. Furthermore, the average fluorescent intensity values of the immunoassay performed using the population of beads that had been sorted and activated in-house was at least 30% greater (data not shown) than that performed using the material supplied by the vendor. These studies suggest that the chemical reactivity of the aldehyde-containing beads can be controlled to increase the immunological reactivity with minimal variation. As a result, the analytical characteristics of agarose bead-based immunoassays can be influenced, for example, to provide decreased detection limits with improvements in inter- and intra-assay variation (see below).

3.3.7 Integrating the Agarose Beads into the Electronic Taste Chip.

The electronic taste chip approach derives many analytical benefits by localizing the immunologically sensitized beads into the sensor array and using pressure-driven flow as afforded by the external fluid pumps to introduce sample and reagents. This configuration efficiently enables multiplexed analyses with excellent analytical characteristics.¹¹⁹ Following the placement of the sensitized beads into the array, the chip is then encased in an optically transparent flow cell, which serves to immobilize the

beads in the wells of the wafer and to allow for optical analysis. Figure 3.1E represents a cross-sectional diagram showing a bead within a well and the associated fluid flow pattern as delivered by the external pumps. Here, the fluids are first directed into an upper reservoir of the flow cell and then forced down through the well to a lower reservoir (~50 μ L total exchange volume) and finally out to waste. Thus, the bead sensors are continuously exposed to a steady stream of sample and reagents. Flow rates up to 5 mL/min are common used for flow cells housing the smaller array sizes (i.e. 3×4 .) and up to 10 mL/min for larger arrays (i.e. 5×7 , 10×10 , etc.)

The ultimate utilization of the agarose immunosensors in the sensor array is also investigated here using a standard protein capture immunoassay. Here the influence of bead diameter on signaling characteristics is evaluated. The spherical diameter of the beads is varied to evaluate the influence of the beads within the confines of the wells on the microfluidic reagent delivery patterns. Small, medium and large populations of beads (~290, 375 and 420 μ m, respectively) are sorted by the computer-aided bead sorter. Individual beads representative of each size population are then placed in adjacent wells of the sensor. Figure 6A and B presents schematics illustrating side and top views, respectively, and the associated space-filling characteristics of each bead size within the well. The objects in the schematics are drawn to scale to represent the true proportions of the bead as it is localized within the well. Clearly, a properly sized bead must be larger than the dimensions of the bottom drain hole (100 μ m square) so it would not be flushed out to waste from the considerable hydrodynamic forces in the flow cell as created by the pressure driven pumps. On the other hand, beads that are too large (>420 μ m diameter) protrude from the top planar surface of the silicon wafer and may be forced to make contact with the upper layer of the transparent plastic flow cell (as shown for the large bead in Figure 3.6A). Over crowded beads result in the disrupted flow of reagents to the “top” surface of the bead where optical interrogation by the CCD is critical. Figure 3.6C is the top-view image of a completed fluorescent immunoassay where each bead size are simultaneously and equally subjected to the forced flow of the fluorescent probe. Figure

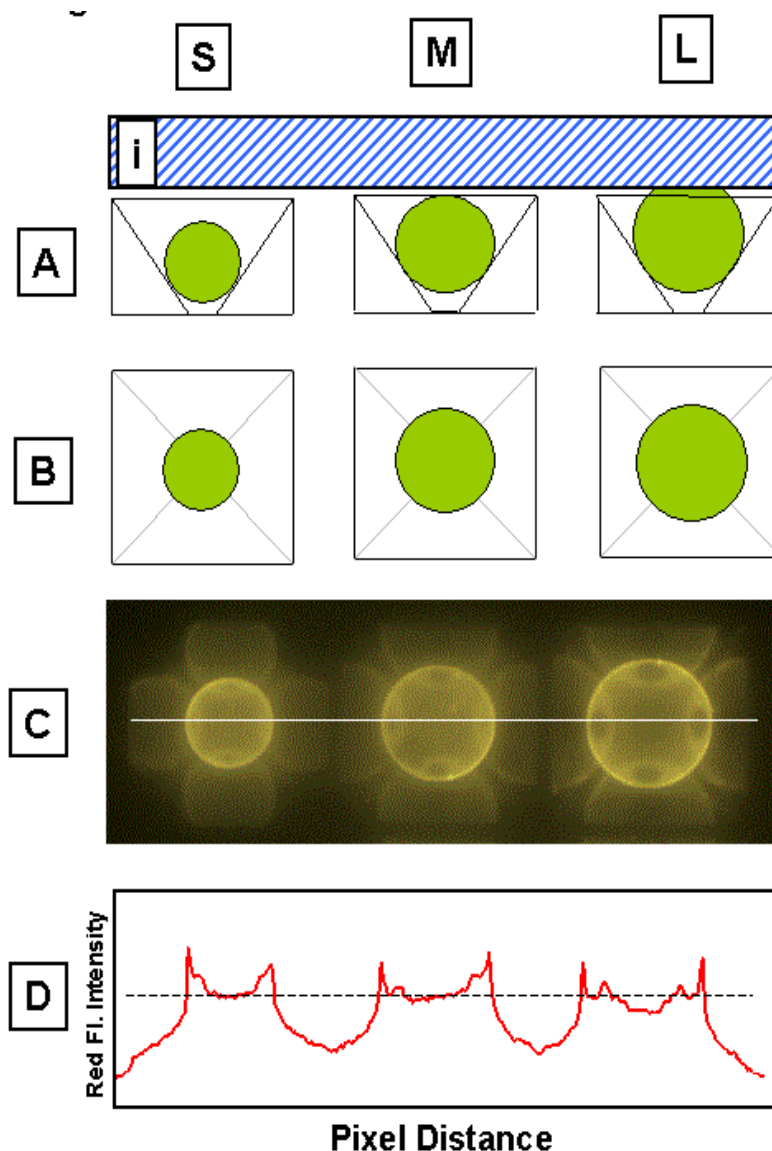


Figure 3.6: The integration of agarose beads into the sensor array is investigated. Populations of beads were sorted into small, medium and large size categories ($S \sim 290 \mu\text{m}$; $M \sim 375 \mu\text{m}$; and $L > 420 \mu\text{m}$). A representative bead from each size category was placed in adjacent wells of the sensor array. Row A illustrates a cross-sectional view of the different sized beads in the confines of the wells. The beads are drawn to scale to represent the space-filling characteristics the beads as they are localized within the wells. In addition, the transparent plastic cover formed by the fluidic flow cell is represented by (i). Note that the large bead was pressed up against the flow cell cover. Row B illustrates the associated top view created from this arrangement. A mouse IgG immunoassay was performed in the flow cell whereby each bead was simultaneously subjected to the same fluorophore-labeled detecting antibody. The associated image of the completed immunoassay is shown in row C. In addition, the line profile across the image is presented in row D. This data depicts the fluorescent intensity as produced according to the 3 bead sizes. Note the dip in fluorescent intensity in the middle of the large bead. This effect is most likely due to the top of the bead pressing against the flow cell thus preventing the flow of reagents.

3.6D is a lateral line profile representing the red pixel intensity as drawn across the 3 beads in the image in Figure 3.6C. Both the top-view image and the line profile reveal that the smallest of the beads, and to some degree the medium sized beads, have the most consistently developed fluorescent signal. This behavior is presumably caused by the more directed flow of immuno-reagent towards the top portion of the beads and may serve to increase reagent penetration effects. The large beads, on the other hand, have a reduced fluorescent intensity as revealed by the “dip” in the line profile. This effect is probably a result of the top portion of the bead being pressed up against the transparent plastic of the flow cell. Thus, fluid is directed to the sides and around the beads inhibiting the fluorescent development. Consequently, the increased and more uniform fluorescent signal is derived by the smaller beads, beads ranging $\sim 290 \pm 30 \mu\text{m}$. Beads of this diameter are considered the most appropriate choice for use in the current generation fluidic cell of the sensor array (wafer thickness $280 \mu\text{m}$).

3.3.8 The Characterization of Superporous and Homogenous Agarose Beads.

As outlined above, the sorting and activating procedures performed on a bulk source of 6% cross-linked agarose beads are used generate a consistent supply of uniform and reactive beads. However, to fully derive the benefits from the capacity of the agarose matrix to act as a 3-dimensional and biocompatible “molecular scaffold”, beads that contained large macroscopic porous channels are desired. Here, attempts are made to engineer a biocompatible sphere with internal pores that enhance the rate of mass transport of reagents and analyte into the entire volume of the bead. Hence, by optimizing a double emulsification procedure first reported by Gustavsson et. al., agarose beads are produced that fit most, if not all, of the physical, chemical and optical criteria described above. Yet, these new beads are different in that they are characterized by 2 sets of pores: 1) normal diffusion pores characteristic of all polymeric agarose materials including the agarose beads described above (now termed homogenous beads); and 2) very wide pores and channels that allow greater accessibility and penetration of fluidic

flow. Thus, this new type of beads is termed here as superporous beads. Figure 3.7A and 3.7B present scanning electron micrographs of both the homogenous and superporous beads, respectively, at both low and high magnifications. The homogenous beads have

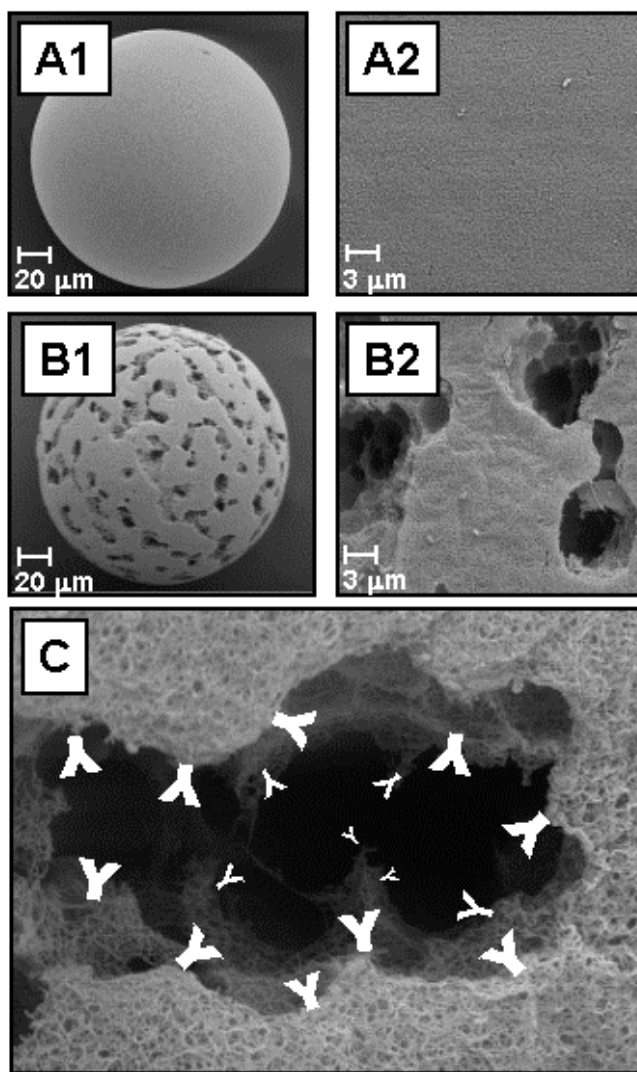


Figure 3.7: Scanning electron micrographs obtained for two types of agarose beads. Low magnification views (315x) are provided for the homogenous (A1) and superporous (B1) beads. Higher magnification views (3000x) are also provided for the homogenous (A2) and superporous (B2) beads. The schematic elements in (C) suggest possible interactions that serve to increase analyte and reagent accessibility as created by the channels of the superporous beads. Here, capture antibodies are shown to penetrate into the interior pores of the channels, thereby enabling the permeation of reagents deeper into the porous superstructure.

relatively smooth and uniform surface features compared to the superporous beads. On the other hand, the superporous beads have irregularly shaped pits or channels (5-20 μm) that penetrate into the interior of the bead (see schematic representation in Figure 3.1E and confocal image in Figure 3.8A ii). By design, these pores structures are expected to allow for deeper and more rapid penetration of sample and reagents into the interior region of the bead. The new porous channels should allow the greater penetration of capture proteins to occur during the immobilization procedure and the subsequent greater penetration of soluble reagents during the flow-based assay. Additionally, the porous channels might be expected to improve the mass transfer of reagents, especially in situations where diffusion through the agarose matrix limits the rate of binding of the molecular interactions. The advantages derived from this new feature may be that an increased number of capture molecules are made present which could increase the probability of analyte binding and its subsequent detection by the signaling strategies used here.

To gain a detailed understanding of the agarose bead microenvironment as well as the molecular weight size-dependence of protein diffusion into the agarose interior, the penetration of the immunoreagents of the model CRP sandwich immunoassay for both homogenous and superporous bead types is visualized using confocal microscopy techniques. Figure 3.8 row I provides schematics of the relevant fluorescent immuno-reagents that are used to analyze the penetration effects. Here, CRP capturing antibody (~150 kDa), purified CRP protein (~120 kDa), and HRP-conjugated CRP detecting antibody (~190 kDa) are each labeled with fluorophore and evaluated individually during the bead-based sandwich immunoassay. Figure 3.8 rows II and III provide illustrative confocal images highlighting the medial bead slices of both the superporous and homogenous beads, respectively.

As these images reveal, the penetration of the fluorescent-labeled CRP capture antibody is continuous throughout the full diameter of both bead types. Macro-porous superstructure in the form of meandering channels and deep indentations can be

distinguished in the superporous beads compared to the uniform agarose structure characteristic of the homogenous beads. In addition, the binding of the fluorescent-

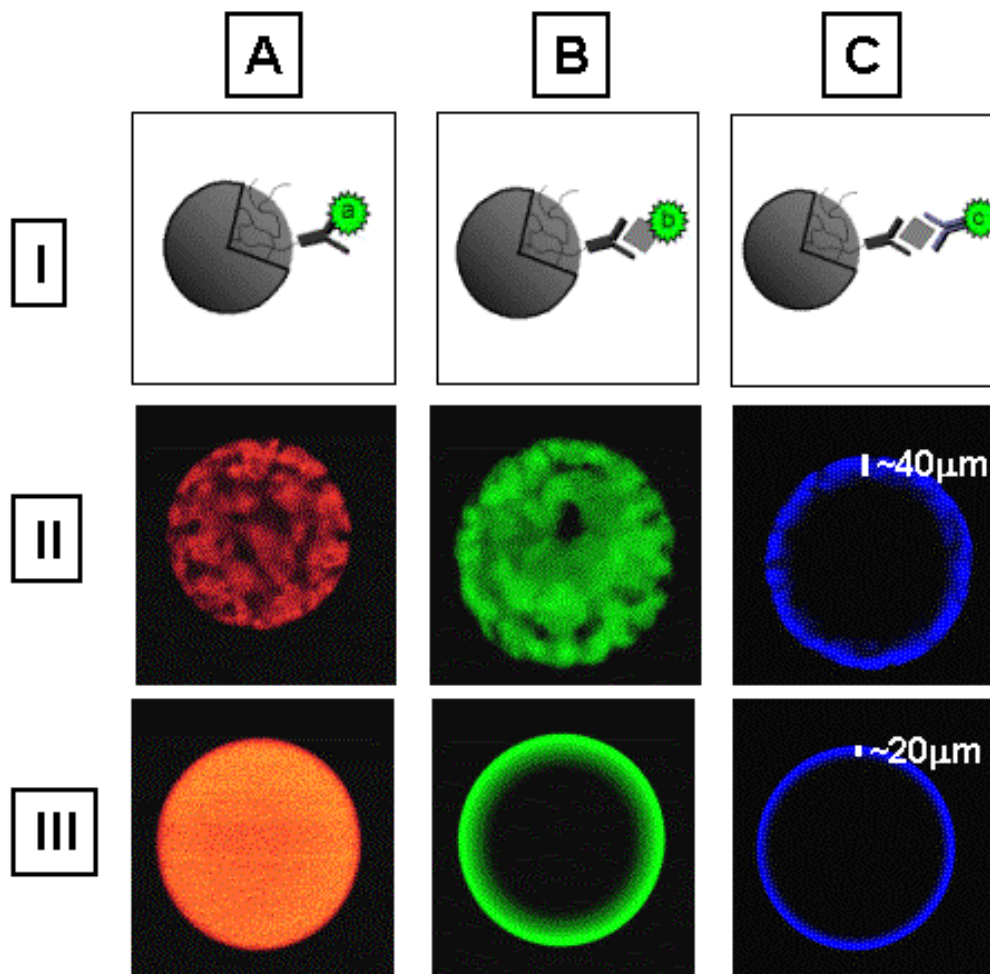


Figure 3.8: To compare the penetration of fluorophore-labeled immunoreagents into the interior regions of the bead, fluorescent medial cross-sectional images of both the homogenous and superporous agarose beads are obtained using confocal microscopy. Row I contains schematic representations of the different immuno-reagents of the CRP sandwich immunoassay used to probe the penetration effects. The images in row II are obtained for the homogenous agarose beads and those provided in row III show the penetration of reagent observed for the superporous beads. Column A shows the penetration of fluorophore-labeled CRP capture antibody (~150 kDa) that occurs during the protein immobilization procedure (total immunocomplex: 150 kDa). Column B shows the penetration of the fluorophore-labeled CRP analyte (~120 kDa) through the beads that had been previously conjugated with unlabeled CRP capture antibody (total immunocomplex: 270 kDa). Column C shows the penetration of the fluorophore and HRP-labeled detecting antibody (~190 kDa) through beads that previously had the immobilized unlabeled capture antibody and bound unlabeled CRP protein (total immunocomplex: 460 kDa).

labeled CRP analyte to the unlabeled capture antibody is observed to penetrate the full diameter of the superporous bead. However, this protein penetrates only through to about the outer third diameter of the homogenous bead. More importantly, the binding of the fluorescent-labeled CRP detecting antibody is observed to penetrate ~40 microns into the superporous bead and ~20 microns into the homogenous bead.

Although these observations confirm the predicted enhanced protein penetrating properties of agarose, the shallow depth that the 460 kDa “full-sandwich” penetrated throughout both bead types is unanticipated. The useable protein fractionation range of agarose beads is commonly reported as a protein fractionation range¹⁵¹ (i.e. 20-1,000 kDa for the homogenous agarose beads used here). In the context of size exclusion chromatography, the penetration of reagents into the outermost region of the bead matrix is all that is required to evoke separation. The fact that 10-20% of the bead exterior region is found to capture the entire sandwich immunocomplex is consistent with this behavior. Furthermore, the 40 μm exterior shell of the homogenous beads leads to an effective signaling pathlength of ~ 80 μm (~40 μm for the homogenous beads) when the appropriate collection optics are used. With further optimization of the pore structure, more complete usage of the entire bead volume is expected. While large improvements in the analyte mass transport effects are observed with the superporous matrix, some restricted diffusion may prevent complete penetration of immuno-reagents into the bead interior during the time course of the assay. Further improvements in analyte permeation are expected upon optimization of pore characteristics.

3.3.9 Comparison of Assay Characteristics of Homogenous and Superporous Agarose Beads.

In addition to the intrinsic interest of protein penetration, it becomes interesting to explore the cause and effect of bead microreactor pore engineering on observed immunoassay analytical characteristics. Dose-response data for the CRP antigen capture immunoassay, where both the homogenous and superporous bead-types are used

independently in the sensor array is obtained using the procedures previously reported.¹¹⁹ In addition, the same CRP assay is performed in the wells of a microtiter plate using established enzyme-linked immunosorbent assay (ELISA) methodologies.^{6,155} Including the dose-response data obtained using the ELISA approach allows us to gauge the performance of the bead-based immunoassay to the established and widely used planar solid-phase immunoassay technique. While this topic is covered in detail in Chapter 4, only the limit of detection, dynamic range and the associated variation of the ELISA immunoassay will be discussed here.

Figure 3.9 compares the CRP dose-response binding curves using the superporous agarose and homogenous agarose beads (plots A and B, respectively). The data for each plot has been normalized to its associated saturated absorbance value induced at high analyte concentrations. The limit of detection determined at 95% confidence is 1 ng/mL CRP for the homogenous bead-based assay and 0.1 ng/mL CRP for the superporous bead-based assay. In addition, the limit of detection using the same confidence level is 10 ng/mL CRP using the ELISA method. Likewise, compared to ELISA, the homogenous bead-based assay had a 10-fold decrease in limit of detection while the superporous bead-based assay exhibits an impressive 100-fold decrease in the limit of detection.

Clearly, the 3-dimensional microenvironment created from the porous agarose bead matrix plays an important role in the observed high quality analytical characteristics. Another important related feature to consider here is that high density of capture antibodies within the bead matrix may result in increased avidity effects of the antibody-antigen binding interaction (i.e. increased probability of bivalent binding events due to the 2 equivalent binding regions typical of the antibody structure).¹⁵⁶ In addition, re-association events (i.e. the re-binding of immuno-reactants that had previously dissociated) are more likely as the dissociation of bound analyte quickly re-binds with the highly localized capture antibody. As a result, the effective ratio of bound to free analyte is increased. In the planar method, however, the capture antibody is limited to a

monolayer on the surface of polystyrene and the increased bivalent interactions and re-association events are not as likely to occur as is the case with the agarose matrix.

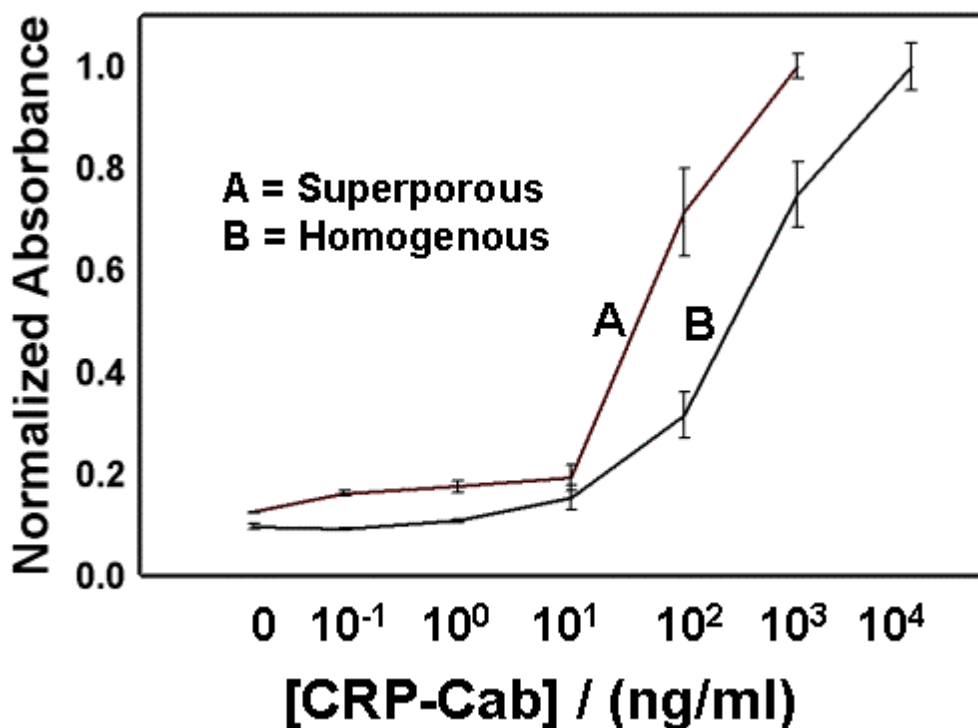


Figure 3.9: Dose-response plots are shown for the CRP sandwich assays completed with superporous and homogenous beads. Plot A is the CRP dose-response curve performed with superporous beads with a limit of detection of 0.1 ng/mL CRP (95% confidence). The assay range ($\sim 0.1 - 1,000$ ng/mL CRP) spans ~ 4 orders of magnitude in analyte concentration before saturating.^x Plot B is the dose-response for the homogenous beads which exhibit a limit of detection of 1 ng/mL CRP. The assay range ($\sim 1 - 10,000$ ng/mL CRP) also spans ~ 4 orders of magnitude before saturating.

The data from Figure 3.9 also illustrates that both the homogenous and superporous bead-based assays exhibit an extended dynamic range compared to the microplate-based assay. Generally, the dynamic range of an immunoassay is considered to extend between 10-90% saturation of the antibody used. This is typically equivalent to 2-3 orders of magnitude in analyte concentration in a conventional immunoassay^{103,157} and is confirmed by the microplate-based CRP assay (data not shown). On the other hand, the dynamic range of the CRP assay using the homogenous agarose beads extends

over 4 orders of magnitude. The range is extended by an order of magnitude in concentration on both the upper and lower limits in concentration compared to the microplate assay. A possible explanation for the expansion of the high concentration side may be due to the heterogeneity in the affinity of capture antibody (and detecting antibody) for the CRP antigen. At the low concentration end, the high immobilization density characteristic of the agarose bead can allow the higher affinity interactions to persevere the vigorous washing due to the bivalent binding of the analyte as transport effects would tend to wash away and thus decrease the more prevalent monovalent interactions characteristic of ELISA.¹⁰³ Indeed, dynamic ranges extending 4-orders of magnitude have been reported for other bead-in-channel methodologies.^{81,103} Interestingly, this attribute becomes even more profound with the superporous bead-based assay and its 100-fold decrease in limit of detection compared to the microplate assay.

Furthermore, another factor that may serve to lower the detection limits of the bead-based assays are the decreased background readings. This attribute is likely due to the inefficient washing procedure common to microplate immunoassays where only 3-4 microwell volumes are exchanged in a typical wash sequence. In contrast, the lower baseline reading for the homogenous and superporous beads may be the result of the more efficient flow-through wash sequence of the taste chip approach where >4,000 exchange volumes occur throughout a typical wash sequence.

3.4 CONCLUSIONS

In summary, materials considerations are explored in this chapter in the context of the selection of bead-based microreactors for use in the electronic taste chip system. Here, 7 different bead types are evaluated with attention paid to optical transparency, fluorescence background, bead size variability, chemical activation, protein conjugation efficiency and bead mechanical strength. While polystyrene is found to be suitable for surface analyses, enhanced assay sensitivity is derived from agarose beads where the internal volume of the beads can be utilized. With engineering of pores into the same

matrix, a more complete utilization of the bead interior region is demonstrated even for full immunocomplexes with molecular weights exceeding 450 kDa.

The process-of-elimination approach discussed above presents a rational method for eliminating the DVB-PS, PS-PEG, PEGA, and PS polymeric bead matrices as candidates for use as the solid-phase in the electronic taste chip methodology. The macroporous agarose beads, on the other hand, exhibited many of the predefined target attributes desired here. For example, the cross-linked agarose beads: 1) are hydrophilic and compatible with a diversity of biological and molecular targets used in taste chip sensing schemes-i.e. DNA/ RNA oligonucleotides¹²², enzymes¹¹⁸, antibodies (see Chapter 4), proteins¹¹⁹, biological toxins, bacterial spores, hemocytes, etc. 2) the beads exhibits negligible non-specific protein or reagent binding effects, 3) the beads facilitate the convenient immobilization of capture protein using simple and established coupling chemistries, 4), they are nearly optically transparent and exhibit minimal fluorescent background readings, 5), they exhibit excellent mechanical stability in conditions of high fluid flow rates and hydrodynamic pressures created by the external fluidic pumps, 6) they possess a porous infrastructure allowing the penetration of biological and chemical reagents, and 7) they are commercially available with no chemical functionality added enabling highly specialized sorting and activation procedures to be performed in-house.

Furthermore, in contrast to ELISA and other planar array techniques where antigen-antibody interactions are built up and limited to a single layer on the bottom surface of the polystyrene microplate well or glass slide^{132,158,159}, the taste chip total analysis system benefits from using the 3-dimensional structure of porous beads. The internal volume of the bead is used as a reaction vessel that serves as the physical structure to support and confine the antigen-antibody interactions. Furthermore, this feature allows for the use of thicker layers of the capture and signal generating agents allowing for the production of larger signals. Finally, the ability to complete a full assay at each site of the sensor array allows for the simultaneous analysis of multiple targets. This capacity is advantageous for use in protein profiling, chemical and biological

warfare agent detection, and medical diagnostics¹¹⁹ and complements well with other multi-analyte detection methodologies.^{160,161}

In the next chapter, focus will be placed on the evaluation of the bead-based immuno-analytical characteristics. Furthermore, these characteristics are compared in even more detail relative to the ELISA technique.

CHAPTER 4: A COMPARISON OF BEAD-BASED IMMUNOASSAYS USING THE ELECTRONIC TASTE CHIP APPROACH TO CONVENTIONAL MICROTITER PLATE-BASED ELISA

4.1 INTRODUCTION

Having identified important materials considerations related to the taste chip approach, emphasis is now placed on establishing a firm understanding of the details related to the bead-based analytical characteristics. In addition, this chapter reviews recent developments in immunoassay techniques and seeks to establish firmly the taste chip approach within the field.

Solid-phase immunoassay techniques, which exploit the highly specific binding interaction of antibodies to their respective target molecules, are a standard tool for disease diagnosis.¹ First generation solid-phase immunoassays are based on the use of microtiter plates and are described as enzyme-linked immunosorbent assays (ELISAs). The heterogeneous immunoassay technique, in which one of the reactants is immobilized to the solid-phase surface of the microtiter plate well, enables the unbound reactants to be efficiently washed away. This now standard methodology is used extensively in the clinical diagnostic settings as well as in the scientific studies for a number of disciplines¹⁵⁵ due to its high selectivity and sensitivity. However, conventional microplate-based ELISA methodologies require large sample volumes, long reagent incubation times and trained personnel to perform the highly repetitive and error prone reagent transfer and washing procedures. In addition, these plate-based techniques do not lend themselves to parallel (i.e. multiplexed) analyses, but rather necessitate the completion of numerous serial tests resulting in proportionate increases in reagent and labor expense.¹⁷

To circumvent these problems, the normal practice in many modern hospital laboratories and medical diagnostic clinics is to batch process specimens and test the samples by ELISA or by analogous closed automated processors.⁵¹ While the turn-

around time to obtain the results of conventional immunological tests at some hospital settings with integrated testing facilities is now as short as a few hours, the same tests completed at remote satellite physician clinics often takes many days to receive the test results. Today's managed health care systems target the goal that patients be diagnosed quickly and efficiently at the point-of-care (POC) (i.e. physician's offices, student health clinics, satellite walk-in clinics, etc.).¹⁶²⁻¹⁶⁴ Unfortunately, the time lapse associated with remote site testing leads to delayed treatment and increases the probability of the patient transmitting the disease. Clearly, the ability to perform immunological assays at the POC and being able to rapidly obtain the results would enable better patient management decisions, improved patient outcome, and would lead to a reduction in the overall cost of care. In an attempt to overcome some of these deficiencies and delays associated with the completion of remote site immunoassays, a number of single use devices have been developed that enable simple and rapid testing at the POC.⁴⁸ The majority of these rapid immunoassay formats use latex agglutination,^{35,40} membrane-based horizontal, and tangential flow-through devices.^{48,49} However, these assays often are not as sensitive as conventional microplate-based ELISA. Further, the membrane-based flow-through devices require large sample volumes and sometimes become clogged with sample matrix components.^{48,49}

In response to the need for more rapid and thorough immuno-analyses, several innovations to the first generation of immuno-analytical methodologies have been developed. Likewise, a second generation of immuno-analytical methodologies has evolved whereby protein arrays within the individual wells of the microtiter plate are used. This adaptation allows for simultaneous detection of multiple analytes at individually addressable sites.^{128,129,154} The advantage of the microarray approach is the possibility of massive parallel measurements, hence minimizing analysis cost and times. Protein microarrays⁶⁹ have been demonstrated on a variety of surfaces such as glass slides,^{65,154} polystyrene,⁶⁸ membrane filters,^{64,66,70} and in the 3-dimensional matrix of polyacrylamide gel pads⁷⁶ and coated glass slides.^{133,134} In addition, a portable "array biosensor" has been demonstrated by Ligler and coworkers that uses a glass microscope

slide as an evanescent waveguide that allows for the simultaneous detection of bacterial, viral and protein analytes.⁷¹

Protein microarrays on glass and polystyrene surfaces have a history of being problematic for assay optimization and Butler et. al. have reported that >90% of monoclonal and 75% of polyclonal antibodies are denatured by physical adsorption to polystyrene.^{131,132} In addition, the use of these “planar” microarrays results in small signal generating path-lengths that necessitates either the use of high-powered light sources for their readout or the use of amplification methodologies that serves to lengthen the analysis time.

Additionally, new multiplexed protein analysis methodologies have been developed recently using polymeric microspheres as the solid-phase platform.^{19,81,91} For example, the use of fluorescent encoded sets of polystyrene microspheres (~5 μm diameter) allows for the multiplexed interrogation of immunochemical and DNA hybridization reactions on the surface of the spheres using flow cytometric techniques.⁸⁹ Further, a high-density fiber optic bundle (500 μm) has been developed that contains ~6,000 individually addressable 3-6 μm etched wells capable of housing functionalized microspheres. Applications of these methodologies have been reported for the multiplexed analyses of solubilized odor compounds,⁸⁵ cellular responses of live cells,⁸⁶ haptens and proteins,⁸⁷ and DNA oligomers.⁸⁸ While these methods have afforded sensitive and specific multiplexed analytical characteristics, their sophisticated instrumentation components have limited their use to research and clinical laboratory settings.

A third generation of technological developments have occurred in the solid-phase immunoassay area involving the use of micro-total analysis systems (μ -TAS), or “lab on a chip” devices.^{93,94} These new devices integrate the technological developments in the photolithography, micromachining, microelectromechanical systems (MEMS), and microfluidics arenas for the construction of miniaturized monolithic testing devices. Advantages conferred by these microfabricated systems include a reduction in size and

reagent consumption leading to lower assay costs, shortened analysis times, increased mass transport and improved thermal diffusion.¹¹⁴ Furthermore, these miniaturized systems when fully developed will lend themselves to multiplexed detection themes. Several reports describing the use of μ -TAS devices for immunological analysis have been recently published.^{81,94,114,165,166} For example, Harrison and coworkers described a multichannel microfluidic device for immunoassays.¹²⁵ This device integrated 6 independent mixing, reaction, and separation manifolds that operate in parallel and are used in conjunction with a single-point fluorescent detector that is equipped with a galvanoscanner. Furthermore, electrokinetic flow was used by Qiu et al. to mix antigen, antibody and diluting buffer to generate on-board a set of calibration standards within a microfluidic device.¹⁶⁷ Likewise, Yager and coworkers have developed a rapid diffusion immunoassay using a simple microfluidic device that places fluid streams in contact and allows for the interdiffusion of the assay components and subsequent detection downstream.¹⁶⁸

While numerous important developments have occurred in recent years related to the general area of immunoassays, there remains today important opportunities for the development of an inexpensive portable flow device that facilitates simple, flexible and cost effective testing in the context of multiplexed biomolecular analyses. To this end, we have developed recently a fourth generation detector system that has been adapted now to solid-phase immunoassay testing. The sensor suite uses a flow-based array structure that we have described as an “electronic taste chip” system. The system employs polymer bead microreactors that are combined with photolithographically etched pits and video chip optical analyses in such a manner that allows for the efficient completion of complex multiplexed immunoassays. This configuration results in the generation of a 2-dimensional array of individually addressable sites composed of 3-dimensional objects. Here, the 3-dimensional microreactors are derived from macroporous agarose beads that can be tailored for porosity and capture agent density to allow for the rapid transport of reagents within the structure. In a recent report, an

application of the electronic taste chip approach was demonstrated for the multiplexed immuno-analysis of the human cardiac risk factors, C-reactive protein (CRP), fibrinogen and interleukin-6.¹¹⁹ Previously, the same system has been adapted and optimized for detection of non-protein based analytes such as acids, metal cations, sugars, DNA oligonucleotides, and biological cofactors.^{111,116-118} All of these analyte classes have been detected rapidly and with high quality assay characteristics using the same electronic taste chip approach.

In this final chapter of the dissertation, the scope and utility of the electronic taste chip approach is expanded to include the simultaneous analysis of multiple proteins related to a number of infectious diseases. Furthermore, the analytical characteristics of the new bead-based immunoassay approach are compared to that of conventional microtiter plate-based ELISA. In doing so, both direct and sandwich type immunoassay formats are optimized for both approaches and are performed using identical immuno-reagents and solid-phase capture antibody immobilization densities. The detection limit, dynamic range, intra- and inter-assay variation, and the time course for signal equilibration are determined for the bead-array approach and compared with the characteristics obtained for the conventional ELISA methodology. Finally, a new procedure for the creation of macro-porous agarose microreactors suitable for the completion of ultra-high sensitivity and high selectivity immunoassays is described and their utility in bead-based immunoassays is defined.

4.2 EXPERIMENTAL SECTION

4.2.1 Reagents

The same CRP-specific immunoreagents were used for both the bead- and microtiter plate-based immunoassays. All CRP antibodies were purchased from Accurate Chemical and Scientific Corp. (Westbury, NY). The capture antibody was a rabbit anti-human CRP reagent and the detecting antibody was a horseradish peroxidase (HRP) labeled rabbit anti-human CRP reagent. Purified human CRP antigen was obtained from Cortex Biochem (San Leandro, CA) and was diluted in phosphate-buffered saline (PBS)

pH 7.4. The bead-based precipitable colorimetric signal was developed using the substrate 3-amino-9-ethylcarbazole (AEC) as purchased from Pierce Biotechnology Inc. (Rockford, IL). The microtiter plate-based soluble colorimetric signal was developed using 3,3',5,5'-tetramethyl benzidine (TMB) also obtained from Pierce Biotechnology Inc. For the signal response experiments, normal mouse IgG was obtained from Caltag Laboratories (Burlingame, CA). The detecting antibody, a rat monoclonal anti-mouse IgG₁ was obtained from Biosource International (Camarillo, CA), was used in both the bead-based and microtiter plate-based experiments. For the bead-based experiments, this antibody was conjugated with the fluorophore, Alexa Fluor® 546 acquired from Molecular Probes (Eugene, OR). The microtiter plate-based experiments used the HRP labeled antibody purchased from Biosource International (Camarillo, CA). Homogenous agarose microbeads (200-450 µm diameter) were obtained from Agarose Bead Technologies (Tampa, FL). Agarose powder (type I-B), sorbitan triolate (Span 85), and polyoxyethylenesorbitan monooleate (Tween 80) were purchased from Sigma Corporation (St. Louis, MO). Hexane (mixture of isomers) was obtained from Fisher Scientific (Fair Lawn, NJ).

4.2.2 The Production of Superporous Agarose Beads

Superporous agarose beads were prepared by adapting a procedure previously described.¹³⁹ An agarose solution was prepared by heating ~2 g of agarose in 50 mL of water to 92°C. The solution was stirred slowly and cooled to 62°C. The stir speed was increased to 1000 rpm and a 62°C suspension consisting of 1.4 mL Tween 80 and 20 mL hexanes was added with agitation for 4.5 min. A second 62°C solution consisting of 14 mL Span 85 and 150 mL hexanes was added and mixed for 1.5 min. The stir speed was then reduced to 500rpm and the reaction was cooled to 30°C. The resulting mixture was transferred to a wire screen sieve (W.S Tyler; Mentor, OH) and washed with water. The beads were then washed with a water:ethanol (50%:50%) solution. Particles with diameters ranging from between 250 and 300 µm were isolated with the sieves and

sonicated in the water:ethanol (50%:50%) solution for 30 minutes followed by another rinse with pure water.

4.2.3 Bead Sorting, Activation and Protein Conjugation Steps

To obtain a population of beads that was uniform in diameter, samples of the commercial source of homogenous agarose beads or the freshly prepared superporous beads were size selected using a series of graded sieves. The bead fractions between 250-300 μm diameter were isolated then further sorted using an automated high-throughput particle analysis/sorting instrument (Union Biometrica; Sommerville, MA). The instrument parameters were set to analyze the size distribution of beads and sort the population according to predefined criteria. As a result, a population of beads was obtained with a variation in diameter of ~5%.

A previously reported procedure was adapted and used to generate reactive aldehyde groups within the agarose matrix.¹⁵³ Briefly, a 1.7 mL volume of settled beads of consistent size (2.0 mL total liquid volume) was added to 1.2 mL of a solution made from 10mL 1M sodium hydroxide, 20 mg sodium borohydride and 3 mL glycidol. This mixture was shaken gently for 18 hours followed by washes with copious amounts of water. Next, 0.7mL of a 0.16 M sodium periodate solution was added to the washed beads to achieve a final volume of 3.2 mL. This mixture was gently shaken for 1 hour followed by washes with copious amounts of water. To increase the pH within the bead microenvironment, the beads were rinsed with ~10mL carbonate buffer at pH 9.6. Analyte-specific capture antibodies were then coupled to the aldehyde activated beads via established reductive amination procedures.¹³⁷

4.2.4 Instrumentation

The components of the electronic taste chip analysis system have been described previously.^{111,116-119} Briefly, individual agarose beads were placed into chemically etched cavities patterned in a square array on a silicon wafer chip. The cavities were created by

an anisotropic etch which yielded inverted pyramidal pits with trans-wafer openings. Patterns of these cavities were arranged to create 3×3 , 3×4 , 4×5 , 5×7 , or 10×10 arrays. The chip with positioned beads was then encased into a plastic fluid flow cell that was held together by a stainless steel housing. Solutions were introduced into the flow cell in an automated fashion using an Amersham Pharmacia Biotech ÄKTA high-pressure liquid chromatography system controlled by Unicorn 3.0 software (Amersham Pharmacia Biotech; Piscataway, NJ). The flow cell assembly was positioned onto a microscope stage that allowed for the microscopic observation of the beads from both transmission and epi-fluorescent perspectives. The beads within the silicon array were exposed to sample and signaling reagents using fluid flow that was directed into an upper reservoir of the flow cell and forced through the wells containing the beads. The fluid then was directed into a bottom reservoir leading to an exit drain. The flow cell was designed to ensure that all introduced fluid passed through the various wells of the sensor array. Finally, the wells were observed through the microscope optics, and images were captured using a 12-bit charge-coupled device (CCD) in conjunction with Image Pro Plus 4.0 software (Media Cybernetics; Silver Spring, MD).

4.2.5 Assay Procedures and Data Collection

Dose-response data for the CRP antigen capture immunoassay, where both the homogenous and superporous bead-types were used independently as the solid-phase, was obtained using the following procedure: Prior to each assay, the inner walls of the fluidic tubing, the flow cell and the beads were blocked by delivering 3% bovine serum albumin (BSA) in PBS at a flow rate of 0.07 mL/min for 30 min. A washing step followed using PBS delivered for 2 min at 2 mL/min. For sample delivery, 1% BSA in PBS was spiked with known amounts of purified CRP and delivered to the flow cell at a rate of 0.03 mL/min for 10-60 min. This procedure was followed by another washing step. The HRP-labeled detecting antibody diluted to an optimized concentration was delivered at a flow rate of 0.07 mL/min for 30 min followed by another washing step.

Finally, the presence of captured analyte was detected by delivering the chromogenic and precipitable AEC mixture for 20 min at 0.07 mL/min followed by a washing step for 1 min at 2 mL/min. The CCD camera then captured the image of the beads.

For all bead-based immunoassays, the flow cell was maintained in a fixed position on the microscope stage throughout the duration of the assay. The CCD camera captured images before and after the delivery of reagents. Digital information was obtained by measuring a consistent area of interest (AOI) for the red, green and blue (RGB) intensities. For the bead-based immunoassays that used a fluorescent signaling scheme, the intensity of the channel that most closely matched the fluorophore's emission maximum was quantified. The beads in the colorimetric CRP assays, which utilized the HRP/AEC detection scheme, developed a reddish-brown coloration that was quantified by measuring the blue pixel intensity of the CCD. In this case, the blue intensity after all reagents, I_{After} , was subsequently converted to the "effective blue absorbance" value, A_B , using Beer's law, $[A_B = -\log(I_{\text{After}}/I_{\text{Before}})]$, where the reference blue intensity of the bead before the immunoassay, I_{Before} , was used.¹¹¹

4.2.6 Intra- and Inter-assay Variation Studies

For the dose response data, at least 4 replicate beads for the CRP assay were included within the array from which the mean absorbance was calculated for the zero CRP-background sample. The limit of detection was defined as the lowest CRP concentration yielding an average absorbance reading at least 2 standard deviations above the mean value recorded for the zero analyte trials. Intra-assay variation was calculated by averaging the coefficient of variation (CV) of the absorbance from 4 replicate trials at each of 8 different CRP concentrations. The CV was expressed as a percentage and defined as the standard deviation of the absorbance from the 4 replicate trials divided by the mean absorbance then multiplied by 100. The inter-assay variation was calculated by repeating the experiment 4 times at the 10 ng/mL CRP level then calculating the CV from the average absorbance values from all 4 trials.

4.2.7 ELISA Studies

For the microtiter plate-based dose response data, the wells of a Nunc Maxisorp 96-well microtiter plate (300 μ L maximum) were incubated with 100 μ L of an optimized concentration of CRP capture antibody overnight at 4° C. The next morning, the plate was emptied and washed 3-fold with 300 μ L PBS (i.e. the washing step). The plate was then blocked with 300 μ L of 3% BSA in PBS for 30 min with circular shaking action followed by another washing step. The same purified CRP dilutions as used for the bead-based assay were used here and incubated with shaking for 1 hour. This procedure was followed by another wash sequence. Next, 100 μ L of the HRP-labeled detecting antibody diluted to the optimized concentration was incubated in the wells with shaking for 30 min. Finally, the presence of captured analyte was visualized using the soluble TMB substrate using the standard procedures provided by the vendor. Then absorbance values were measured in a SPECTRAmax[®] Plus Microplate Spectrophotometer (Molecular Devices; Sunnyvale, CA).

For these experiments, the average of 4 replicate trials of the zero CRP-containing sample was used to determine the limit of detection as defined above. The intra- and inter-assay variation was evaluated in the same manner as the bead-based immunoassay as described above.

4.2.8 Bead Characterization

To insure the selected bead populations did not produced unwanted imaging artifacts within the silicon chip cavities, the beads were measured outside the chip in control studies and found to exhibit the correct spherical diameters as allowed by the dimensions of the cavities. Thus, the beads could be imaged directly within the chip cavities without optical artifacts (i.e. beads that were too large to fit in the flow cell housing).

To illustrate the penetration of immunoreagents, medial cross-sectional images of beads were obtained on a LEICA (Exton, PA) TCS 4D laser scanning confocal

microscope. Fluorophore-labeled CRP capture antibody was immobilized to both types of beads using the normal reductive amination methods. These beads were then imaged with the confocal microscope to obtain the medial cross-sectional image. Next, beads with unlabeled capture antibody were reacted with fluorophore-labeled CRP antigen and imaged as such. Likewise, beads with unlabeled capture antibody and bound unlabeled CRP antigen were reacted with fluorophore-labeled detecting antibody then imaged. All reagents were allowed to react overnight to minimize diffusion effects.

Scanning electron micrograph images of the plain agarose and porous bead types were obtained on the LEO Model-1530 scanning electron microscope (Carl Zeiss Inc., North America). Bead samples that were previously stored in aqueous solution were prepared for the SEM by exchanging the solvent with ethanol. Then a subsequent solvent exchange was performed with hexa-methyl di-silazane (HMDS) and dried overnight in a dessicator. The samples were then coated with 8 nm of gold and platinum alloy (50:50 by weight) and imaged in the SEM.

4.3 RESULTS AND DISCUSSION

A preliminary assessment of the assay characteristics from a typical microtiter plate-based immunoassay as compared to that of a multiplexed immunoassay performed using the electronic taste chip approach reveals a number of distinct advantages for the latter approach. For example, a single well of a microtiter plate typically requires 50-200 μL of sample volume and measures only one analyte. During the course of an assay, many manual washing/reagent transfer steps are required with sample and reagent incubation times typically lasting 1 to 16 hours.⁶ Here, the rate of the antigen/antibody association is often limited by diffusion of macromolecules to the solid-liquid interface which often leads to the depletion of reactants close to the surface.^{9,169} However, with the electronic taste chip approach, a single 100 μL sample aliquot may be directed over and through a 10×10 array of beads, allowing for the simultaneous measurement of up to 100 analytes. Here, pressure driven flow and recirculation loops allow for the rapid

delivery of reagents and sequestration of analyte at/to the various bead microreactor sites. Automated sample injection, fluid pumping and valve sequencing allows for the elimination of all manual fluid handling steps. Redundant tests can also be performed by loading the bead array with multiple bead replicates to facilitate better analytical characteristics. Finally, the effect of pressure-driven flow serves to minimize diffusional limitations and the opportunity to continuously recirculate sample and reagents allows the efficient delivery of small sample volumes (see below).

The bead-based immunoassay system here studied exploits a series of sensitized agarose microbeads ($\sim 275\ \mu\text{m}$ diameter) that are placed within the micromachined wells of a silicon wafer. Figure 4.1A provides a scanning electron micrograph illustrating a 3×4 array of bead populated micromachined wells. Since an individual bead's selectivity is determined by the specificity of the covalently linked capture protein, beads that are selective for a separate analyte can be placed with known location within each well of the array. Thus, the 3×4 array shown in Figure 4.1A has the capacity to analyze up to 12 different analytes simultaneously. Similarly, 10×10 arrays now prepared routinely by our laboratory using similar methodologies have the ability to detect simultaneously up to 100 different protein analytes.

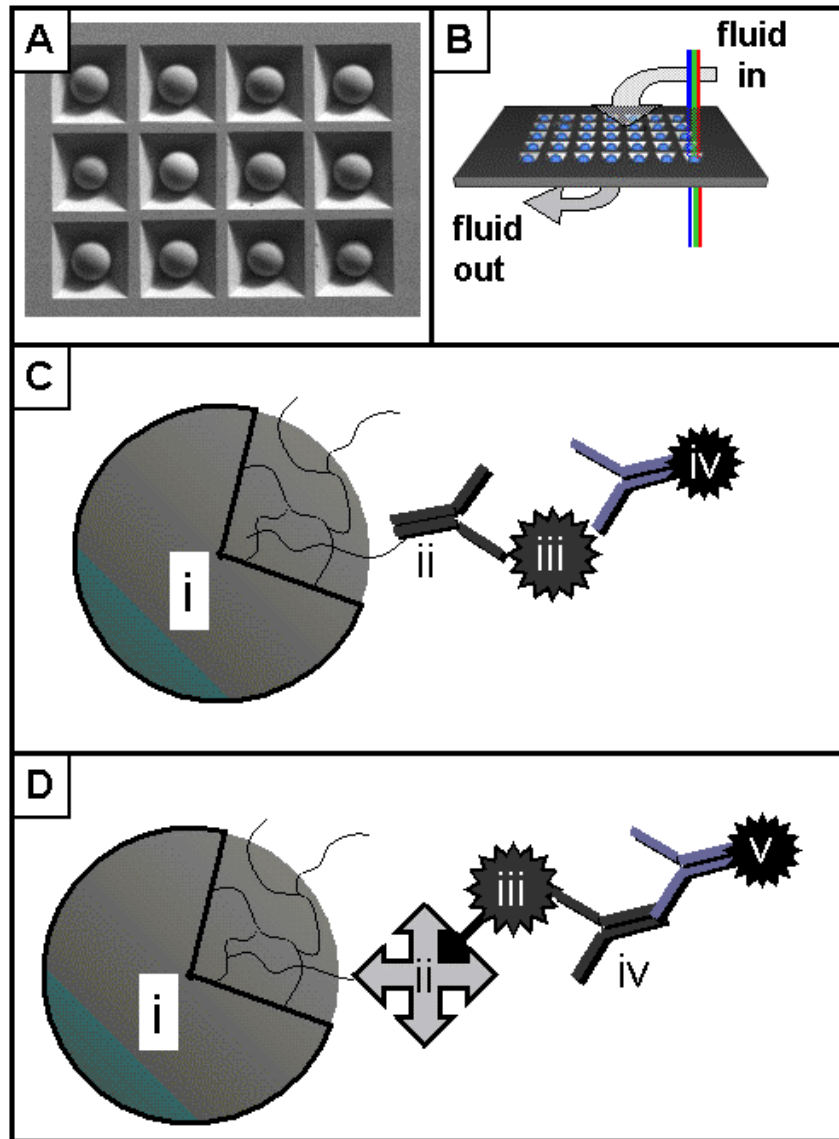


Figure 4.1: Bead-based sensor array system. (A) A scanning electron micrograph shows the beads placed into chemically etched pyramidal pits patterned on a silicon chip. (B) Schematic showing an etched silicon wafer with pits, which extend through the entire thickness of the silicon wafer creating square openings on the bottom side of the chip. These openings provide both optical access to the bead element and serve as a drain for the reaction/analysis chambers. (C) Immunocomplex schematic for a typical antigen capture assay. An agarose bead of $\sim 250\ \mu\text{m}$ diameter (i) is conjugated with capture antibody (ii); the protein analyte (iii) binds to the capture antibody and is visualized with the HRP-labeled detecting antibody (iv). Color development is achieved with an enzyme-catalyzed precipitating chromophore that effectively stains the bead. (D) Immunocomplex schematic for a typical antibody capture assay. The agarose bead (i) is conjugated with avidin (ii) and then bound with biotinylated antigen (iii). The target antibody (iv) is visualized with a fluorophore-labeled detecting antibody (v).

Following the placement of sensitized beads into the array, the array element is then encased in an optically transparent flow cell, which serves to immobilize the beads in the chip and to allow for optical analysis. Figure 4.1B highlights the fluid flow pattern as delivered by the external pumps, which sequentially administer in an automated manner the sample, buffers, and immunoreagents. Initially, fluid is directed into an upper reservoir of the flow cell and then forced down through the wells to a lower reservoir (~50 μ L total exchange volume) and finally out to waste.¹¹¹ The flow cell readily accommodates flow rates up to 5 ml/min through the smaller array sizes (i.e. 3×4) and as high as 10 mL/min for larger arrays (i.e. 5×7 , 10×10 , etc.) Consequently, rapid and effective washing occurs as ~4,000 bead dead volumes are delivered throughout a typical washing step. This combination of chip and integrated fluidic channels enables reagents to be brought rapidly and efficiently into contact with the positioned beads. In addition, by rearranging the tubing and pump flow components, the reagents can be recirculated through the chip allowing multiple passes for reagent interactions.

Figure 4.1C shows the relevant immunocomplex that is formed during a typical bead-based “sandwich” assay, where the analyte is captured and detected by separate analyte-specific antibodies. In this case, the bead becomes sensitized by covalently linking the capture antibody directly to the agarose beads using reductive amination.¹³⁶ With this approach, an immunoassay is performed by successively delivering the analyte-containing sample to the bead array. Then, an analyte-specific detecting antibody that has been conjugated to a fluorophore or enzyme is delivered. Identification and quantification of the analyte follows by discriminating the fluorescent or colorimetric optical signals acquired by the charge-coupled device (CCD).^{111,116-119}

The same chip-based platform is readily adapted to miniaturized multiplexed antibody capture assays. For an antibody capture immunoassay, antigen-specific antibodies are detected in the sample (i.e. human serum) to indicate previous exposure to viral or bacterial pathogens.¹⁷ Likewise, in the bead-based approach, the antibody generating protein (i.e. the antigen) is linked directly to the agarose beads using reductive

amination. The immunoassay is performed in an analogous fashion as described above. In certain cases, antigens are found to be difficult to link to the bead using reductive amination (i.e. for certain proteins with few accessible free amines). In such cases, the strong biotin-avidin binding interaction can be exploited as an alternative antigen docking strategy as shown in Figure 4.1D. Here, the docking moiety, avidin, is readily anchored to the agarose matrix using reductive amination. This biological tetrameric binding system is used in conjunction with its biotin ligand which is attached to the capture antigen using the amine reactive N-hydroxysuccinimide (NHS) biotin ester.¹⁷⁰ The biotinylated capture protein is then allowed to bind to the avidin-coupled agarose creating an extremely stable noncovalent bond. This modular binding methodology is convenient and efficient while remaining unaffected by wide extremes of pH, temperature and denaturing agents. With these approaches, immunoassays are performed by successively delivering the analyte-containing sample to the bead array. Then, analyte-specific detecting antibodies are injected through the flow cell followed by the measurement of the optical signal.

As opposed to the planar surface of a microwell used in standard ELISA procedures, the electronic taste chip approach here described exploits agarose beads that serve as 3-dimensional microreactors. The use of the interior gel-matrix of agarose beads is commonly employed in protein purification techniques such as size-exclusion chromatography.¹³⁹ Techniques of this type separate molecules based on size where molecules above the gel exclusion limit become excluded from the agarose matrix and quickly pass through the column in the void volume with the aid of the mobile liquid phase. In contrast, molecules small enough to enter into the pores of the agarose effectively become sequestered and spatially localized within the gel matrix, requiring longer times to exit the column. Similarly, for the bead-based immunoassays, the gel porosity of the agarose bead microreactors allows for the penetration of immunoreactants into the interior regions of the bead, thereby creating a 3-dimensional volume for the sequestration of analyte. Furthermore, the bead also acts as a cuvette whereby the generated signal is localized in the confined volume of the bead. The longer pathlength

here established enables the production of larger signals. Hence, higher assay signal to noise ratios and thus greater sensitivity can be achieved relative to other more commonly exploited planar immunoassay strategies (see below).

4.3.1 Comparison of Signal Response Rates. To compare the signal response rates for the bead- and microtiter plate-based assays, a simple two-component antigen/antibody system is used to monitor signal generation rates. Here, purified mouse immunoglobulin (IgG) is employed as the antigen and a labeled monoclonal antibody specific to mouse IgG is used as the detecting antibody. Because the amount of antigen bound to the two solid-phase supports influences the rate of signal generation (data not shown), the protein loading densities are chosen to be approximately the same for both methods. The amount of mouse IgG bound to a series of beads is determined by mass balance measurements using the absorbance of the protein at 280 nm.¹⁷¹ By the same token, the amount of protein bound to an individual well of the microtiter plate is determined with the aid of a bicinchoninic acid (BCA) protein quantification procedure.¹⁷² Using these carefully completed procedures, wells and beads loaded with similar amounts of antigen (205 ng mouse IgG per well and 200 ng mouse IgG per bead) are used to compare signal generation rate data for both systems.

The time evolution of the optical response from the microtiter plate-based assays is monitored sequentially in the wells of multiple microplates as the experiment progressed. Here, a 5.0×10^{-5} mg/mL solution of HRP-labeled monoclonal rat anti-mouse IgG is allowed to react in separate wells for each of eight different incubation times (10, 20, 40, 60, 120, 210, 300 and 1500 min). The signals are developed after each incubation time using the TMB substrate and measured for absorbance on a standard microtiter plate reader. This series of experiments is performed with two variations: 1) without plate shaking and 2) with plate agitation at the optimized speed. The condition with no shaking is chosen since the rate of the antigen/antibody interaction is likely limited by the rate of diffusion of the antibodies to the planar surface.⁹ Previously,

Nygren et. al. demonstrated that the binding of antibodies to the solid-phase immobilized antigen continued slowly for 72 hours without ever reaching a saturation level due to the slow diffusion of antibodies and the effect of high surface concentrations of immobilized antigen causing the localized depletion of the antibody near the surface of the solid-phase.¹⁷³ In addition, the rate of antibody binding to surface immobilized antigen above a critical surface concentration ($>1 \text{ pmol/cm}^2$) was found previously to be limited by steric hindrance and a subsequent reorganization of the layer of bound antibodies.⁹ Thus, in order to track the influence of these limitations, other experiments were also performed with the vigorous circular rotation (shaking) of the microplates. The effect of shaking of the ELISA is studied here since shaking can be used to increase mass transport effects.^{174,175}

The time evolution data for both types of plate-based experiments is shown in Figure 4.2A. These experiments reveal a number of interesting factors. First, the stationary plates (Figure 4.2A plot ii) do not reach their limiting equilibrium response during the entire 1,500 minute incubation time. On the other hand, the signal response of the shaking condition (Figure 4.2A plot i) is found to change dramatically over the first ~100 minutes while reaching full saturation near the end of the full 1,500 minute incubation period. These results suggest that the strong agitation of the microtiter plate accelerates the formation of the majority of the possible immunocomplexes. However, it is clear that some additional antigen-antibody binding interactions do occur, but on a longer time scale requiring extended incubation periods. This delayed response may be due to the high surface concentration of the immobilized antigen ($>2 \text{ pmol/cm}^2$) whereby steric hindrance associated with immunocomplex formation requires further reorganization of the antibodies at the surface. The observed time delay and lack of equilibration of antibody binding during the extended incubation period is compatible with the observations of others.¹⁷³ Other authors that evaluated the equilibration of antibody binding using agitated conditions report maximal binding occurs in as little as 1 hour⁴⁴ to up to 16 hours.¹⁷⁶ A second important observation apparent in Figure 2A is that the inclusion of the solution agitation procedure leads to a dramatic increase in signal

magnitude relative to the analogous experiments completed with the stationary solutions. This effect is likely due to increased antigen/antibody binding events caused by the more effective delivery of reagents fostered by the shaking procedure. Thirdly, the overall signal levels for both plate-based experiments types are quite small. Accordingly, the microtiter plate procedure does not allow for the use of direct detection methodologies. Rather, enzyme amplification procedures following the formation of the completed immunocomplex are required to monitor the reaction sequence in all cases.

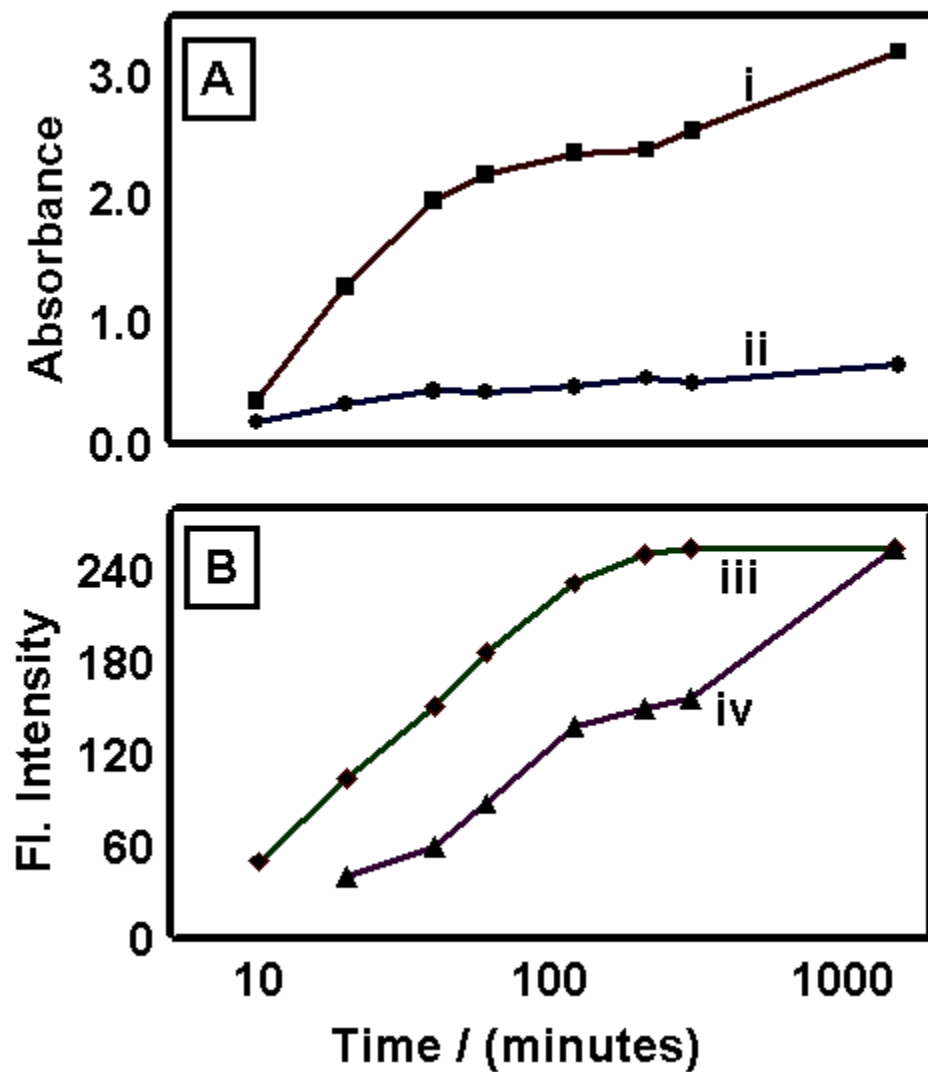


Figure 4.2: Assay signal time-course for antigen-antibody equilibration. A rat anti-mouse IgG₁ monoclonal antibody was reacted with immobilized antigen and monitored for reaction equilibration using (A) conventional microtiter wells where plot (i) shows the condition with mixing via a microtiter plate shaker at an optimized speed and plot (ii) shows the condition without mixing. (B) The lower panel shows data from the experiments using homogenous beads as the solid-phase where plot (iii) reveals the behavior for reagents being recirculated at an optimized flow rate of 9 ml/min and plot (iv) summarizes data recorded for the reagents being recirculated at the slowest rate allowed by the fluidic pump system of 0.01 ml/min.

On the other hand, the signal levels derived for the bead-based analogous experiments are significantly greater. Likewise, the use of direct fluorescence detection is possible and this attribute allows for the real-time monitoring of the complex formation using epi-fluorescent techniques. More specifically, a 5.0×10^{-5} mg/mL solution of fluorophore-labeled monoclonal rat anti-mouse IgG is recirculated through the flow cell at 2 different flow rates of 9 and 0.01 mL/min. Here, the faster flow rate (Figure 4.2B plot iii) represents the optimized condition where signal saturation is obtained rapidly and the slower flow rate (Figure 4.2B plot iv) is that associated with the lowest possible flow rate afforded by the fluidic pumps used here. For these experiments, single beads are monitored for their capacity to capture labeled antibody from the fluid stream by measuring fluorescent intensity as a function of time. The results for these pressure-driven flow experiments are provided in Figure 4.2B. Here it is interesting to note that fully saturated signals are acquired at both flow rates during the same time course of the experiment. A number of additional trials not shown here reveal that the final signal level for the other flow rates also approach the same values within experimental error. For these experiments, there is a consistent trend whereby the faster the flow rate that is used, the shorter the time to reach equilibrium and signal saturation. However, above ~ 10 ml/min for this size array (3×4), the rate of immunocomplex formation reaches a maximum level. At the upper limit of useful flow rates, the signal saturation occurs at ~ 300 minutes.

From the time evolution experiments, it becomes clear that both fluid agitation as well as pressure-driven flow provide significant advantages relative to shortening the time required for immunocomplex formation and reagent delivery. It is interesting to note here that despite the fact that the bead-based approach requires analyte and reagent penetration into the bead interior region (see below), the additional step not required for the planar plate-based approach does not force the bead-based to be slower than the planar methodology. Apparently, the benefits derived from the chip-based forced flow over-compensate for the additional time required for reagent/analyte penetration into the

bead interior. The advantages of pressure-driven flow at reducing diffusion effects and increasing equilibration rates has been reported in other biosensor methodologies.^{7,81} Further decreases in bead-based immunocomplex formation times are to be expected following the inclusion of macropores within the bead structure (see below).

4.3.2 Immunoreagent Penetration. While other bead-based sensing strategies have been developed, prior work here has been completed where signal generation is localized at the surface of the bead spheres. For example, methods using ~ 3 μm beads (87% methylstyrene 13% divinylbenzene copolymer) localized at the distal face of an etched imaging fiber have been demonstrated for the simultaneous detection of multiple protein targets.⁸⁷ Further, evaluation of a suspended set of sensitized ~5 μm polystyrene beads by flow cytometry was demonstrated previously for the multiplexed detection of various cytokines and serum proteins.^{89,91} With the electronic taste chip, on the other hand, it is possible to utilize the 3-dimensional volume of the macroporous bead to effectively increase the associated signal generating pathlength and, thus, improve the overall analytical performance of the system.

As described in Chapter 3 whereby the bead matrix dependence of immunoassays was explored, it was determined that agarose beads are well suited for the chip-based analysis of various bio-molecules.^{111,119} The properties of the agarose matrix that make it suitable for such bioassays include its hydrophilic nature, optical clarity, lack of nonspecific absorption effects, chemical and mechanical stability, and its high protein binding capacity.

Given the past literature precedent for the use of agarose beads in protein purification based on affinity chromatography¹³⁶ and the importance of the size separation of analytes within the bead matrix of gel exclusion chromatography,^{148,149} it seemed likely that not only the surface, but also the interior regions of the beads may contribute to the signal generating capacity of the bead microreactors. A detailed understanding of the agarose bead microenvironment as well as the molecular weight-

size dependence of protein diffusion into the agarose interior, thus, becomes important enroute to full optimization of the micro-bead array's assay characteristics. Based on simple Beer's law considerations, it is clear that the full advantage of using the bead approach relative to planar methods could be realized if all the reagents of an immunoassay permeate can throughout the entire volume of the bead during the time scale of the assay.

In order to explore the time dependence of immunoreagents permeation into the interior region of the agarose beads, a series of experiments were designed and executed whereby the penetration of fluorescent immunolabels was visualized using confocal microscopy. Figure 4.3 column I provides illustrative confocal images recorded during the time course of a typical sandwich assay. These images highlight the medial bead slices that explore the penetration of immunoreactants into the interior region of the homogenous agarose beads. Here, a CRP capturing antibody (~150 kDa), purified CRP protein (~120 kDa), and HRP-conjugated detecting antibody (~190 kDa) are each labeled with fluorescent dye and evaluated individually during the bead-based sandwich immunoassay. From an analysis of these images, it becomes clear that the capture antibody is immobilized throughout the entire volume of the bead while the CRP antigen penetrates only through to the outer third of the diameter of the bead. Most significantly, the detecting antibody penetrates to only about the outer 10% (20 μm) of the bead's diameter.

While the expected size exclusion limit for this formulation of beaded agarose is ~5,000 kDa, the full sandwich (totaling ~460 kDa) is found to penetrate only partially through the volume of the bead. The useable protein fractionation range of this type of agarose bead is typically reported as a molecular weight range (i.e. 10-5,000 kDa for the homogenous agarose beads used here) and is typically measured by monitoring the chromatographic elution profiles of protein standards by UV spectroscopy.¹⁴⁸ In the context of such applications, the penetration of reagents into the outermost region of the bead matrix is all that is required to evoke separation. The fact that ~10% of the bead

exterior region is found to capture the entire sandwich immunocomplex is consistent with this behavior. Furthermore, the 20 μm exterior shell of the beads leads to an effective

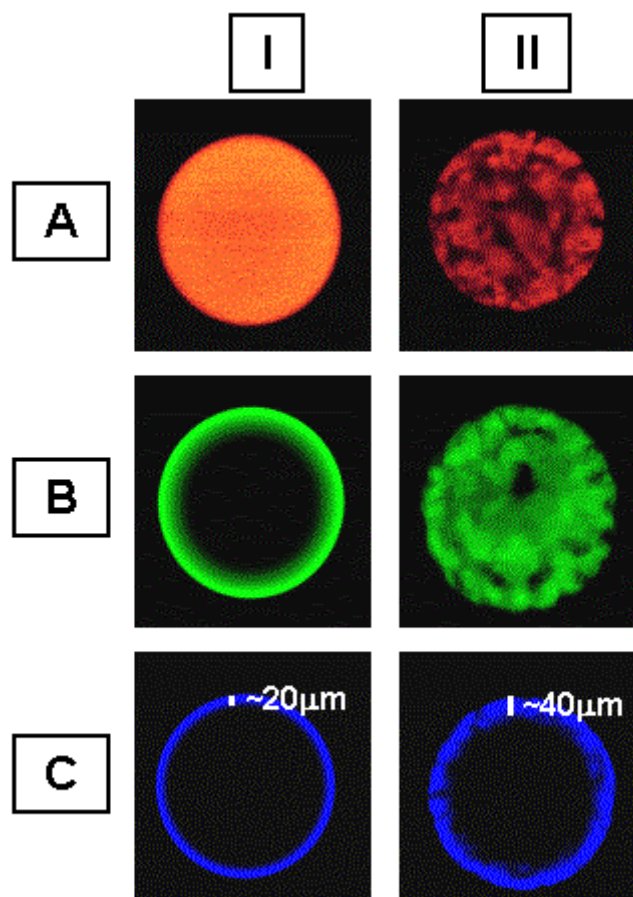


Figure 4.3: Fluorescent medial cross-sectional images of agarose beads obtained using confocal microscopy, which probe the penetration within these beads of fluorophore-labeled immunoreagents. The images in left column (I) are obtained for the homogenous agarose beads and those provided in the right column (II) show the behavior observed for the superporous agarose beads. Row A shows the penetration of the fluorophore-labeled CRP capture antibody (~150 kDa) that occurs during the protein immobilization procedure. Row B shows the penetration of the fluorophore-labeled CRP (~120 kDa) through beads that had been previously conjugated with unlabeled CRP capture antibody. Row C shows the penetration of the fluorophore-labeled detecting antibody (~150 kDa) through beads that previously had the immobilized unlabeled capture antibody (~150 kDa) and bound unlabeled CRP protein (~120 kDa).

signaling pathlength of $\sim 40 \mu\text{m}$ when appropriate collection optics are used. This relatively large signal layer thickness significantly exceeds the signal capacity obtained

more typically from planar approaches such as ELISA methodology. The larger capture areas as well as the higher density of capture probes are important factors that contribute to the high sensitivity of the bead-array approach (see below).

While significant penetration of immunoreagents into the bead interior is noted for typical assay times of 10-60 minutes, nonetheless only about 10% of the diameter of the bead is utilized. In an attempt to enable immunoreagents to penetrate further into the interior volume of the bead, a new series of beaded agarose is created. The new type of agarose bead (termed here as superporous) is prepared in-house using a double emulsification procedure that produces an evenly distributed network of very wide pores, meandering throughout the thickness of the bead. More specific details of the superporous bead preparation and characterization will be provided in future publications. The confocal images of the superporous beads provided in Figure 4.3 Column II show that both the capture antibody and analyte penetrated the entire thickness of the bead while the detecting antibody penetrated through to the about outer 40 μm of the bead diameter, effectively doubling the signal generation layer thickness. With further bead preparation optimization, additional improvement in capture volume is expected. However, even at this early stage of development, it is clear that the electronic taste chip analysis systems benefits from the use of the superporous beads by allowing a thicker layer of detecting reagents for the generation of signal.

To further characterize the features of the homogenous and superporous agarose beads, scanning electron micrographs are acquired as provided in Figure 4.4. The electron micrographs reveal the homogeneous beads to be very nearly spherical with smooth and uniform surface features. The superporous beads are also nearly spherical in shape, but have multiple indentations and pits at their surfaces and throughout their interior regions. In some cases, pores or channels ($\sim 10\text{-}40\text{ }\mu\text{m}$ wide) penetrate throughout the interior region of the bead as evidenced by the medial cross-sectional images shown in Figure 4.3 Column II. Collectively, the results of Figures 4.3 and 4.4 suggest that the inclusion of the pores serves to increase the bead surface area while

providing better solution access into the interior region of the beads, which serves to minimize the diffusional distances of immunoreactants. Accordingly, the physical appearance of the beads in the electron micrographs is therefore consistent with the improvement in the immunoreactant permeation characteristics observed by the protein labeled confocal measurements.

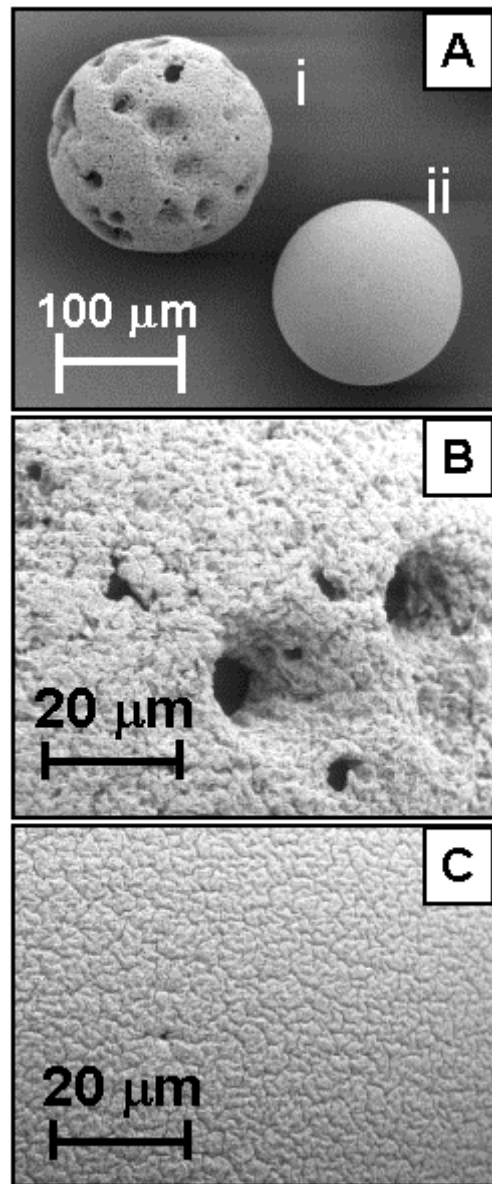


Figure 4.4: Scanning electron micrographs obtained for two types of agarose beads. (A) Low magnification (254x) views are provided for a superporous agarose bead (i) and a homogenous agarose bead (ii). Higher magnification images (2000x) are also provided for the superporous bead (B) and the homogenous bead (C).

4.3.3 Comparison of Assay Characteristics. In addition to the intrinsic interest of protein penetration, it becomes interesting to explore the cause and effect of bead

microreactor pore engineering on observed immunoassay analytical characteristics. With this in mind and with further attention to be paid to comparisons with conventional ELISA methodologies, the CRP sandwich assay analytical parameters are defined. Here, attempts are made to optimize the methods for lowest detection threshold and widest dynamic range. Further, to ensure that a fair and valid comparison is made, important experimental conditions that may affect the ultimate assay performance are considered. For example, the same immunoreagents (capture antibody, enzyme-labeled detecting antibody and CRP antigen) are used and the inherent sensitivity of enzyme substrate systems of the bead- and plate-based methods (AEC vs. TMB) are selected to be comparable.¹⁷⁷ In addition, the CRP antigen and detecting antibody incubation times are maintained at 1 hour and 30 min, respectively, to emulate the incubation times established in high-volume ELISA methodologies.¹

Figure 4.5 compares the CRP dose-response binding curves using conventional microtiter plates, superporous agarose beads, and homogenous agarose beads (plots A, B and C, respectively). The data for each plot has been normalized to its associated saturated absorbance value obtained at high analyte concentrations. The limit of detection determined at 95% confidence is found to be $\sim 10^{-11}$ M for the microplate-based assay, $\sim 10^{-12}$ M for the homogenous bead-based assay and $\sim 10^{-13}$ M for the superporous bead-based assay. Here, the homogenous bead-based assay yields a 10-fold decrease in limit of detection while the superporous bead-based assay affords a 100-fold decrease in the limit of detection as compared to the microplate based-assay. The significant decreases in detection threshold obtained here are consistent with the information derived from the above-mentioned confocal studies.

The inclusion of interconnected pores within the beads lead to a high density of capture antibodies within the interior region of the matrix that may lead to an increased avidity (i.e. increased probability of multivalent binding events) of the antibody-antigen binding interaction.¹⁵⁶ Consequently, the dissociation of bound analyte within such restricted regions that are lined with additional capture antibodies might be expected to foster rapid recapture leading to an

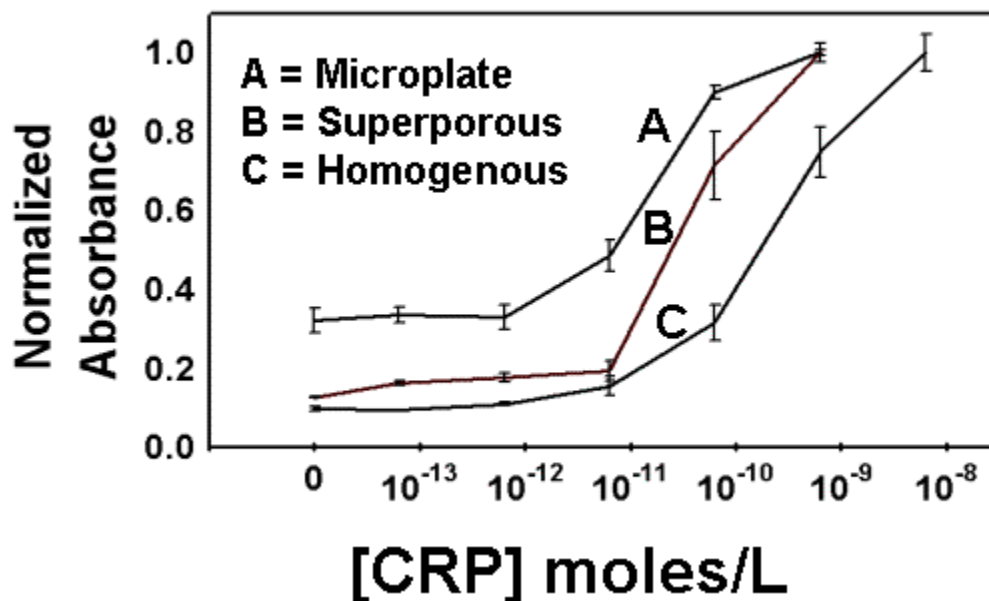


Figure 4.5: The dose-response plots are shown for CRP sandwich assays completed with A) the conventional microplate-based ELISA, B) the superporous agarose beads and C) the homogeneous agarose beads. The microplate dose response curve is characterized by high background readings as illustrated by the higher baseline along the y-axis. The linear dynamic range of this plot spans two orders of magnitude in analyte concentration ($\sim 10^{-11}$ M - 10^{-9} M CRP) before saturating. Plot B is the superporous bead-based CRP dose response with the lowest limit of detection at $\sim 10^{-13}$ M CRP. A region of linearity ($\sim 10^{-13}$ - 10^{-11} M CRP) extends well beyond the dose response of the microplate and may be due to the high avidity effects caused by high capture protein immobilization density. Another region of linearity for this plot extends from $\sim 10^{-11}$ - 10^{-9} M CRP where the signal saturates beyond the detectable range of the digital camera. Plot C is the dose response for the homogenous beads which exhibits a limit of detection of $\sim 10^{-12}$ M CRP. The detectable response extends to $\sim 10^{-8}$ M CRP (~ 4 orders of magnitude) before the signal saturates beyond the detectable range of the digital camera.

increased proportion of bound analyte that quickly re-associates with the highly localized capture antibody thereby increasing the effective ratio of bound to free analyte. Thus, the likelihood that a captured analyte molecule will completely dissociate from the bead matrix is reduced. Likewise, the bound complexes are more likely to survive vigorous washing regimes. Under such circumstances, the reduction of background caused by nonspecific binding interactions can be decreased substantially with vigorous washes without signal loss caused by antigen dissociation into the fluid stream.

In order to support this conjecture, kinetic studies are also performed to evaluate the rate of analyte dissociation as a function of capture protein loading density. Here, the dissociation of a monoclonal anti-mouse IgG₁ antibody from mouse IgG bound to homogenous beads is compared with that using surface plasmon resonance techniques (SPR).¹⁷⁸ The SPR related experiments use a dextran microlayer (100 nm +/- 20 nm) for protein immobilization that is loaded at the nearly maximal concentration of $\sim 10^{-4}$ M IgG (or ~ 2 IgG molecules per 100 nm²). These conditions simulate a planar biosensor surface with a high protein immobilization density and thus increase the likelihood of bivalent interactions and re-association events.¹⁵⁶ The dissociation rate constant, k_d , is determined by fitting the dissociation data (i.e. continuous buffer flow after ligand saturation) to a homogeneous dissociation model represented by the equation:

$$R=R_0 \exp[-k_d(t-t_0)]. \quad \text{Eq. 15}$$

The effective k_d value for the high loading condition is determined to be $\sim 10^{-5}$ s⁻¹. Similarly, when the IgG capture protein loading level on the planar biosensor surface is decreased by 10-fold, the effective k_d was found to be $\sim 10^{-3}$ s⁻¹. The 100-fold increase in displacement rate observed for the low loading case here is consistent with the presence of low-density receptor loadings where monovalent interactions are dominant. On the other hand, the high loading level appears to foster less frequent displacements due to increased multivalent interactions. These effects are seen commonly observed in SPR techniques⁷ and ELISA methodologies.¹⁷⁴

To probe the effect of protein loading density on the rate of analyte dissociation using the 3-dimensional agarose matrix, homogenous beads are loaded with two concentrations of mouse IgG representing both low and high protein immobilization conditions (~ 65 and 200 ng IgG per bead or $\sim 10^{-5}$ M IgG). After a fluorescent anti-mouse IgG probe is bound to nearly saturated conditions, the rate of ligand dissociation is monitored using the epi-fluorescent procedures as described above and the effective k_d value is calculated using the same dissociation model as used for the above described

SPR data. Interestingly, both low and high immobilization densities yield a dissociation rate constant of $\sim 10^{-5} \text{ s}^{-1}$, implying that both bead-based loading values yield high avidity conditions. This data corroborates the assertion that high capture protein immobilization densities are present within the beads. Such loading levels serve to minimize the rate of complete dissociation of antigen/antibody binding interactions. When combined with the observations made by the confocal measurements along with the 10-fold decrease in detection thresholds afforded by the superporous beads, it becomes possible that high avidity binding pockets are created in these engineered beads. These results suggest that this feature may contribute in an important way the decrease in detection limits afforded by the agarose bead-based assays.

Figure 4.5 also shows that the microplate dose-response curve has increased background as revealed by the significant low concentration high absorbance signal. This undesirable feature may be due to the inefficient washing procedure common to microplate immunoassays where only 3-4 microwell volumes are exchanged in a typical wash sequence. Alternatively, problems with nonspecific binding caused by non-ideal antibody to plate associations may contribute to this parasitic signal. In contrast, the lower baseline reading for the homogenous and superporous beads can be attributed to the more efficient wash sequence used with the bead-based approach. Likewise, the reduced background caused by the more efficient flow-through washing strategy is responsible in part for the lower detection thresholds achieved by the bead-based assays. Further, the presence of a more ideal environment for the antibodies within the agarose matrix may also contribute to the observed reduction in background.

Additionally, data from Figure 4.5 reveals that both the homogenous and superporous bead-based assays have an extended dynamic range compared to the microplate-based assay. Generally, the linear dynamic range of an immunoassay is considered to extend between 10-90% saturation of the antibody used. This is typically equivalent to 2-3 orders of magnitude in analyte concentration in a conventional immunoassay.^{103,157} Indeed, these typical expectations are met by the microplate-based CRP assay in Figure 4.5A. The dynamic range of the CRP assay using the homogenous

agarose beads in Figure 4.5C, on the other hand, is extended by an order of magnitude in concentration on both the upper and lower limits in concentration compared to the microplate assay in Figure 4.5A. Possible explanations for the extended dynamic range may include both avidity considerations¹⁰³ (extending the lower limit) as well as the enhanced transport effects associated with integrated fluidics systems.¹⁷⁹ Thus, the increased protein immobilization density can allow higher affinity interactions to persevere the vigorous washing due to the (higher affinity) bivalent binding of the analyte¹⁰³ and, as a result, enables the lower concentrations of analyte to be detected. This attribute becomes even more profound with the superporous bead-based assay and its 100-fold decrease in limit of detection compared to the microplate assay. Finally, the extension of the linear range of the homogenous bead-based in the upper limit of concentration may be due to the increased protein loading capacity of the agarose bead matrix. Thus, at high analyte concentration, an increased amount of immunoreagents may be used to generate signal as compared to the limited protein binding capacity of the planar microwell surfaces. Dynamic ranges extending 4-orders of magnitude have been reported for other bead-in-channel methodologies.^{81,103}

To further evaluate the bead-based assay characteristics, the intra-assay variation of the bead-based immunoassay system is determined by averaging the coefficient of variation (CV) of the absorbance from 4 replicate trials at each of 8 different analyte concentrations. The inter-assay variation is obtained for bead and ELISA approaches for measurements acquired at the 10 ng/mL CRP concentration. For the intra-assay variance for ELISA, well-to-well differences on the same plate are evaluated; while for the taste-chip, bead-to-bead differences within the same chip are explored. Under these conditions, intra-assay CV values of 6.5% for ELISA, 9.5% for the homogenous beads and 9.7% for the superporous beads are obtained. For the inter-assay values, plate-to-plate and chip-to-chip differences are evaluated for both approaches. Here, the inter-assay CV is obtained at 19% for the ELISA, 13% for the homogenous beads and 27% for the porous beads. The results show slightly more scatter for both the homogenous and superporous bead intra-assay variation. The procedure for producing the superporous

beads at the time of this writing has not yet been fully optimized to minimize variation in porosity and agarose composition. It is expected that future optimizations in flow design and bead production procedures will yield even more consistent results. On the other hand, the inter-assay variation was the lowest for the homogenous beads. This could be an effect of the capture protein immobilization process whereby many thousands of beads are simultaneously sensitized in the same reaction vessel. The wider plate-to-plate variation of the ELISA may be an effect of the time and temperature differences when binding capture protein to different plates. Furthermore, it should be noted that the ELISA procedure requires numerous manual rinsing and reagent delivery steps. Likewise, large person to person differences in assay characteristics have been reported.¹⁸⁰⁻¹⁸² The chip-based assays on the other hand, employ automated fluidics that when fully optimized have the potential to exhibit highly reproducible, operator independent assay characteristics. At present, the major sources of error for the bead-based assay include bead-to-bead size/activation levels as well as differences in the well-to-well fluid delivery characteristics. While the former may be improved with bead size sorting and protein conjugation optimization, the latter will require further studies of fluid delivery characteristics within these bead-chip composite systems. Fundamental studies in these areas are currently in progress.

4.3.4 Multianalyte Detection Capacity. Perhaps the most significant advantage of the micro-bead array approach is its capacity to detect multiple analytes simultaneously. Applications are envisioned where the multiplexed screening of disease-related biomarkers would lead to a more comprehensive analysis of serum-based biomarker concentrations and hence, provide earlier and more rapid diagnoses.^{161,183} Furthermore, this feature would be complimented by the electronic taste chip's capability to analyze for multiple antigenic determinants from the same disease-causing agent, thus, leading to more accurate diagnoses. Some of these features are shown in Figure 4.6 which illustrates the multiplexed detection of antibodies to medically-relevant viral diseases such as Influenza; Hepatitis A,B and C; and HIV-1 and HIV-2; etc. In these experiments, the

multiplexing capabilities of the bead array are demonstrated using homogenous beads that are immobilized with various medically relevant viral disease antigens. To obtain this data, human blood serum spiked with various combinations of polyclonal antibodies to the viral antigens is used. Figure 4.6A illustrates the intra-disease multiplexing capability where two separate tests for Hepatitis B are performed simultaneously. Here, a serum-based analysis of antibodies sensitized to Hepatitis B surface antigen as well as Hepatitis B core antigen is shown. Figure 4.6B demonstrates a multi-disease screening test where specific antibodies to both Hepatitis B surface antigen and HIV gp41 are simultaneously detected. In addition to demonstrating the multiplexed capabilities, these experiments show the selectivity of the bead-based approach is preserved without interference effects from human serum components.

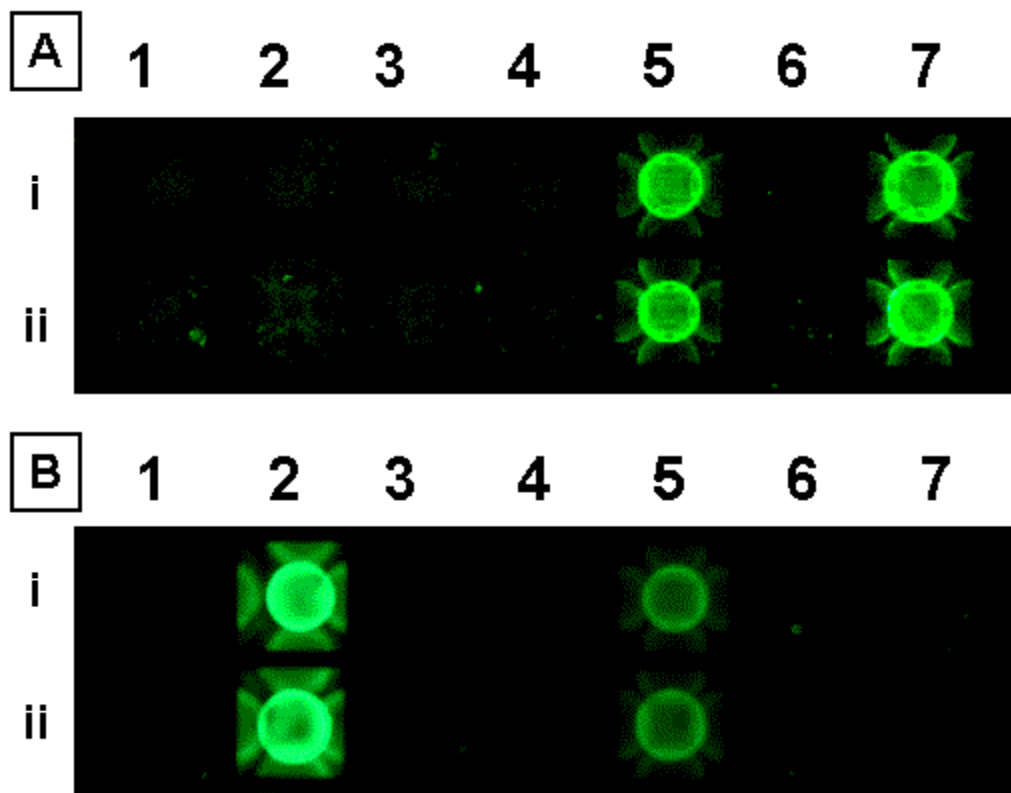


Figure 4.6: The multiplexing capabilities of the bead-based sensor array system are demonstrated in case (A) for two specific serum-based antibodies to Hepatitis B. Here, human serum was spiked with polyclonal antibody to Hepatitis B core antigen and polyclonal antibody to Hepatitis B surface antigen. The solution was delivered to the sensor array containing the sensitized beads in columns 1-7. Two replicate beads (top row holds replicate #1, bottom row holds replicate #2) were placed in the wells of the array where column (1) = HIV-2 gp36; (2) = HIV-1 gp41; (3) = Hepatitis A; (4) = Hepatitis C NS-4; (5) = Hepatitis B core antigen; (6) = Influenza A; (7) = Hepatitis B surface antigen. The captured antibodies were then visualized using a fluorophore-labeled secondary detecting antibody. Similarly, case (B) shows a multi-disease screening assay is demonstrated in (B) where column (1) = bovine serum albumin; (2) = Hepatitis B surface antigen; (3) = Mumps; (4) = Hepatitis C NS4; (5) = HIV-1 gp41/120; (6) = Cytomegalovirus; (7) Influenza A. As in the prior example, (i) and (ii) provide data for the replicate trials as performed in the same evaluation.

Although the multiplexed simultaneous analysis for 7 different analytes is demonstrated here, the aforementioned 10×10 arrays have been prepared and used in selected experiments demonstrating an effective methodology that further extends the capabilities of existing multianalyte detection themes. Upon implementation of this technology, the delays associated with sending samples to remote testing facilities would

be eliminated while resulting in more rapid patient diagnoses and, thus, earlier implementation of therapeutic strategies. Another benefit of this approach is the possibility of identifying disease states that were not previously anticipated. For example, the initial symptoms of HIV infection often resemble those of infectious mononucleosis. In a recent case study, it was reported that ~1% of the patients suspected of having infectious mononucleosis actually had the primary HIV-1 infection instead.¹¹⁵ Thus, when fully developed such a multiplexed disease screening approach would serve to reduce the number of misdiagnosed medical conditions often associated with diseases showing similar symptoms. Here the completion of cost effective tests which screen simultaneously for both common and non-common infections would become possible as would the identification of the presence of various bio-threat agents.

4.4 CONCLUSIONS

The electronic taste chip immunoassay detection capabilities described within this chapter compliments previous developments of other multiplexed approaches such as planar arrays^{75,154} and bead-based assays.^{71,89} Attempts have been made to establish firm comparisons completed under controlled conditions between the new chip-based approach and the established prior “gold standard” methodology based on ELISA plate techniques. In completing the studies, the chip-based approach reveals a number of significant advantages relative to the prior standard. First, the combination of the silicon chip and microfluidics creates channels for the efficient delivery of reagents and washes to the agarose sensors. Further, a typical washing step achieves 4000-fold more wash volumes per well while using 1/10th the total liquid volume compared to ELISA. Second, multiplexing using the taste chip approach greatly reduces the required manual steps and reagent cost. Third, the ability to tailor a particular assay to meet sensitivity or dynamic range requirements is made possible by the bead sensor exchangeability feature of the electronic taste chip approach. Moreover, the production of superporous beads is a powerful demonstration that the bead micro-environment can be modified to benefit the

analytical characteristics of an immunoassay. Lastly, and perhaps most importantly, the analytical characteristics (response time, detection threshold, dynamic range and precision) of electronic taste chip immunoassays are shown to be comparable to, and in many cases, exceed the performance of conventional ELISA. These characteristics, along with the capacity to multiplex, strongly validate the utility of the electronic taste chip approach in performing multiplexed immunochemical analyses.

Another benefit of this approach is the possibility of identifying disease states that were not previously anticipated. For example, the initial symptoms of HIV infection often resemble those of infectious mononucleosis. In a recent case study, it was reported that ~1% of the patients suspected of having infectious mononucleosis actually had the primary HIV-1 infection instead.¹¹⁵ Thus, when fully developed such a multiplexed disease screening approach would serve to reduce the number of misdiagnosed medical conditions often associated with diseases showing similar symptoms. Here the completion of cost effective tests which screen simultaneously for both common and non-common infections would become possible as would the identification of the presence of various bio-threat agents.

REFERENCES

1. Wild, D. (ed.) *The Immunoassay Handbook*, pp. 118-39 (Nature Publishing Group, New York, 2001).
2. Rony, P.R. Hollow fiber enzyme reactors. *Journal of the American Chemical Society* **94**, 8247-8 (1972).
3. www.antibodyresource.com/antibody.html.
4. Butler, J.E. (ed.) *Immunochemistry of Solid-Phase Immunoassay*, pp. 277-91 (CRC Press, Boca Raton, 1991).
5. Purich, D.L. & Allison, R.D. *Handbook of Biochemical Kinetics*, pp. 129-42 (Academic Press, San Diego, 2000).
6. Wild, D. (ed.) *The Immunoassay Handbook*, pp. 3-40 (Nature Publishing Group, New York, 2001).
7. Myszka, D.G. Kinetic analysis of macromolecular interactions using surface plasmon resonance biosensors. *Current Opinion in Biotechnology* **8**, 50-57 (1997).
8. Glasner, R.W. Antigen-antibody binding and mass transport by convection and diffusion to a surface: A two-dimensional computer model of binding and dissociation kinetics. *Analytical Biochemistry* **213**, 152-61 (1993).
9. Stenberg, M. & Nygren, H. Kinetics of antigen-antibody reactions at solid-liquid interfaces. *Journal of Immunological Methods* **113**, 3-15. (1988).
10. Scatchard, G. Excess free energy and related properties of solutions containing electrolytes. *Journal of the American Chemical Society* **90**, 3124-7 (1968).
11. Paul, S.M., Hulihan-Giblin, B. & Skolnick, P. (+)-Amphetamine binding to rat hypothalamus: relation to anorexic potency of phenylethylamines. *Science* **218**, 487-90 (1982).
12. Rodbard, D. & Catt, K.J. Mathematical theory of radioligand assays. Kinetics of separation of bound from free. *Journal of Steroid Biochemistry* **3**, 255-73 (1972).
13. Nygren, H. & Stenberg, M. Kinetics of antibody-binding to surface-immobilized antigen: influence of mass transport on the enzyme-linked immunosorbent assay (ELISA). *Journal of Colloid and Interface Science* **107**, 560-6 (1985).

14. Munson, P.J. & Rodbard, D. LIGAND: a versatile computerized approach for characterization of ligand-binding systems. *Analytical Biochemistry* **107**, 220-39 (1980).
15. Purich, D.L. & Allison, R.D. *Handbook of Biochemical Kinetics*, p. 92 (Academic Press, San Diego, 2000).
16. Khalifa, M.B., Choulier, L., Lortat-Jacob, H., Altschuh, D. & Vernet, T. BIACORE data processing: an evaluation of the global fitting procedure. *Analytical Biochemistry* **293**, 194-203. (2001).
17. Rose, N.R. (ed.) *Manual of Clinical Laboratory Immunology*, Part 1 (ASM Press, Washington D.C., 1997).
18. Rose, N.R. (ed.) *Manual of Clinical Laboratory Immunology*, Part 2 (ASM Press, Washington D.C., 1997).
19. Bangs, L.B. New developments in particle-based immunoassays: introduction. *Pure and Applied Chemistry* **68**, 1873-1879 (1996).
20. Watt, A.P., Morrison, D., Locker, K.L. & Evans, D.C. Higher Throughput Bioanalysis by Automation of a Protein Precipitation Assay Using a 96-Well Format with Detection by LC-MS/MS. *Analytical Chemistry* **72**, 979-984 (2000).
21. Butler, J.E. (ed.) *Immunochemistry of Solid-Phase Immunoassay*, p. 3-26 (CRC Press, Boca Raton, 1991).
22. Greenwood, F.C., Hunter, W.M. & Glover, J.S. The preparation of ¹³¹I-labeled human growth hormone of high specific radioactivity. *Biochemistry Journal* **89**, 114-23 (1963).
23. Wild, D. (ed.) *The Immunoassay Handbook*, pp. 159-76 (Nature Publishing Group, New York, 2001).
24. Porstmann, B., Porstmann, T., Nugel, E. & Evers, U. Which of the commonly used marker enzymes gives the best results in colorimetric and fluorimetric enzyme immunoassays: horseradish peroxidase, alkaline phosphatase or beta-galactosidase? *Journal of Immunological Methods* **79**, 27-37. (1985).
25. Palaniappan, V. & Terner, J. Resonance Raman spectroscopy of horseradish peroxidase derivatives and intermediates with excitation in the near ultraviolet. *Journal of Biological Chemistry* **264**, 16046-53 (1989).
26. www.moleculardevices.com.

27. Strobel, H.A. *Chemical Instrumentation: A Systematic Approach*, pp. 516-36 (John Wiley & Sons, New York, 1989).
28. Coghlan, J.P. et al. Hybridization histochemistry. *Analytical Biochemistry* **149**, 1-28 (1985).
29. Soini, E. & Kojola, H. Time-resolved fluorometer for lanthanide chelates - a new generation of nonisotopic immunoassays. *Clinical Chemistry* **29**, 65-8 (1983).
30. Kricka, L.J., Voyta, J.C. & Bronstein, I. Chemiluminescent methods for detecting and quantitating enzyme activity. *Methods in Enzymology* **305**, 370-390 (2000).
31. Agbaria, R.A., Oldham, P.B., McCarroll, M., McGown, L.B. & Warner, I.M. Molecular Fluorescence, Phosphorescence, and Chemiluminescence Spectrometry. *Analytical Chemistry* **74**, 3952-3962 (2002).
32. Strobel, H.A. *Chemical Instrumentation: A Systematic Approach*, p. 283 (John Wiley & Sons, New York, 1989).
33. Butler, J.E. (ed.) *Immunochemistry of Solid-Phase Immunoassay*, pp. 67-83 (CRC Press, Boca Raton, 1991).
34. Kricka, L.J. Strategies for immunoassay. *Pure and Applied Chemistry* **68**, 1825-1830 (1996).
35. Farhat, S.E. et al. Rapid detection of infectious mononucleosis-associated heterophile antibodies by a novel immunochromatographic assay and a latex agglutination test. *Journal of Clinical Microbiology* **31**, 1597-600 (1993).
36. Hussain, Z., Stoakes, L., John, M.A., Garrow, S. & Fitzgerald, V. Detection of methicillin resistance in primary blood culture isolates of coagulase-negative staphylococci by PCR, slide agglutination, disk diffusion, and a commercial method. *Journal of Clinical Microbiology* **40**, 2251-2253 (2002).
37. Karmali, M.A., Petric, M. & Bielaszewska, M. Evaluation of a microplate latex agglutination method (Verotox-F assay) for detecting and characterizing verotoxins (Shiga toxins) in *Escherichia coli*. *Journal of Clinical Microbiology* **37**, 396-399 (1999).
38. Trabelsi, A., Peenze, I., Pager, C., Jeddi, M. & Steele, D. Distribution of rotavirus VP7 serotypes and VP4 genotypes circulating in Sousse, Tunisia, from 1995 to 1999: emergence of natural human reassortants. *Journal of Clinical Microbiology* **38**, 3415-9. (2000).

39. Percival, D.A. The measurement of hormones and bacterial antigens using rapid particle-based immunoassays. *Pure and Applied Chemistry* **68**, 1893-1895 (1996).
40. Sheehan, C. & Carreiro, E. Evaluation of five kits for detecting choriogonadotropin in urine. *Clinical Chemistry* **31**, 875-6 (1985).
41. Strobel, H.A. *Chemical Instrumentation: A Systematic Approach*, p. 373 (John Wiley & Sons, New York, 1989).
42. Strobel, H.A. *Chemical Instrumentation: A Systematic Approach*, pp.363-68 (John Wiley & Sons, New York, 1989).
43. Statistica Experimental Design (StatSoft; Tulsa, OK).
44. Butler, J.E. (ed.) *Immunochemistry of Solid-Phase Immunoassay*, pp. 47-65 (CRC Press, Boca Raton, 1991).
45. Lopez, M., Fleisher, T. & deShazo, R.D. Use and interpretation of diagnostic immunologic laboratory tests. *JAMA* **268**, 2970-90. (1992).
46. Rose, N.R. (ed.) *Manual of Clinical Laboratory Immunology*, pp. 77-107 (ASM Press, Washington D.C., 1997).
47. www.cdc.gov/epo/mmwr/preview/mmwrhtml/00001431.htm.
48. Hesterberg, L.K.C., Mark, A. An Overview of Rapid Immunoassays. *Laboratory Medicine* **27**, 41-46 (1996).
49. Giles, R.E., Perry, K.R. & Parry, J.V. Simple/rapid test devices for anti-HIV screening: do they come up to the mark? *JOURNAL OF MEDICAL VIROLOGY* **59**, 104-9. (1999).
50. Kopchick, J.J. et al. Perspective: Proteomics-see "spots" run. *Endocrinology* **143**, 1990-1994 (2002).
51. Sokoll, L.J. & Chan, D.W. Clinical Analyzers. Immunoassays. *Analytical Chemistry* **71**, 356R-362R (1999).
52. Hamwi, A. et al. Evaluation of turbidimetric high-sensitivity C-reactive protein assays for cardiovascular risk estimation. *Clinical Chemistry (Washington, DC, United States)* **47**, 2044-2046 (2001).

53. Bevan, C.D. & Lloyd, R.S. A High-Throughput Screening Method for the Determination of Aqueous Drug Solubility Using Laser Nephelometry in Microtiter Plates. *Analytical Chemistry* **72**, 1781-1787 (2000).
54. Montagne, P., Cuilliere, M.L., Mole, C., Bene, M.C. & Faure, G. Microparticle-enhanced nephelometric immunoassay of lysozyme in milk and other human body fluids. *Clinical Chemistry (Washington, D. C.)* **44**, 1610-1615 (1998).
55. Cheung, V.G. et al. Making and reading microarrays. *Nature Genetics* **21**, 15-19 (1999).
56. Young, R.A. Biomedical discovery with DNA arrays. *Cell* **102**, 9-15 (2000).
57. Lockhart, D.J. & Winzeler, E.A. Genomics, gene expression and DNA arrays. *Nature (London)* **405**, 827-836 (2000).
58. Chee, M. et al. Accessing genetic information with high-density DNA arrays. *Science* **274**, 610-614 (1996).
59. Debouck, C. & Goodfellow, P.N. DNA microarrays in drug discovery and development. *Nature Genetics* **21**, 48-50 (1999).
60. Li, J., Chen, S. & Evans, D.H. Typing and subtyping influenza virus using DNA microarrays and multiplex reverse transcriptase PCR. *Journal of Clinical Microbiology* **39**, 696-704 (2001).
61. Prix, L., Uciechowski, P., Bockmann, B., Giesing, M. & Schuetz, A.J. Diagnostic biochip array for fast and sensitive detection of K-ras mutations in stool. *Clinical Chemistry* **48**, 428-435 (2002).
62. Gray, D.E., Case-Green, S.C., Fell, T.S., Dobson, P.J. & Southern, E.M. Ellipsometric and Interferometric Characterization of DNA Probes Immobilized on a Combinatorial Array. *Langmuir* **13**, 2833-2842 (1997).
63. www.affymetrix.com.
64. Lueking, A. et al. Protein Microarrays for Gene Expression and Antibody Screening. *Analytical Biochemistry* **270**, 103-111 (1999).
65. MacBeath, G. & Schreiber, S.L. Printing proteins as microarrays for high-throughput function determination. *Science (Washington, D. C.)* **289**, 1760-1763 (2000).

66. Huang, R.-P., Huang, R., Fan, Y. & Lin, Y. Simultaneous Detection of Multiple Cytokines from Conditioned Media and Patient's Sera by an Antibody-Based Protein Array System. *Analytical Biochemistry* **294**, 55-62 (2001).
67. Mendoza, L.G. et al. High-throughput microarray-based enzyme-linked immunosorbent assay (ELISA). *BIOTECHNIQUES* **27**, 778-88. (1999).
68. Silzel, J.W., Cercek, B., Dodson, C., Tsay, T. & Obremski, R.J. Mass-sensing, multianalyte microarray immunoassay with imaging detection. *Clinical Chemistry* **44**, 2036-2043 (1998).
69. MacBeath, G. Protein microarrays and proteomics. *Nature Genetics* **32**, 526-532 (2002).
70. De Wildt, R.M.T., Mundy, C.R., Gorick, B.D. & Tomlinson, I.M. Antibody arrays for high-throughput screening of antibody-antigen interactions. *Nature Biotechnology* **18**, 989-994 (2000).
71. Rowe, C.A. et al. Array Biosensor for Simultaneous Identification of Bacterial, Viral, and Protein Analytes. *Analytical Chemistry* **71**, 3846-3852 (1999).
72. Taitt, C.R., Anderson, G.P., Lingerfelt, B.M., Feldstein, M.J. & Ligler, F.S. Nine-Analyte Detection Using an Array-Based Biosensor. *Analytical Chemistry* **74**, 6114-6120 (2002).
73. Sapsford, K.E., Charles, P.T., Patterson, C.H., Jr. & Ligler, F.S. Demonstration of four immunoassay formats using the array biosensor. *Analytical Chemistry* **74**, 1061-1068 (2002).
74. Anderson, G.P., Breslin, K.A. & Ligler, F.S. Assay development for a portable fiberoptic biosensor. *ASAIJ Journal* **42**, 942-946 (1996).
75. Ligler, F.S. et al. Array biosensor for multi-analyte sensing. *Proceedings of SPIE-The International Society for Optical Engineering* **3258**, 50-55 (1998).
76. Arenkov, P. et al. Protein Microchips: Use for Immunoassay and Enzymatic Reactions. *Analytical Biochemistry* **278**, 123-131 (2000).
77. Drobyshev, A.L., Zasedatelev, A.S., Yershov, G.M. & Mirzabekov, A.D. Massive parallel analysis of DNA-Hoechst 33258 binding specificity with a generic oligodeoxyribonucleotide microchip. *Nucleic Acids Research* **27**, 4100-4105 (1999).

78. Broude, N.E., Woodward, K., Cavallo, R., Cantor, C.R. & Englert, D. DNA microarrays with stem-loop DNA probes: preparation and applications. *Nucleic Acids Research* **29**, e92/1-e92/11 (2001).
79. www.PerkinElmer.com.
80. Raboni, S.M. et al. Comparison of latex agglutination with enzyme immunoassay for detection of rotavirus in fecal specimens. *American Journal of Clinical Pathology* **117**, 392-394 (2002).
81. Sato, K., Tokeshi, M., Kimura, H. & Kitamori, T. Determination of Carcinoembryonic Antigen in Human Sera by Integrated Bead-Bed Immunoassay in a Microchip for Cancer Diagnosis. *Analytical Chemistry* **73**, 1213-1218 (2001).
82. Spiro, A., Lowe, M. & Brown, D. A bead-based method for multiplexed identification and quantitation of DNA sequences using flow cytometry. *Applied and Environmental Microbiology* **66**, 4258-4265 (2000).
83. Swartzman, E.E., Miraglia, S.J., Mellentin-Michelotti, J., Evangelista, L. & Yuan, P.-M. A homogeneous and multiplexed immunoassay for high-throughput screening using fluorometric microvolume assay technology. *Analytical Biochemistry* **271**, 143-151 (1999).
84. Martens, C., Bakker, A., Rodriguez, A., Mortensen, R.B. & Barrett, R.W. A Generic Particle-Based Nonradioactive Homogeneous Multiplex Method for High-Throughput Screening Using Microvolume Fluorimetry. *Analytical Biochemistry* **273**, 20-31 (1999).
85. Albert, K.J., Walt, D.R., Gill, D.S. & Pearce, T.C. Optical multibead arrays for simple and complex odor discrimination. *Analytical Chemistry* **73**, 2501-2508 (2001).
86. Biran, I. & Walt, D.R. Optical imaging fiber-based single live cell arrays: A high-density cell assay platform. *Analytical Chemistry* **74**, 3046-3054 (2002).
87. Szurdoki, F., Michael, K.L. & Walt, D.R. A duplexed microsphere-based fluorescent immunoassay. *Analytical Biochemistry* **291**, 219-228 (2001).
88. Epstein, J.R., Lee, M. & Walt, D.R. High-Density Fiber-Optic Genosensor Microsphere Array Capable of Zeptomole Detection Limits. *Analytical Chemistry* **74**, 1836-1840 (2002).
89. Fulton, R.J., McDade, R.L., Smith, P.L., Kienker, L.J. & Kettman, J.R., Jr. Advanced multiplexed analysis with the FlowMetrix system. *Clinical Chemistry* **43**, 1749-1756 (1997).

90. Oliver, K.G., Kettman, J.R. & Fulton, R.J. Multiplexed analysis of human cytokines by use of the FlowMetrix system. *Clinical Chemistry (Washington, D. C.)* **44**, 2057-2060 (1998).
91. Vignali, D.A. Multiplexed particle-based flow cytometric assays. *Journal of Immunological Methods* **243**, 243-55. (2000).
92. Pickering, J.W. et al. A multiplexed fluorescent microsphere immunoassay for antibodies to pneumococcal capsular polysaccharides. *American Journal of Clinical Pathology* **117**, 589-596 (2002).
93. Reyes, D.R., Iossifidis, D., Auroux, P.-A. & Manz, A. Micro Total Analysis Systems. 1. Introduction, Theory, and Technology. *Analytical Chemistry* **74**, 2623-2636 (2002).
94. Auroux, P.-A., Iossifidis, D., Reyes, D.R. & Manz, A. Micro Total Analysis Systems. 2. Analytical Standard Operations and Applications. *Analytical Chemistry* **74**, 2637-2652 (2002).
95. Harrison, D.J. et al. Micromachining a miniaturized capillary electrophoresis-based chemical analysis system on a chip. *Science* **261**, 895-7 (1993).
96. Jacobson, S.C., Hergenroder, R., Koutny, L.B., Warmack, R.J. & Ramsey, J.M. Effects of Injection Schemes and Column Geometry on the Performance of Microchip Electrophoresis Devices. *Analytical Chemistry* **66**, 1107-13 (1994).
97. Effenhauser, C.S., Manz, A. & Widmer, H.M. Manipulation of Sample Fractions on a Capillary Electrophoresis Chip. *Analytical Chemistry* **67**, 2284-7 (1995).
98. Emrich Charles, A., Tian, H., Medintz Igor, L. & Mathies Richard, A. Microfabricated 384-lane capillary array electrophoresis bioanalyzer for ultrahigh-throughput genetic analysis. *Analytical Chemistry* **74**, pp. 5076-83. (2002).
99. Burns, M.A. et al. An integrated nanoliter DNA analysis device. *Science* **282**, 484-487 (1998).
100. Paegel, B.M., Yeung, S.H.I. & Mathies, R.A. Microchip bioprocessor for integrated nanovolume sample purification and DNA sequencing. *Analytical Chemistry* **74**, 5092-5098 (2002).
101. Seong, G.H. & Crooks, R.M. Efficient mixing and reactions within microfluidic channels using microbead-supported catalysts. *Journal of the American Chemical Society* **124**, 13360-13361 (2002).

102. Oleschuk, R.D., Shultz-Lockyear, L.L., Ning, Y. & Harrison, D.J. Trapping of bead-based reagents within microfluidic systems. On-chip solid-phase extraction and electrochromatography. *Analytical Chemistry* **72**, 585-590 (2000).
103. Buranda, T. et al. Biomolecular recognition on well-characterized beads packed in microfluidic channels. *Analytical Chemistry* **74**, 1149-1156 (2002).
104. Fodor, S.P. et al. Light-directed, spatially addressable parallel chemical synthesis. *Science* **251**, pp. 767-73. (1991).
105. Waters, L.C. et al. Microchip Device for Cell Lysis, Multiplex PCR Amplification, and Electrophoretic Sizing. *Analytical Chemistry* **70**, 158-162 (1998).
106. Hadd, A.G., Raymond, D.E., Halliwell, J.W., Jacobson, S.C. & Ramsey, J.M. Microchip Device for Performing Enzyme Assays. *Analytical Chemistry* **69**, 3407-3412 (1997).
107. Barker, S.L.R., Tarlov, M.J., Canavan, H., Hickman, J.J. & Locascio, L.E. Plastic Microfluidic Devices Modified with Polyelectrolyte Multilayers. *Analytical Chemistry* **72**, 4899-4903 (2000).
108. Petersen, K.E. Silicon as a mechanical material. *IEEE Trans. Electron Devices* **ED-70**, pp. 420-57 (1982).
109. Hoche, J., Buttgenbach, S., Pittschellis, R. & Hesselbach, J. Silicon microgripper for micro-assembly realized by photolithography and fast anisotropic silicon etching. *Proceedings of SPIE-The International Society for Optical Engineering* **3519**, 13-21 (1998).
110. Kim, Y. & Neikirk, D. Micromachined Fabry-Perot Cavity Pressure Transducer. *IEEE Photonics Technology Letters* **7**, pp. 1471-73 (1995).
111. Goodey, A. et al. Development of multianalyte sensor arrays composed of chemically derivatized polymeric microspheres localized in micromachined cavities. *Journal of the American Chemical Society* **123**, 2559-2570 (2001).
112. De Boer, M.J. et al. Micromachining of buried micro channels in silicon. *Journal of Microelectromechanical Systems* **9**, 94-103 (2000).
113. Schasfoort, R.B.M., Schlautmann, S., Hendrikse, J. & Van Den Berg, A. Field-effect flow control for microfabricated fluidic networks. *Science* **286**, 942-945 (1999).
114. Sanders, G.H.W. & Manz, A. Chip-based microsystems for genomic and proteomic analysis. *TrAC, Trends in Analytical Chemistry* **19**, 364-378 (2000).

115. Rosenberg, E.S., Caliendo, A.M. & Walker, B.D. Acute HIV infection among patients tested for mononucleosis. *NEW ENGLAND JOURNAL OF MEDICINE* **340**, 969. (1999).
116. Savoy, S. et al. Solution-based analysis of multiple analytes by a sensor array: toward the development of an "electronic tongue". *Proceedings of SPIE-The International Society for Optical Engineering* **3539**, 17-26 (1998).
117. Lavigne, J.J. et al. Solution-Based Analysis of Multiple Analytes by a Sensor Array: Toward the Development of an "Electronic Tongue". *Journal of the American Chemical Society* **120**, 6429-6430 (1998).
118. Curey, T.E. et al. Characterization of multicomponent monosaccharide solutions using an enzyme-based sensor array. *Analytical Biochemistry* **293**, 178-184 (2001).
119. Christodoulides, N. et al. A microchip-based multianalyte assay system for the assessment of cardiac risk. *Anal. Chem.* **74**, 3030-3036 (2002).
120. McCleskey, S.C., Griffin, M.J., Schneider, S.E., McDevitt, J.T. & Anslyn, E.V. Differential receptors create patterns diagnostic for ATP and GTP. *Journal of the American Chemical Society* **125**, 1114-1115 (2003).
121. Goodey, A.P. & McDevitt, J.T. Multishell Microspheres with Integrated Chromatographic and Detection Layers for Use in Array Sensors. *Journal of the American Chemical Society* **125**, 2870 (2003).
122. Ali, M. et al. DNA Hybridization and Discrimination of Single-Nucleotide Mismatches Using Chip-Based Microbead Arrays. *submitted to Analytical Chemistry* (2003).
123. Floriano, P., Goodey, A.P., Tsau, A.S. & McDevitt, J.T. Application of Artificial Neural Networks to the Taste Chip System: Molecular Level Design Considerations for Array Sensors. *submitted to Analytical Chemistry* (2003).
124. Aratani, K. et al. Surface micromachined tuneable interferometer array. *Sensors and Actuators A* **43**, pp. 17-23 (1994).
125. Cheng, S.B. et al. Development of a multichannel microfluidic analysis system employing affinity capillary electrophoresis for immunoassay. *Analytical Chemistry* **73**, 1472-1479 (2001).
126. Emrich, C.A., Tian, H., Medintz Igor, L. & Mathies Richard, A. Microfabricated 384-lane capillary array electrophoresis bioanalyzer for ultrahigh-throughput genetic analysis. *Analytical Chemistry* **74**, pp. 5076-83. (2002).

127. Ekins, R.P. & Chu, F.W. Multianalyte microspot immunoassay-microanalytical \"compact disk\" of the future. *Clinical Chemistry (Washington, DC, United States)* **37**, 1955-67 (1991).
128. Roda, A. et al. Microtiter format for simultaneous multianalyte detection and development of a PCR-chemiluminescent enzyme immunoassay for typing human papillomavirus DNAs. *Clinical Chemistry* **48**, 1654-1660 (2002).
129. Wiese, R., Belosludtsev, Y., Powdrill, T., Thompson, P. & Hogan, M. Simultaneous multianalyte ELISA performed on a microarray platform. *Clinical Chemistry* **47**, 1451-1457 (2001).
130. Roth, F., Burkart, T. & Muhlemann, K. A new multiantigen immunoassay for the quantification of IgG antibodies to capsular polysaccharides of *Streptococcus pneumoniae*. *Journal of Infectious Diseases* **176**, 526-529 (1997).
131. Butler, J.E. et al. The physical and functional behavior of capture antibodies adsorbed on polystyrene. *Journal of Immunological Methods* **150**, 77-90 (1992).
132. Qian, W. et al. Immobilization of antibodies on ultraflat polystyrene surfaces. *Clinical Chemistry* **46**, 1456-1463 (2000).
133. Sommer, M. et al. Parallel immunoassays on HydroGel biochips using microspot arrays. *Proceedings of SPIE-The International Society for Optical Engineering* **4626**, 49-57 (2002).
134. Afanassiev, V., Hanemann, V. & Wolfl, S. Preparation of DNA and protein micro arrays on glass slides coated with an agarose film. *Nucleic Acids Research* **28**, e66, ii-v (2000).
135. Parsons, R.G. et al. Multianalyte assay system developed for drugs of abuse. *Clinical Chemistry (Washington, DC, United States)* **39**, 1899-903 (1993).
136. Hermanson, G.T. *Immobilized Affinity Ligand Techniques*, 1-136 (Academic Press, San Diego, 1992).
137. Borch, R.F., Bernstein, M.D. & Durst, H.D. Cyanohydridoborate anion as a selective reducing agent. *Journal of the American Chemical Society* **93**, 2897-904 (1971).
138. Ternynck, T. & Avrameas, S. Polyacrylamide-protein immunoadsorbents prepared with glutaraldehyde. *FEBS Letters* **23**, 24-8 (1972).
139. Gustavsson, P.-E. & Larsson, P.-O. Superporous agarose, a new material for chromatography. *Journal of Chromatography, A* **734**, 231-240 (1996).

140. Meldal, M. Properties of solid supports. *Methods in Enzymology* **289**, 83-104 (1997).
141. Bayer, E. Protein synthesis. *Angewandte Chemie* **103**, 117-33 (See also *Angew. Chem., Int. Ed. Engl.*, 1991, 30(2), 113-29) (1991).
142. Sherrington, D.C. Preparation, structure and morphology of polymer supports. *Chemical Communications (Cambridge)*, 2275-2286 (1998).
143. Toy, P.H., Reger, T.S. & Janda, K.D. Tailoring polystyrene solid-phase synthesis resins: incorporation of flexible cross-linkers. *Aldrichimica Acta* **33**, 87-93 (2000).
144. Kates, S.A. et al. "High-load" polyethylene glycol-polystyrene (PEG-PS) graft supports for solid-phase synthesis. *Biopolymers* **47**, 365-380 (1999).
145. Meldal, M. PEGA: a flow-stable polyethylene glycol-dimethylacrylamide copolymer for solid-phase synthesis. *Tetrahedron Letters* **33**, 3077-80 (1992).
146. Fahrner, R.L., Whitney, D.H., Vanderlaan, M. & Blank, G.S. Performance comparison of protein A affinity-chromatography sorbents for purifying recombinant monoclonal antibodies. *Biotechnology and Applied Biochemistry* **30**, 121-128 (1999).
147. Margel, S. Agarose-polyaldehyde microsphere beads: synthesis and biomedical applications. Cell labeling, cell separation, affinity chromatography, and hemoperfusion. *Applied Biochemistry and Biotechnology* **8**, 523-39 (1983).
148. Andersson, T., Carlsson, M., Hagel, L., Pernemalm, P.A. & Janson, J.C. Agarose-based media for high-resolution gel filtration of biopolymers. *Journal of Chromatography* **326**, 33-44 (1985).
149. Horak, D., Hradil, J. & Benes, M.J. Packings for size exclusion chromatography: preparation and some properties. *ACS Symposium Series* **635**, 190-210 (1996).
150. Hjerten, S. Preparation of agarose spheres for chromatography of molecules and particles. *Biochim. Biophys. Acta* **79**, 393-8 (1964).
151. Hjerten, S. & Eriksson, K.O. High-performance molecular sieve chromatography of proteins on agarose columns: the relation between concentration and porosity of the gel. *Analytical Biochemistry* **137**, 313-17 (1984).
152. Hagel, L. Characteristics of modern media for aqueous size exclusion chromatography. *ACS Symposium Series* **635**, 225-248 (1996).

153. Shainoff, J.R. Zonal immobilization of proteins. *BIOCHEMICAL AND BIOPHYSICAL RESEARCH COMMUNICATIONS* **95**, 690-5. (1980).
154. Mendoza, L.G. et al. High-throughput microarray-based enzyme-linked immunosorbent assay (ELISA). *BioTechniques* **27**, 778, 780, 782-786, 788 (1999).
155. Hage, D.S. Immunoassays. *Analytical Chemistry* **71**, 294R-304R (1999).
156. Muller, K.M., Arndt, K.M. & Pluckthun, A. Model and simulation of multivalent binding to fixed ligands. *Analytical Biochemistry* **261**, 149-158 (1998).
157. Koertge, T.E. & Butler, J.E. The relationship between the binding of primary antibody to solid-phase antigen in microtiter plates and its detection by the ELISA. *Journal of Immunological Methods* **83**, 283-99 (1985).
158. Brash, J.L. & Lyman, D.J. Adsorption of plasma proteins in solution to uncharged, hydrophobic polymer surfaces. *Journal of Biomedical Materials Research* **3**, 175-89 (1969).
159. Cantarero, L.A., Butler, J.E. & Osborne, J.W. The adsorptive characteristics of proteins for polystyrene and their significance in solid-phase immunoassays. *Analytical Biochemistry* **105**, 375-82 (1980).
160. McGlennen, R.C. Miniaturization technologies for molecular diagnostics. *Clinical Chemistry (Washington, DC, United States)* **47**, 393-402 (2001).
161. Roberts, D.C.K. Biomarkers, yesterday, today and tomorrow: the basis for health claims. *Asia Pac J Clin Nutr* **11**, S87-9. (2002).
162. St-Louis, P. Status of point-of-care testing: promise, realities, and possibilities. *Clinical Biochemistry* **33**, 427-40 (2000).
163. Fleisher, M. & Schwartz, M.K. Automated approaches to rapid-response testing. A comparative evaluation of point-of-care and centralized laboratory testing. *American Journal of Clinical Pathology* **104**, S18-S25 (1995).
164. Rainey, P.M. Outcomes assessment for point-of-care testing. *Clinical Chemistry* **44**, 1595-1596 (1998).
165. Dodge, A., Fluri, K., Verpoorte, E. & de Rooij, N.F. Electrokinetically Driven Microfluidic Chips with Surface-Modified Chambers for Heterogeneous Immunoassays. *Analytical Chemistry* **73**, 3400-3409 (2001).

166. Yang, T., Jung, S.-y., Mao, H. & Cremer, P.S. Fabrication of Phospholipid Bilayer-Coated Microchannels for On-Chip Immunoassays. *Analytical Chemistry* **73**, 165-169 (2001).
167. Qiu, C.X. & Harrison, D.J. Integrated self-calibration via electrokinetic solvent proportioning for microfluidic immunoassays. *Electrophoresis* **22**, 3949-3958 (2001).
168. Hatch, A. et al. A rapid diffusion immunoassay in a T-sensor. *Nature Biotechnology* **19**, 461-465 (2001).
169. Stenberg, M., Werthen, M., Theander, S. & Nygren, H. A diffusion limited reaction theory for a microtiter plate assay. *Journal of Immunological Methods* **112**, 23-9 (1988).
170. Becker, J.M., Wilchek, M. & Katchalski, E. Irreversible inhibition of biotin transport in yeast by biotinyl-p-nitrophenyl ester. *Proceedings of the National Academy of Sciences of the United States of America* **68**, 2604-7 (1971).
171. Smith, E.L. & Coy, N.H. The absorption spectra of immune proteins. *J. Biol. Chem.* **164**, 367-70 (1946).
172. Brenner, A.J. & Harris, E.D. A quantitative test for copper using bicinchoninic acid. *Analytical Biochemistry* **226**, 80-4 (1995).
173. Nygren, H., Werthen, M. & Stenberg, M. Kinetics of antibody binding to solid-phase-immobilised antigen. Effect of diffusion rate limitation and steric interaction. *Journal of Immunological Methods* **101**, 63-71. (1987).
174. Nygren, H., Czerkinsky, C. & Stenberg, M. Dissociation of antibodies bound to surface-immobilized antigen. *Journal of Immunological Methods* **85**, 87-95. (1985).
175. Mushens, R.E. & Scott, M.L. A fast and efficient method for quantification of monoclonal antibodies in an ELISA using a novel incubation system. *Journal of Immunological Methods* **131**, 83-9. (1990).
176. Engvall, E., Jonsson, K. & Perlmann, P. Enzyme-linked immunosorbent assay. II. Quantitative assay of protein antigen, immunoglobulin G, by means of enzyme-labeled antigen and antibody-coated tubes. *Biochimica et Biophysica Acta* **251**, 427-34 (1971).
177. Pierce Biotechnology Inc. (Rockford, IL) rates the sensitivity of their enzyme substrates on a qualitative scale (Low, Med, High, Very High). One-Step Slow TMB and 3-amino-9-ethylcarbazole (AEC) were purchased from Pierce and both were rated as having medium sensitivity.

178. Johnsson, B., Loefaas, S. & Lindquist, G. Immobilization of proteins to a carboxymethyldextran-modified gold surface for biospecific interaction analysis in surface plasmon resonance sensors. *Analytical Biochemistry* **198**, 268-77 (1991).
179. Holt, D., Rabbany, S.Y., Kusterbeck, A.W. & Ligler, F.S. Advances in flow displacement immunoassay design. *Reviews in Analytical Chemistry* **18**, 107-132 (1999).
180. Franciotta, D. et al. TE671 cell-based ELISA for anti-acetylcholine receptor antibody determination in myasthenia gravis. *Clinical Chemistry (Washington, D. C.)* **45**, 400-405 (1999).
181. Azcona-Olivera, J.I., Abouzied, M.M., Plattner, R.D. & Pestka, J.J. Production of monoclonal antibodies to the mycotoxins fumonisins B1, B2, and B3. *Journal of Agricultural and Food Chemistry* **40**, 531-4 (1992).
182. Escande, C., Chevalier, P., Verdier, F. & Bourdon, R. Sensitive radioimmunoassay and enzyme-linked immunosorbent assay for the simultaneous determination of chloroquine and its metabolites in biological fluids. *Journal of Pharmaceutical Sciences* **79**, 23-7 (1990).
183. Jungblut, P.R. et al. Proteomics in human disease. Cancer, heart, and infectious diseases. *Electrophoresis* **20**, 2100-2110 (1999).

VITA

Marc David Rodriguez was born in San Antonio, Texas on July 26, 1969, the son of Henry Edmund Rodriguez and Mary Angela Rodriguez. During his high school years, he and his family lived in Nürnberg, Germany where he completed his work at Nürnberg American High School. He then returned to Texas in 1987 and in 1988 began a Bachelor of Science degree in Marine Science (Oceanography) at Texas A&M University in Galveston, Texas. He completed the Bachelor of Science in 1993 and began work as an environmental technician at various industrial plant operations in Houston, Texas. His ambition grew, and in 1996 pursued a Bachelors of Science in Chemistry at the University of Texas in San Antonio in order to fulfill the admission requirements of a graduate chemistry degree. In 1998, he obtained the B.S. in Chemistry and was soon accepted to the Graduate School of the University of Texas in Austin. At the University of Texas, he specialized in Analytical Chemistry with specific focus on array-based immunoassay systems. He was supported financially by teaching freshman chemistry laboratory and received a fellowship by the National Science Foundation Integrated Graduate Educational and Research Training Program (IGERT).

Permanent Address: 3547 Red Oak, San Antonio, TX 78230.

This dissertation was typed by Marc D. Rodriguez.